NUMERICAL ANALYSIS OF NEWTONIAN AND NON-NEWTONIAN FERROFLUID PIPE FLOW UNDER CONSTANT AND OSCILLATING MAGNETIC FIELDS

by

Mehmet Can Büyükçayır

M.S., Mechanical Engineering, Boğaziçi University, 2019

Submitted to the Institute for Graduate Studies in
Science and Engineering in partial fulfillment of
the requirements for the degree of
Master of Science

Graduate Program in Your Program

Boğaziçi University

2019

ACKNOWLEDGEMENTS

I owe a deep sense of gratitude to my thesis supervisor Prof. Kunt Atalık for his support and help for completing this thesis. His inspiration, enthusiasm and dynamism have helped me to complete my thesis.

I am extremely thankful to my father Ibrahim Buyukcayir, my mother Zuhal Buyukcayir and my sister Neslihan Erbas for their constant encouragement throughout my years of study.

Finally, I must express my very profound gratitude to my girlfriend Nur Evren for providing me with unfailing support and continuous encouragement throughout the process of writing this thesis. This accomplishment would not have been possible without her. Thank you.

ABSTRACT

NUMERICAL ANALYSIS OF NEWTONIAN AND NON-NEWTONIAN FERROFLUID PIPE FLOW UNDER CONSTANT AND OSCILLATING MAGNETIC FIELDS

In this study the effects of constant and oscillating magnetic fields on axi-symmetric laminar pipe flow are studied. The analyses cover both Newtonian and non-Newtonian ferro fluids exhibiting both shear thinning and shear thickening effects. The magnetic field is created by a current carrying conductor laying along the axis of the pipe and the magnetic force is implemented to the momentum equation. The first part of the study covers the constant magnetic field and the second part covers oscillating magnetic field cases. The effect of the constant magnetic field on magnetic entrance length, friction factor and velocity profiles are studied. The constant magnetic field and power law index have a decreasing effect on magnetic entrance length for both non-Newtonian and Newtonian fluids, however the Reynolds number is directly proportional with the magnetic entrance length. The friction factor is directly proportional with the induced magnetic field and the power law index whereas it is inversely proportional with the Reynolds number. Also flatter velocity profiles are observed under magnetic effects. Compared to constant magnetic field, wavy flow patterns form under oscillating magnetic fields and further increasing the magnetic field strength leads to the development of vortices in the pipe. Compared to constant magnetic field, higher gradients of oscillating magnetic field creates higher magnetic effects as a results higher vorticity values are obtained. Non-dimensional vorticity values reveal that the vorticity is directly proportional with the induced magnetic field and inversely proportional with Reynolds number and power law index.

ÖZET

NEWTONYEN VE NEWTONYEN OLMAYAN FERROMANYETİK AKIŞKAN MODELLERİ İÇİN SABİT VE SALINIMLI MANYETİK ALANIN BORU İÇİ AKIŞ ÜZERİNDEKİ ETKİLERİNİN SAYISAL ANALİZİ

Boru içi akış sırasında ferro parçacıklı akışkan üzerindeki manyetik alan uygulanması sonucu ortaya çıkan etkiler incelenmiştir. Newtonyen ve Newtonyen olmayan akışkanlar için laminer boru içi akışın sayısal analizi yapılmıştır. Manyetik alan boru boyunca ilerleyen bir iletken tarafından yaratılmış bunun sonucunda oluşan manyetik kuvvet momentum denklemine uygulanmıştır. Tezin birinci kısmı sabit manyetik alan altındaki boru içi akışları, ikinci kısmı ise salınımlı manyetik alan altındaki boru içi akışları kapsamaktadır. Sabit manyetik alanın giriş bölgesi uzunluğu, sürtünme faktörü ve hız profili üzerindeki etkisi çalışılmıştır. Giriş bölgesi uzunluğunun, hem Newtonyen hem de Newtonyen olmayan akışkanlar için sabit manyetik alan ve üstel indeks ile azaldığı öte yandan Reynolds sayısı ile arttığı gözlemlenmiştir. Sürtünme faktörünün ise manyetik alan ve üstel indeks ile doğru, Reynolds sayısı ile ters orantılı olduğu görülmüştür. Ayrıca sabit manyetik alan etkisinde daha düz hız profilleri görülmüştür. Sabit manyetik alan ile kıyaslandığında, salınımlı manyetik alan etkisinde dalgalı akım çizgileri oluşmuştur ve salınımlı manyetik alan şiddeti daha da arttırıldığında boru içinde girdapların oluştuğu görülmüştür. Sabit manyetik alana kıyasla salınımlı manyetik alanın yüksek eğimleri daha güçlü manyetik etkilere sebep olup daha büyük vortisite değerlerinin gözlemlenmesine yol açmıştır. Boyutsuz vortisite değerleri, vortisitenin manyetik alan ile doğru, Reynolds sayısı ve üstel indeks ile ters orantılı olduğu görülmüştür.

TABLE OF CONTENTS

LIST OF FIGURES

LIST OF TABLES

LIST OF SYMBOLS

B	Magnetic Flux Density
C_f	Friction Factor
$\overrightarrow{F}$	Magnetic Force
H	Magnetic Field
I	Electrical Current
I_0	Non- Dimensional Current
L_m	Magnetic Entrance Length
M	Magnetization
m	Consistency Coefficient
N	Magnetic Interaction Parameter
n	Power Law Index
p	Pressure
r	Radius
Re	Reynolds Number
T	Stress Tensor
t	time
U_∞	Inlet Velocity
$\overrightarrow{V}$	Velocity
κ	Susceptibility
μ_0	Magnetic Permeability
μ	Viscosity
$\overrightarrow{\omega}$	Angular Velocity
$\overrightarrow{\Omega}$	Vorticity
ρ	Density
τ_{wall}	Wall Shear Stress

LIST OF ACRONYMS/ABBREVIATIONS

2D	Two Dimensional
FEM	Finite Element Modelling
MHD	Magnetohydrodynamics

1. INTRODUCTION

1.1. Literature Survey

Ferro fluids are becoming more and more widespread in the recent years as they offer control of the flow through different parameters like entrance length, friction factor, velocity profile, vorticity etc. Magnetohydrodynamics, denoted as MHD, is another field of fluid mechanics where the effect of magnetism on the flow characteristics is studied. Moreau [3] describes MHD as the phenomena in which an electrically conducting fluid interacts with a magnetic field. As it is known electrically conducting fluids respond to applied magnetic fields. During a fluid flow when a strong external magnetic field is applied, flow characteristics are influenced from this and the flow behaves differently than the case where magnetism is not involved. Ferro fluids can be described and/or modeled as the mixture of ferro particles with the base fluid. They can be created artificially by adding ferro particles like aluminum oxide to the base fluid water or fluids like blood can be modeled as a ferro fluid since blood cells contain iron as ferro particle. In most ferro fluids the diameter of the ferro particles varies from $1nm$ to $1\mu m$. Most of the ferro particles are metals, metal alloys, metallic compounds or oxides. Most of the applications involve the interaction of the ferro fluid with an induced magnetic or electric field therefore it is expected that ferro particles enhance the magnetic and/or conducting properties of the base fluid. Voltairas *et al.* [4] studied the hydrodynamics of magnetic drug targeting where they presented a self-consistent ferrohydrodynamic theory of magnetic drug targeting. Voltairas et al expressed the magnetization as a function of the induced magnetic field and ferro fluid susceptibility. Oldenburg *et al.* [1] concluded that the magnetization and the induced magnetic field are related to each other with an arctangent function in form of:

$$\overrightarrow{M} = \alpha \quad atan\left\{\frac{\beta}{\mu_0}\vec{H}\right\}(1.1) \tag{1.1}$$

where α and β are the magnetization curve parameters, μ_0 is the magnetic permeability, $\overrightarrow{M}$ is the magnetization and $\vec{H}$ is the magnetic field. Oldenburg [1] also revealed

that for lower orders of induced magnetic fields the magnetization vs. magnetic field relationship can be linearized and the magnetization can be expressed as the multiplication of induced magnetic field with a constant susceptibility value which is defined as the measure of response of a material to an induced magnetic field.

Malekzadeh, Hedarnissab and Dabir [5] investigated the magnetic field effect on fluid flow characteristics in a pipe for laminar flow. They investigated the magnetic field influence on the skin friction factor for potassium hydroxide water solution with 30 percent weight experimentally and numerically. Their results revealed that the skin friction factor rises almost linearly with the magnetic field for the case of a laminar steady fully developed flow under transverse magnetic fields. They also found out that the fully developed velocity profile becomes flatter when a transverse magnetic field is applied. In addition to this Malekzadeh [5] *et al.* used the definition of the magnetic entrance length which is the entrance length under induced magnetic field. Their results revealed that the induced magnetic field and the magnetic entrance length are inversely proportional.

Solis and Martin [6] performed torque density measurements on vortex fluids produced by symmetry-breaking rational magnetic fields. They measured the torque densities occurring in rotational flows produced by ac-ac-dc tri-axial magnetic field. By tuning these magnetic fields they could control the vorticity axis of the rotational flow and orient it along any of the three orthogonal magnetic field component axes. They obtained the torque density dependence on the phase angle, field strength, particle shape and frequency. The particles used in the experiment are spheres, platelets and rods. The intensity of the rotational flow could be controlled by the selection of the phase angle between biaxial fields or the amplitude of the dc field. The results of torque measurements showed that such flows are as effective as flows occurring from vortex magnetic fields. The combination of tri-axial fields with vortex magnetic fields can provide strong, controllable rotational flows that can result in good mixing and heat and mass transfer.

Sheikholeslami *et al.* [7] studied a nanofluid filled enclosure in the presence of magnetic field by control volume finite element method to obtain the effects of nanoparticle volume fraction, Rayleigh number, Hartmann number on flow and heat transfer characteristics. The geometry consists of an outer and an inner cylinder and the nanofluid is between those two cylinders. The inner cylinder undergoes uniform heat flux and outer cylinder is kept at constant temperature. Aluminum oxide water nanofluid is used. To calculate effective thermal conductivity and viscosity of nanofluid Koo-Kleinstreuer-Li correlation is implemented. Results reveal that the increase of Rayleigh number caused convection to be the dominant heat transfer mechanism than conduction. Presence of the magnetic field caused the velocity field to be suppressed due to retarding effect of the Lorentz force. Therefore intensity of convection becomes significantly less. Also the conduction heat transfer mechanism is more pronounced at high Hartmann numbers as it suppresses the velocity field and decreases the effect of convection.

Akay *et al.* [8]. performed an experimental investigation of the root flow in a horizontal axis wind turbine. Their research investigated the flow behavior and its features in the blade's root region of a horizontal axis wind turbine by using stereoscopic particle image velocimetry technique. In order to quantify the vorticity Akay used the definition of the non-dimensional vorticity in which the vorticity is non-dimensionalized by the velocity and characteristic length.

Adiguzel [9] studied the flow problem around aat the near wal circular cylinder under the action of magnetostatics effects for both Newtonian and Power Law fluid. His results revealed that the vortex shedding formation may be delayed for both Newtonian and power law ferro fluid under induced magnetic field. He also used the definition of the interaction parameter which is a non-dimensional number characterizing magnetic effects to inertia effects.

Weier, Fey, Geberth and Mutschke *et al.*. [10] studied boundary layer control by means of wall parallel Lorentz forces. They studied the influence of streamwise Lorentz force on the flow along a flat plate for seawater. Their experimental results revealed that for sufficiently high electromagnetic forces a strong acceleration occurs near the

wall. They also obtained a transitional boundary layer of almost constant thickness. In addition to this the fluctuating streamwise velocity component is suppressed due to the accelerating effect of the Lorentz force. The results also show that compared to uncontrolled case there is an 80 percent drag reduction for the case where Lorentz forces are applied. This drag reduction can be explained by the momentum gain resulting from the Lorentz forces. The results also revealed that the skin friction factor increases when Lorentz forces are applied.

Gazeau [11] performed a ferro fluid, which includes cobalt ferrite magnetic particles, rigid rotation under alternating magnetic field experiment. His results revealed that the magnetic particles within the fluid can behave as nano motors or nano generators in nano-scaled applications.

Papadopoulos [12] studied ferro fluid pipe flow under the influence of the magnetic field of a cylindrical coil. The cylindrical coil has a finite length and the flow configuration is chosen similar to bioengineering applications. The parameters studied are magnetic field strength, ferro particle volume concentration and dimensions of the coil. His results revealed that the effect of the magnetic field is stronger near the limits of the coil. The parabolic profile of the velocity is not affected but the pressure drop varied significantly in the magnetic field. The pressure drop linearly depends on the volume concentration of the magnetic particles. His results also revealed that the Kelvin force density, which occurs in momentum equation due to magnetic effects and depends on the gradients of the magnetic field, mainly affects and dominates the flow.

1.2. Objective

The study is conducted to reveal the effect of the induced magnetic field on ferro fluids for both Newtonian and power law ferro fluids. The first part of the study includes constant magnetic field applied to Newtonian and power law ferro fluids and the second part of the study includes oscillating magnetic field applied to the same ferro fluids. The problem is solved for $2D$ axis-symmetric pipe flow with a certain diameter and length. Laminar incompressible Newtonian and power law fluid model

is implemented. Gravitational effects are neglected and the only body force acting on the fluid is the magnetic force. The magnetization is assumed to be uncoupled with the velocity vector and is a function of the induced magnetic field only. It is assumed that the fluid magnetizes when the magnetic field is applied and there is no phase difference between the magnetic field and the magnetization. The analytical form of the magnetic field induced by current carrying conductor is implemented to the magnetic force calculation and momentum equation. No slip boundary condition is assumed at the wall. The purpose of this study is to express the effect of constant magnetic field on the Newtonian and power law ferro fluid at different Reynolds numbers and non- dimensional electrical current values. Power law indices cover both shear thinning and shear thickening ferro fluids and the Reynolds numbers are in laminar flow range. The magnetic field is created by a current carrying conductor and the magnetic force resulting from this magnetic field is applied to the momentum equation. In addition to these this study is also conducted to express the effect of oscillating magnetic field on both Newtonian and power law ferro fluids. The oscillating magnetic field is created with the same technique. The effect of the constant and oscillating magnetic field on magnetic entrance length, friction factor, velocity distribution and vorticity is studied.

1.3. Outline of the Thesis

This thesis includes the mathematical modeling and the solution in Chapter 2, results in Chapter 3 and conclusion in Chapter 4. Chapter 2 includes the mathematical formulation. The governing equations for Newtonian and power law ferro fluid models and the magnetic force created by the current carrying conductor and its application to the momentum equation are given. Non-dimensional parameters and equations are also revealed in this chapter.

Chapter 3 includes the validation of the numerical analyses for the entrance length for the Newtonian fluid. Results of the magnetic entrance length and the friction factor are given for both Newtonian and power law ferro fluid. The effect of the magnetic field on the velocity profile is also included.

In the second part of the study the effect of the oscillating magnetic field on Newtonian and power law ferro fluid is given. Non- dimensional vorticity is defined and vorticity and vortex formation are compared under different oscillating magnetic fields. Chapter 4 is the conclusion.

2. MATHEMATICAL FORMULATION

2.1. Magnetic Field of a Current Carrying Conductor

The magnetic flux density B induced by the current carrying conductor is defined as:

$$B = \mu_0 \frac{I}{2\pi r} \tag{2.1}$$

where μ_0 is the vacuum permeability, I is the current and r is the radius around the conductor.The magnetic field H (A/m) induced by the current carrying conductor is expressed as the ratio of the magnetic flux density B and the vacuum permeability. The magnetic field has the same magnitude at all points on a circle, centered on the conductor, which has the radius r around the conductor, and the direction of B is tangent to that circle.

The induced magnetization M of a ferro fluid is defined as an arc tangent expression with two material parameters α (A/m) and β (m/A) as:

$$M = \alpha \quad arctan\left\{\frac{\beta}{\mu_0} H\right\} \tag{2.2}$$

Figure 2.1 reveals the relationship between the induced magnetization of the ferro fluid and the applied magnetic field. It can be seen that for the magnetic field of interest there is a linear relationship between magnetization and the magnetic field. Therefore the magnetization equation can be linearized as:

$$M = \frac{\kappa}{\mu_0} H \tag{2.3}$$

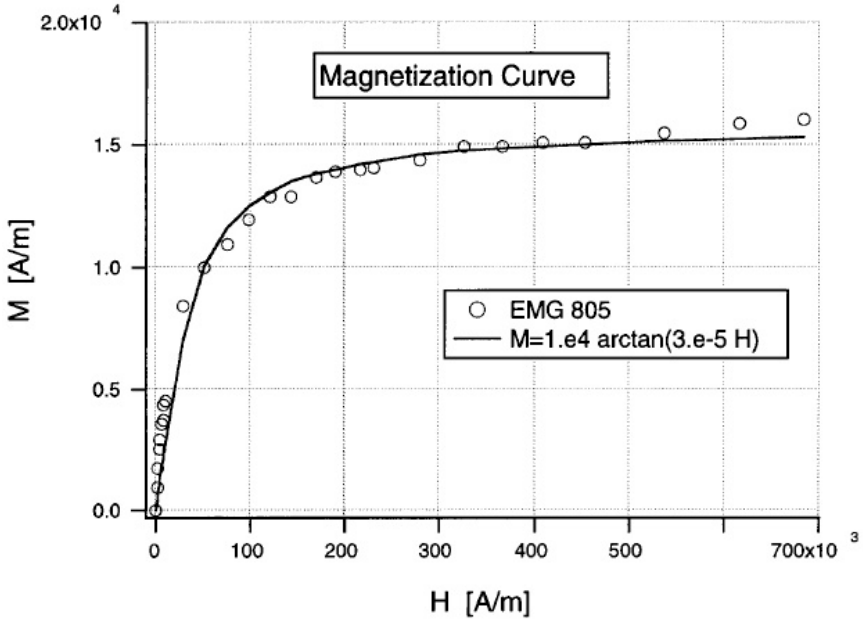

Figure 2.1. Magnetization vs. Magnetic Field for Ferro Fluid EMG 805 [1]

The product of two material parameters α and β, is called the magnetic susceptibility κ,. It is a dimensionless number revealing the degree of magnetization of a material to the applied magnetic field.

2.2. Mass and Momentum Conservation and Definition of Stress Tensor for Newtonian and non- Newtonian Fluids

The mass conservation and momentum equations for the flow of an incompressible fluid are given as:

$$\frac{\partial \rho}{\partial t} + \nabla.(\rho \overrightarrow{V}) = 0 \tag{2.4}$$

$$\rho \left\{ \frac{\partial \overrightarrow{V}}{\partial t} + \vec{V}.\nabla \vec{V} \right\} = \nabla.T + \vec{F} \tag{2.5}$$

$\overrightarrow{V}$ is the velocity vector, ρ is the density, μ is the viscosity, t is the time $\overrightarrow{F}$ is the body force and T is the stress tensor. In this work steady state problem is considered. The stress tensor T is defined as:

$$T = -pI + F(D) \tag{2.6}$$

where p is the thermodynamic pressure, I is the identity tensor and $F(D)$ is a function of the rate of deformation tensor. F(D) is defined as:

$$F(D) = \alpha_0 I_D + \alpha_1 II_D D + \alpha_2 III_D D^2 \tag{2.7}$$

where I_D, II_D and III_D are the invariants of the rate of deformation tensor and α_1, α_2 and α_3 are the expansion coefficients. If a fluid is Newtonian then the stress field is linearly related to the rate of deformation field, therefore α_2 is equal to 0 as D^2 is non linear. α_1 is equal to 2μ and α_0 is equal λ where μ and λ are the viscosity coefficients. The stress tensor equation becomes:

$$T = \quad -pI + \lambda I_D I + 2\mu D \tag{2.8}$$

$$\nabla.T = \quad -\nabla p + (\lambda + \mu)\nabla\nabla.\overrightarrow{V} + \mu\nabla^2\vec{V} \tag{2.9}$$

For incompressible Newtonian fluids the rate of deformation tensor the second term in the right hand side of Equation (2.10) vanishes and the momentum equation becomes:

$$\rho\left\{\frac{\partial\overrightarrow{V}}{\partial t} + \vec{V}.\nabla\vec{V}\right\} = -\nabla p + \mu\nabla^2\overrightarrow{V} + \vec{F} \tag{2.10}$$

Different models are used to model non- Newtonian fluids. In this work Ostwald de Waele or the power law model is used to model the ferro fluid as a non- Newtonian material. Fluids showing decreasing viscosity with increasing shear rate are called shear thinning whereas fluids showing increasing viscosity with increasing shear rate are called shear thickening. It is very useful to predict the viscosity under intermediate shear rates however it may not be accurate to predict the viscosity under very low and very high shear rates. Viscosity of a power law fluid is given as:

$$\mu(D) = m \quad II_D^{\frac{n-1}{2}} \tag{2.11}$$

where M and n are called consistency coefficient and power law index respectively and are empirical curve fitting parameters. Fluids with power law index less than one are called shear thinning whereas fluids with power law index higher than one are called shear thickening. For a Newtonian fluid the power law index becomes one and the consistency factor is equal to the value of the constant viscosity.

2.3. Magnetic Force Acting on the Fluid

The term $\overrightarrow{F}$ defines the body force acting on the fluid. The Induced magnetic field occurring by the current carrying conductor creates a magnetic force on the fluid and it is included as a body force in the momentum equation. In the previous section the magnetic field induced by the current carrying conductor and the induced magnetization of the fluid were given in Equations (2.1) and (2.4), respectively.

Assuming that the ferro particles in the fluid do not interact with each other the magnetic force equation is given as:

$$\overrightarrow{F} = \mu_0 M \nabla H \tag{2.12}$$

Finally the momentum equation for a fluid in the presence of a magnetic field created by a current carrying conductor becomes:

$$\rho \left\{ \frac{\partial \overrightarrow{V}}{\partial t} + \vec{V}.\nabla \vec{V} \right\} = -\nabla p + \mu \nabla^2 \overrightarrow{V} + \mu_0 M \nabla H \tag{2.13}$$

The Velocity is non-dimensionalized by the inlet velocity U_∞, the length is non-dimensionalized with the diameter of the pipe d, the magnetic field is non- dimensionalized by the unit magnetic field B_0 and the magnetization is non-dimensionalized by $\frac{B_0^2}{\mu_0}$.The non-dimensional form of the momentum equation is given as:

$$\rho \left\{ \frac{\partial \overrightarrow{V}}{\partial t} + \vec{V}.\nabla \vec{V} \right\} = -\nabla p + \frac{1}{Re} \nabla^2 \overrightarrow{V} + N\vec{F} \tag{2.14}$$

where N is the magnetic interaction parameter, which is the ratio of the magnetic effects to the inertia effects, and Re is the Reynolds number, which is the ratio of inertia effects to viscous effects and they are given as:

$$N = \frac{B^2}{\mu_0 \rho U_\infty^2} \tag{2.15}$$

$$Re = \frac{\rho U_\infty d}{\mu} \tag{2.16}$$

2.4. Geometry and Mesh Selection

The analyses are conducted for 2-D axi-symmetric pipe shown in Figure 2.2. As it is mentioned before, the magnetic field has the same magnitude at all points centered on the conductor and is inversely proportional with the radius of the circle created by these centered points. In this analysis current carrying conductor flows through the center of the pipe and the radius of the magnetic field circles increase along r direction. The no slip boundary condition is applied at pipe walls. The ferro fluid has a uniform velocity in the inlet and zero pressure boundary condition is applied in the exit of the pipe. The pipe has three sections. In the first section no magnetic field is applied and the flow develops fully before reaching the magnetic region. In the second section of the pipe the so called magnetic section begins. The fluid enters the magnetic region and redevelops in that region under the effect of the induced magnetic field. Then it enters to the third region where there is no induced magnetic field and the fluid redevelops as there is no magnetic field applied to it. For illustrative purposes Figure 2.3 reveals the contour plot of the velocity magnitude of the Newtonian ferro fluid at Reynolds Number 100 under the induced magnetic field. The effect of the magnetic field on the fluid can be seen in the second section of the pipe.

As it is revealed in Figure 2.4 mapped face meshing is used for the analysis. To test the mesh independency the results for five different meshes are compared. These meshes differ in the element number and the element numbers used in the analyses are 340000, 160000, 120000, 80140, 40014 and 4800. The mesh independency test is conducted for Newtonian fluid. It is tested for the friction factor and fully developed velocity profile. Table 2.1 reveals the friction factor comparison for each element number. Results reveal that the friction factor converges to 0.08 after the element number of 120000. Considering the accuracy of the analyses maximum element number of 160000 is chosen and to avoid numerical complexity element number of 340000 is not chosen. Fanning friction factor is defined as:

$$C_f = \frac{16}{Re} \tag{2.17}$$

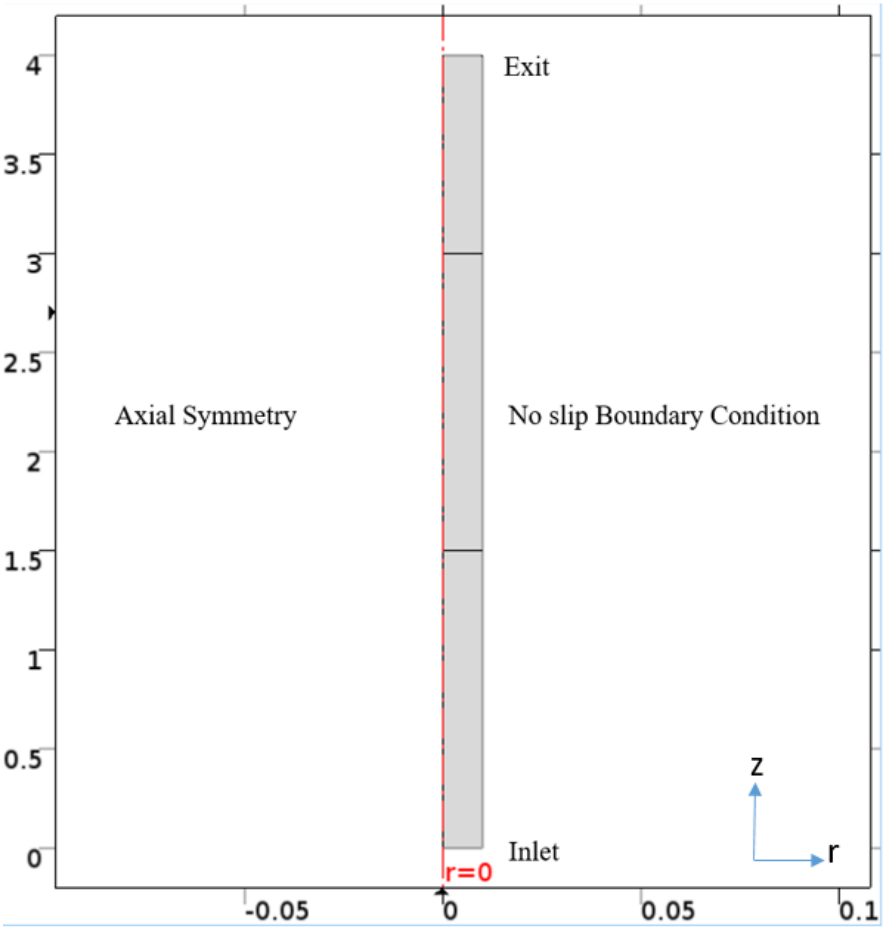

Figure 2.2. Geometry of the Pipe and Boundary Conditions

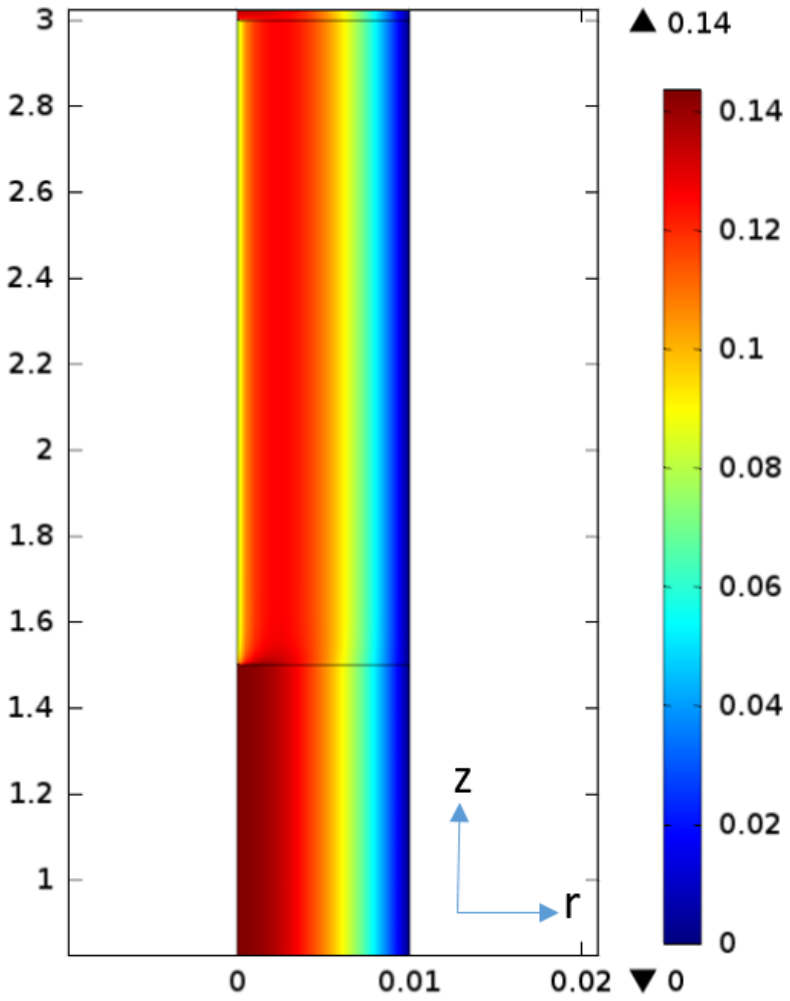

Figure 2.3. Contour Plot of the Velocity Magnitude of Newtonian Ferro Fluid Under Induced Magnetic Field

Comparing results with equation (2.18) maximum element number of 160000 reveals accurate results for the friction coefficient.

Figure 2.5 reveals the mesh independency testing of the velocity profile. Dashed lines stand for maximum element numbers of 340000 and 160000 whereas the dotted lines stand for 120000, 80140 and 4014. As it is seen in Figure 2.5 the velocity converges with increasing element number. As the dashed lines fall onto each other and considering the computation efforts the maximum element number of 160000 is chosen.

Table 2.1. Friction Factor Comparison for Mesh Independency Test.

Element Number	340000	160000	120000	80140	40014	4800
Friction Factor	0.08	0.08	0.08	0.077	0.068	0.056

2.5. Numerical Method

The COMSOL program is used to conduct the numerical analyses. It utilizes the Finite Element Modelling (FEM). The geometry is defined in the same program and the velocity and pressure equations are solved for the given geometry. The volume force is also included to the momentum equation. The analytical solution of the magnetic force due to induced magnetic field created by a current carrying conductor is implemented as a volume force to the momentum equation. All the magnetic parameters such as magnetization and the electrical current are defined in the program manually. Equal order Lagrangian linear functions are used for velocity and pressure fields. The convergence criterion is chosen to be 10^{-6}.

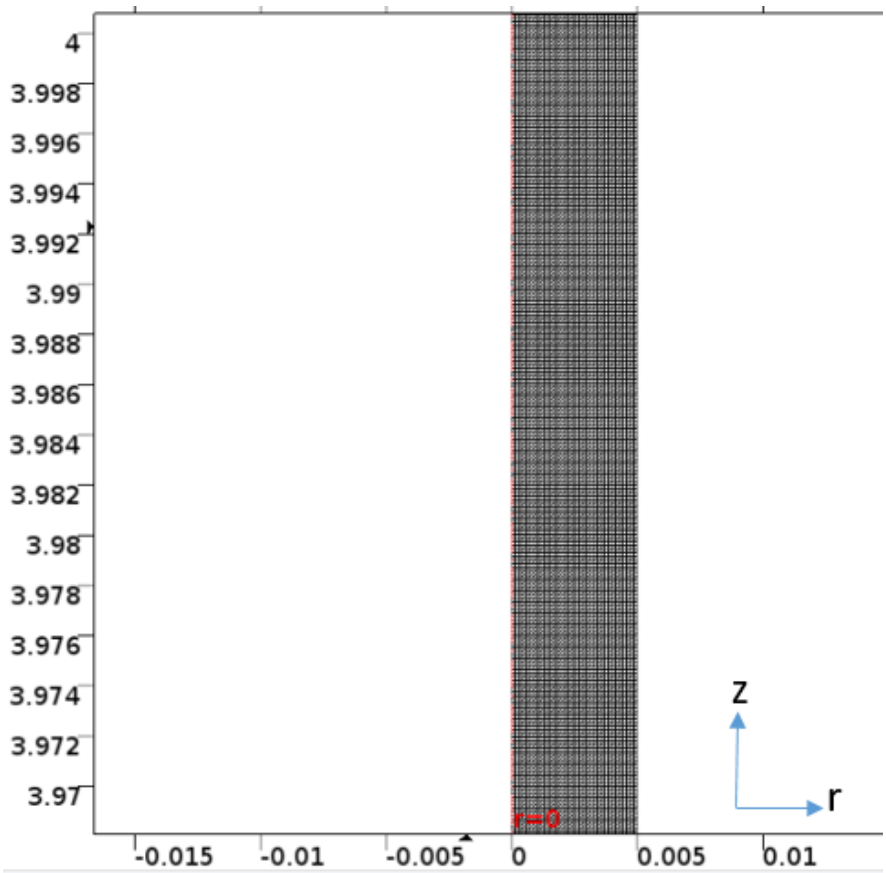

Figure 2.4. Mapped Face Mesh with Maximum Element Size of 5×10^{-4}

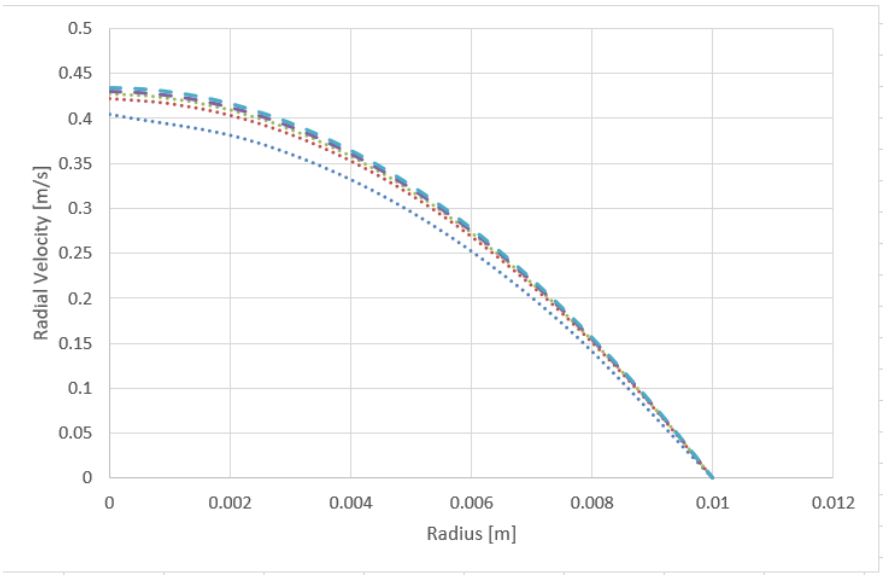

Figure 2.5. Velocity Profiles at $Re = 2000$ for Mesh Independency Test

3. RESULTS AND DISCUSSION

The study consists of two main parts. The analyses in the first part of the study are conducted to express the effect of the induced constant magnetic field created by the current carrying conductor on Newtonian and power law ferro fluids. Changes on the entrance lengh L_e, friction factor C_f and velocity profile under different magnitudes of magnetic fields are studied.

The analyses in the second part are conducted to express the effect of oscillating induced magnetic field on Newtonian and power law ferro fluid. Its effect on stream lines and vortices created by oscillating magnetic field within the ferrofluid are studied. Changes on the non-dimensional vorticity at different Reynolds numbers, magnetic fields and power law indices are shown.

As it is mentioned before the magnetic field created by the current carrying conductor is a function of the electrical current and the radius around the current carrying conductor. The radius around the current carrying conductor is limited by the diameter of the pipe, therefore the magnetic field is tuned by the value of the electrical current. Calvo [13] defines the non-dimensional flow rate as a function of the non-dimensional current, which is given as the ratio of the electrical current to the unit Ampere scale. In this study, as it is mentioned before the magnetic field created by the current carrying conductor depends on the radius around the path of the current carrying conductor. Therefore in addition to the definition of Calvo [13] the non-dimensional electrical current is non-dimensionalized by the characteristic length, which is the radius of the pipe. The non-dimensional current is given as:

$$I_0 = \frac{I}{d}\frac{\bar{L}}{\bar{I}} \tag{3.1}$$

where I and d are the electrical current and diameter and $\bar{I}$ and $\bar{L}$ are the unit current and unit length respectively.

The first part of the analyses are conducted for Reynolds Number from Re=100 to Re=1200 increasing by 100, for non-dimensional currents of I_0= 75, 100 and 150.

The entrance length is the first parameter on which the effect of the induced magnetic field is observed. When a fluid enters to the pipe it has a certain pressure. When the velocity profile develops the pressure value decreases nonlinearly across the pipe. When the velocity fully develops the fluid reaches the entrance length and the pressure starts to drop linearly. Figure 3.1 reveals the pressure change of a viscous fluid before and after it reaches to the entrance length. The entrance length of the Newtonian fluids is proportional with the Reynolds number and the diameter of the pipe. For power law fluids in addition to that it is inversely proportional with the power law index.

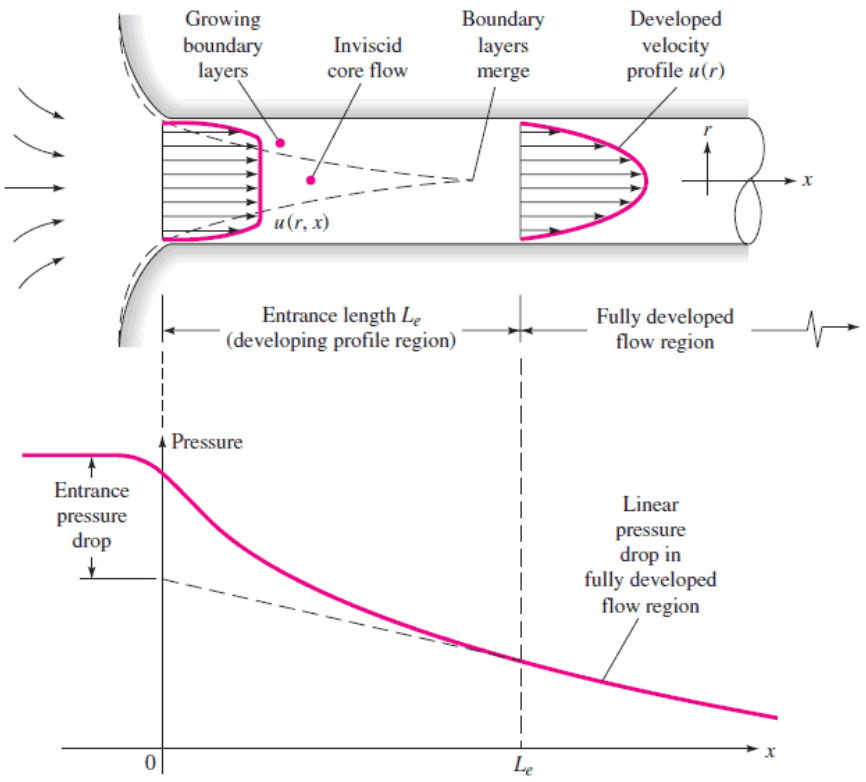

Figure 3.1. Pressure Change in a Pipe Flow Before and After Entrance Length [2]

The effect of the induced magnetic field on the friction factor, which is the second parameter affected, is also studied for Newtonian and power law ferro fluids in this work. Friction factor is the nondimensionalized wall shear stress. For Newtonian fluids the wall shear stress τ_w is given as:

$$\tau_w(r) = \mu\dot{\gamma} \tag{3.2}$$

and for power law fluids it is given as:

$$\tau_w(r) = m\dot{\gamma}^n \tag{3.3}$$

where $\dot{\gamma}$ is the shear rate. The analyses are conducted for two dimensional axi-symmetric pipe, therefore the rate of deformation reduces to:

$$\dot{\gamma}^n = \left[\frac{\partial w}{\partial r}\right]^n \tag{3.4}$$

where w is the axial velocity. The Friction factor, which is the non-dimensional wall shear stress, is given as:

$$C_f = \frac{\tau_w}{0.5\rho U_\infty^2} \tag{3.5}$$

where $0.5\rho U_\infty^2$ is the dynamic pressure.

3.1. Constant Magnetic Field Cases

The entrance length of a Newtonian fluid for laminar flow, on which there is no acting body force, is given as:

$$\frac{L_e}{d} = 0.06Re \tag{3.6}$$

where L_e is the entrance length and d is the diameter of the pipe.

To test the validity of the analyses the entrance length is calculated and plotted for 5 different cases in which there is no magnetic force acting on the fluid. The results are plotted together with the entrance length curve in Equation (3.5). Figure 3.2 reveals the validation of the data from the analyses. Dots are the results obtained in the analyses whereas line is the curve for the entrance length with the slope of 0.06.

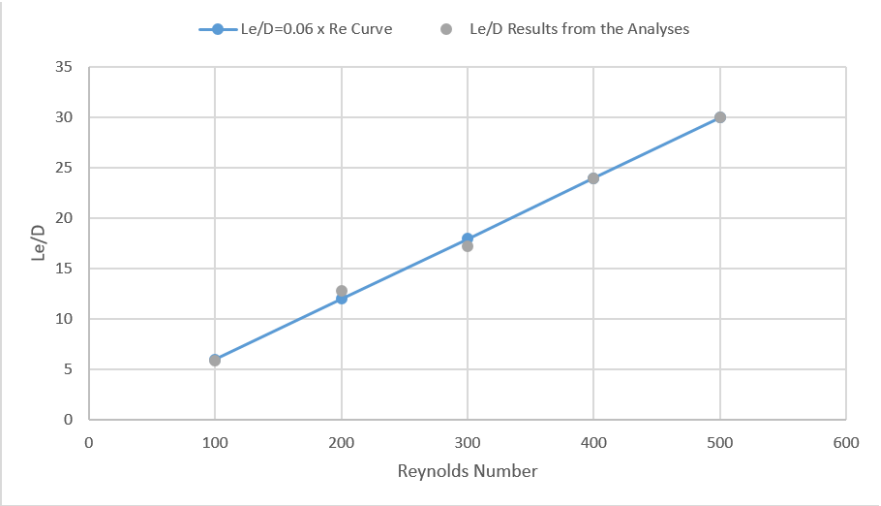

Figure 3.2. Entrance Length Results Obtained in the Analyses and Comparison With Entrance Length Formula

For a Newtonian fluid, on which no body force is exerted, the entrance length is defined as the distance in which the velocity profile fully develops. If it is a cylindrical pipe flow the fully developed velocity profile is in parabolic form. In the case of an induced magnetic field acting on the fluid, magnetic entrance length L_m is defined. As it is mentioned before the analyses are conducted for a cylindrical pipe with three sections. In the first section there is no induced magnetic field and the flow develops without any forces acting to it. In the second section of the pipe the induced magnetic field starts and the magnetic force starts to act on the fluid. Due to the magnetic force the velocity profile of the fluid starts to reshape and redevelops itself in the magnetic section of the pipe. The distance in which the fluid redevelops itself in the magnetic field

is defined as the magnetic entrance length L_m in this work. Similar to the definition of the entrance length L_e, the magnetic entrance length L_m is determined by using the pressure drop versus axial distance in the pipe. The point where pressure starts to drop linearly in the magnetic section of the pipe is taken as the magnetic entrance length.

3.1.1. Magnetic Entrance Length for Newtonian Ferro Fluid

Figures from 3.3 to 3.14 reveal the velocity magnitude contour plots for Reynolds numbers 200, 400, 600 and 800 for non-dimensional currents of $I_0 = 75, 100$ and 150. The magnitude of the induced magnetic field is directly proportional to the non-dimensional electrical current. Plots reveal that the influence of the induced magnetic field on the ferro fluid increases with increasing induced magnetic field. This can be seen directly with the color change of the velocity contours when the ferro fluid enters to the magnetic region of the pipe. With increasing induced magnetic field, the transition from fully developed velocity profile to fully developed magnetic velocity profile is sharper.

The magnetic entrance length and the induced magnetic field are inversely proportional. With increasing non-dimensional electric current the entrance length decreases and the ferro fluid velocity profile develops itself in a smaller distance along the pipe. Similar to the entrance length, the magnetic entrance length is also directly proportional with the Reynolds number. With increasing Reynolds number the magnetic entrance length also increases and the ferro fluid velocity profile develops itself in a larger distance along the pipe.

As it is mentioned before the analyses are conducted for Reynolds number starting from 100 to 1200 with induced magnetic fields created by non-dimensional currents of I_0=75, 100 and 150. The magnetic entrance length values, which is obtained from the pressure drop vs axial length along the pipe curve, are plotted on a single graph for Newtonian ferro fluid.

Malekzadeh *et al.* [5] also revealed in their results that the magnetic entrance length decreases with increasing magnetic field. As the force acting on the fluid becomes larger the new velocity profile develops itself in a smaller distance. However Malekzadeh [5] uses an electrically conducting fluid. As a result the induced magnetic field is related to the current density and instead of the magnetic interaction parameter Hartman number appears when the momentum equation is non-dimensionalized. However, ferro fluid is used in this study which is different than Malekzadeh [5]. For the Newtonian fluid case same trends are observed to Malekzadeh [5] and the magnetic entrance length and the magnetic field are inversely proportional and the magnetic entrance length is directly proportional with the Reynolds number.

Figure 3.15 shows the distribution of the magnetic entrance length value for each analysis. Results reveal the relationship between the magnetic entrance length, Reynolds number and non-dimensional current as:

$$\frac{L_m}{d} = 0.1637 \quad 0.325 \quad \frac{Re}{I_0} \tag{3.7}$$

Equation (3.8) reveals a linear relationship between the magnetic entrance length, Reynolds number and the non-dimensional current. Non-dimensional current is non-dimensionalized by the radius of the pipe as the magnetic field acting on the fluid is limited by the pipe wall. In addition to these, results revealed that there is an inverse relationship between non-dimensional current and the magnetic entrance length for a constant non-dimensional current value.

3.1.2. Magnetic Entrance Length for Power Law Ferro Fluid

In order to understand the effect of the induced magnetic field on non- Newtonian ferro fluids the analyses are conducted for the power law fluids with power law indices $n = 0.6, 0.7, 0.8, 0.9$ and 1.1 for non dimensional currents of $I = 75, 100$ and 150. The same definition of the magnetic entrance length, which is the start of the linear pressure drop in the magnetic region of the pipe, is followed for power law ferro fluid as well.

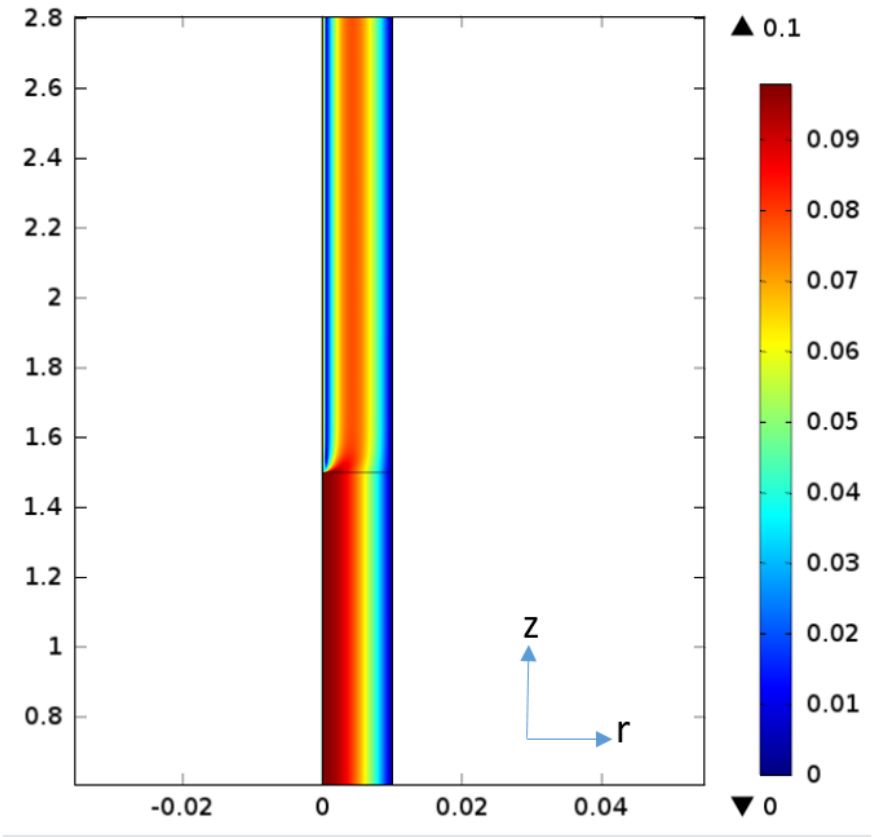

Figure 3.3. Velocity Magnitude Contour Plot for Re=200 and $I_0 = 150$

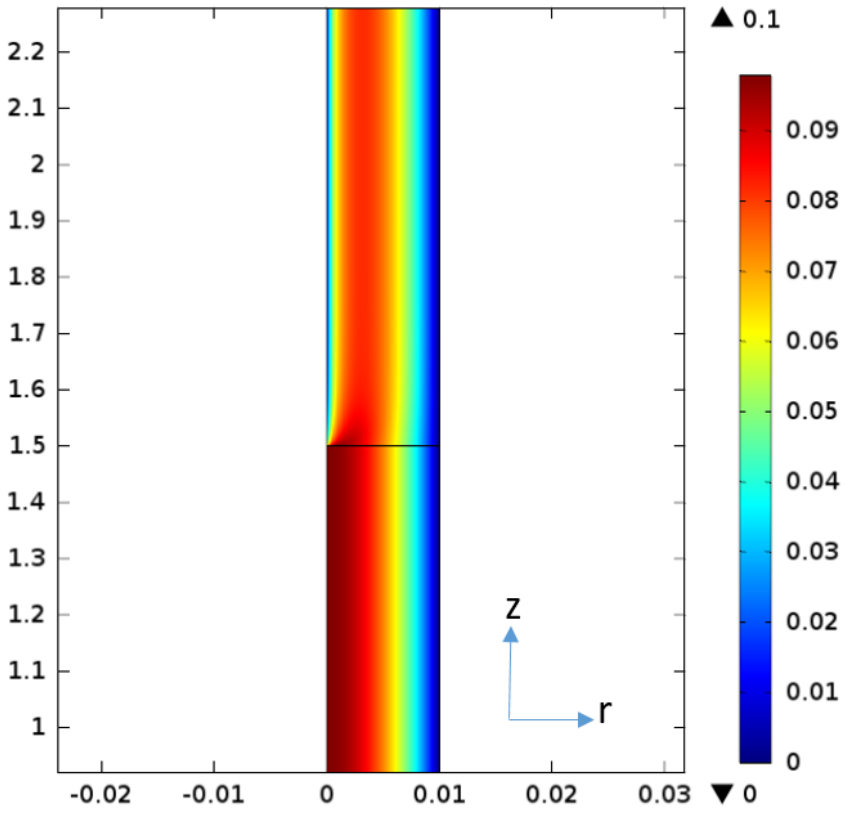

Figure 3.4. Velocity Magnitude Contour Plot for Re=200 and $I_0 = 100$

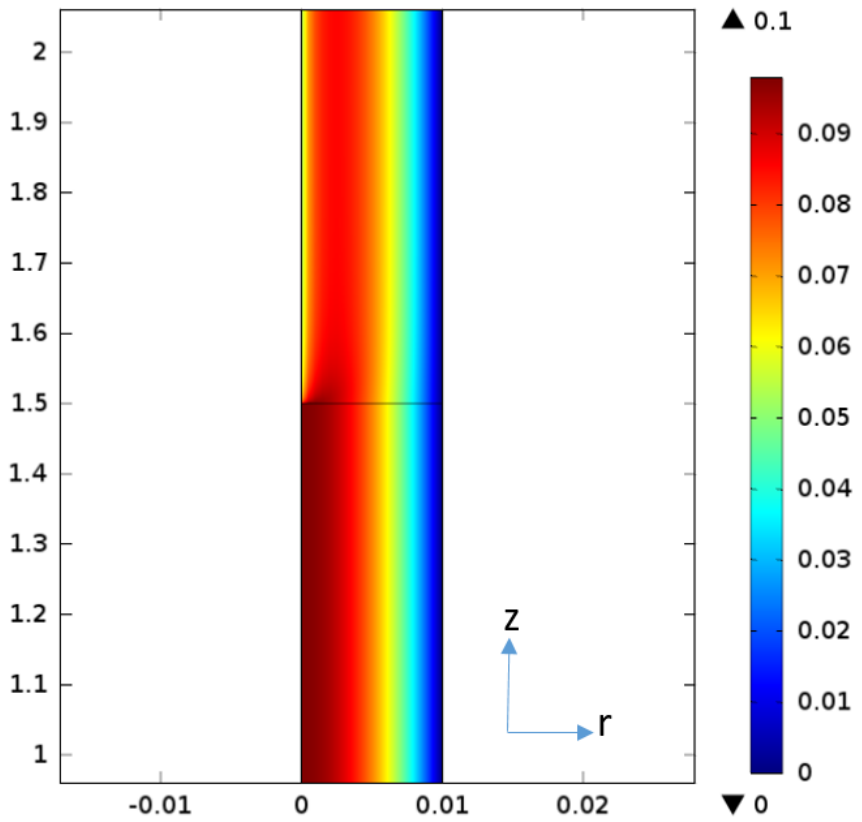

Figure 3.5. Velocity Magnitude Contour Plot for Re=200 and $I_0 = 75$

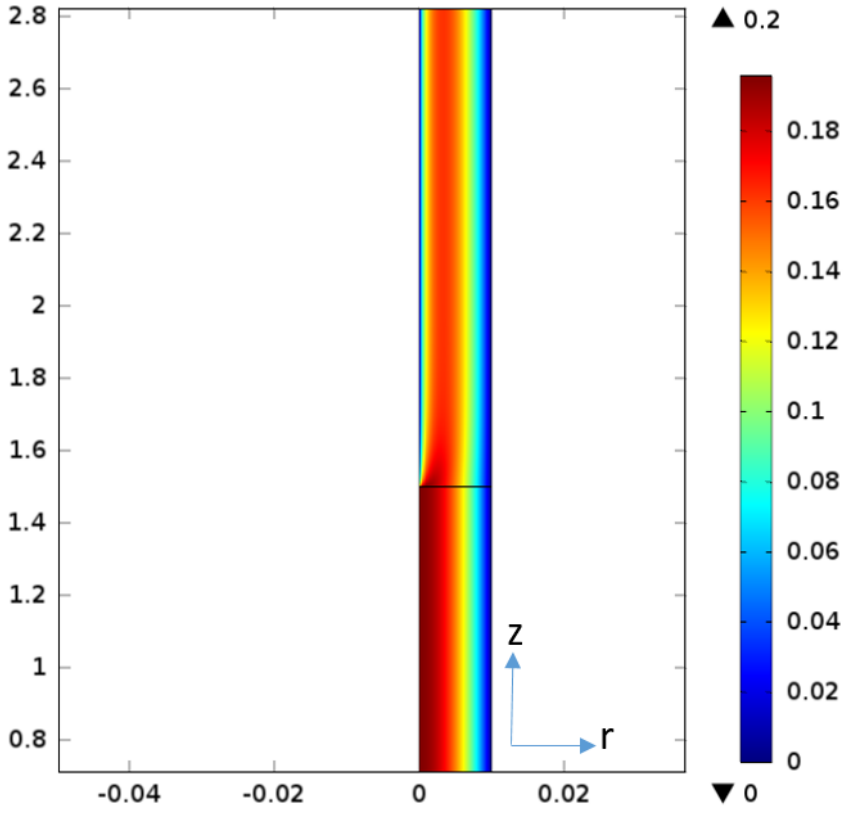

Figure 3.6. Velocity Magnitude Contour Plot for Re=400 and $I_0 = 150$

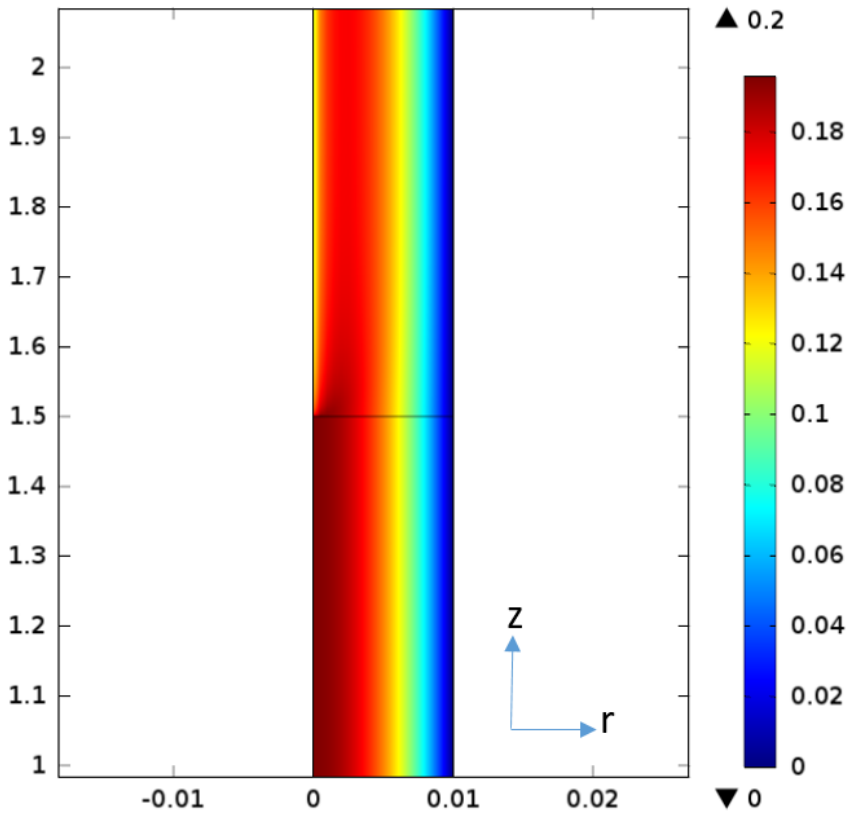

Figure 3.7. Velocity Magnitude Contour Plot for Re=400 and $I_0 = 100$

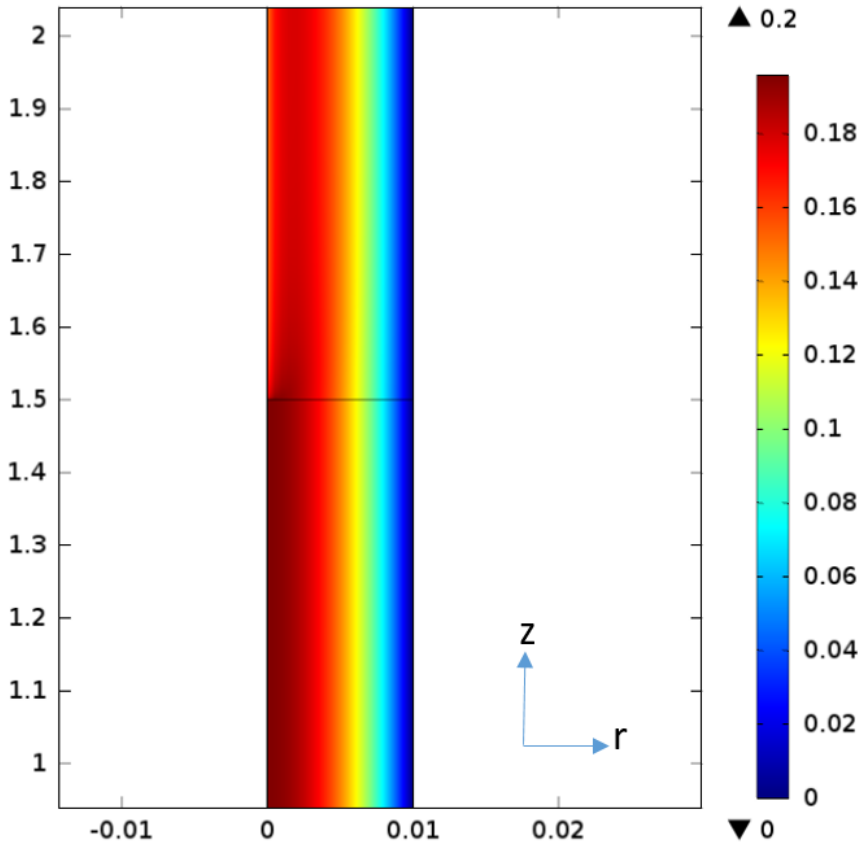

Figure 3.8. Velocity Magnitude Contour Plot for Re=400 and $I_0 = 75$

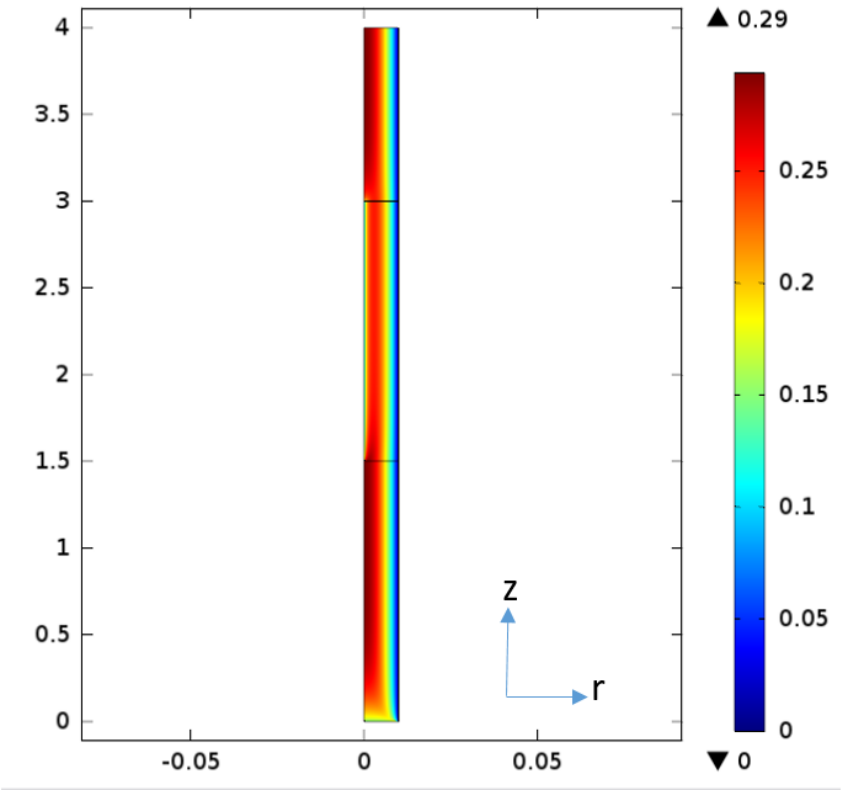

Figure 3.9. Velocity Magnitude Contour Plot for Re=600 and $I_0 = 150$

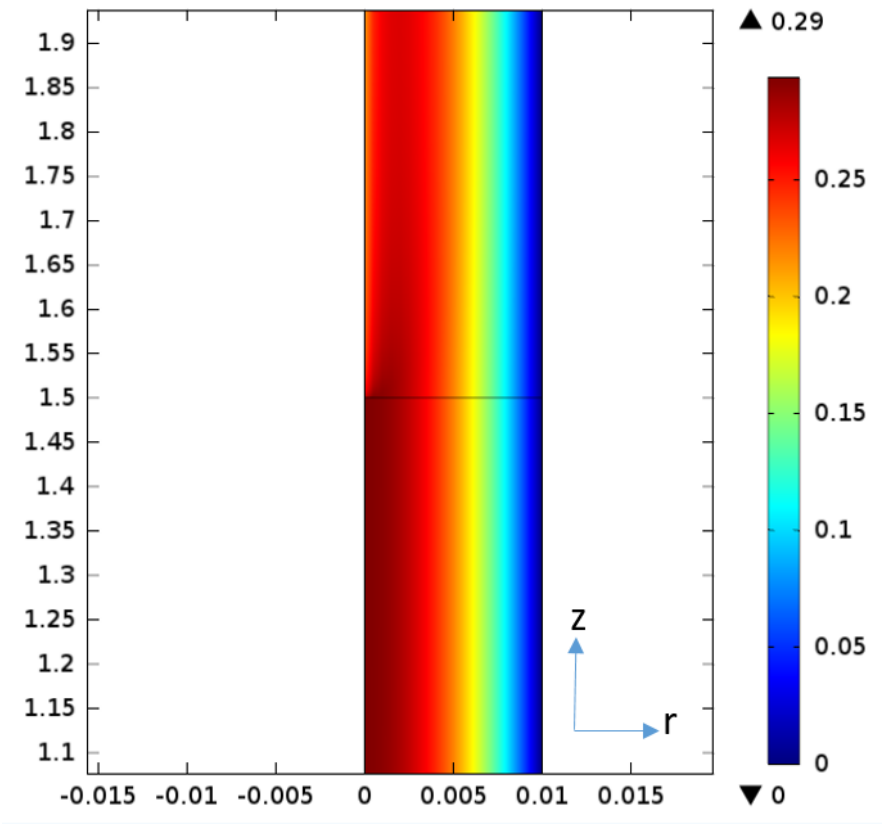

Figure 3.10. Velocity Magnitude Contour Plot for Re=600 and $I_0 = 100$

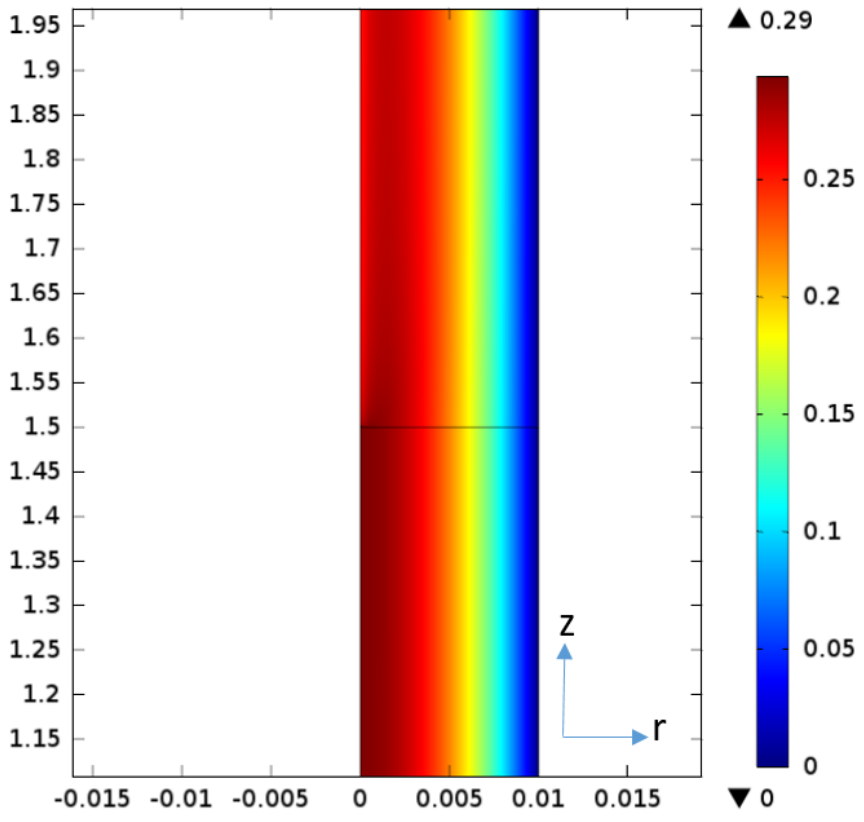

Figure 3.11. Velocity Magnitude Contour Plot for Re=600 and $I_0 = 75$

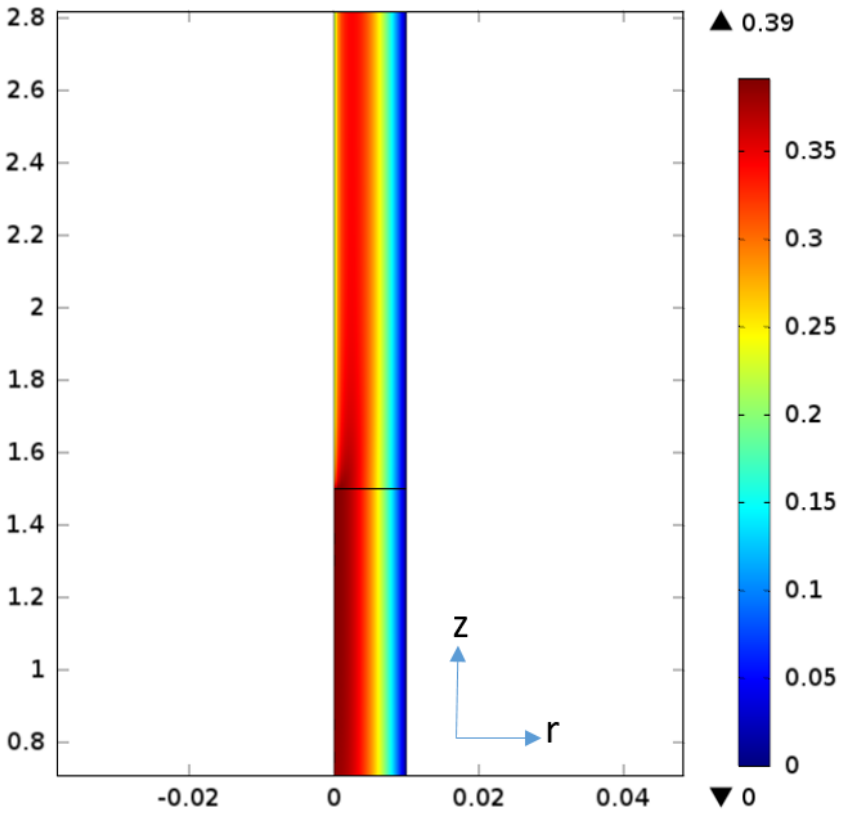

Figure 3.12. Velocity Magnitude Contour Plot for Re=800 and $I_0 = 150$

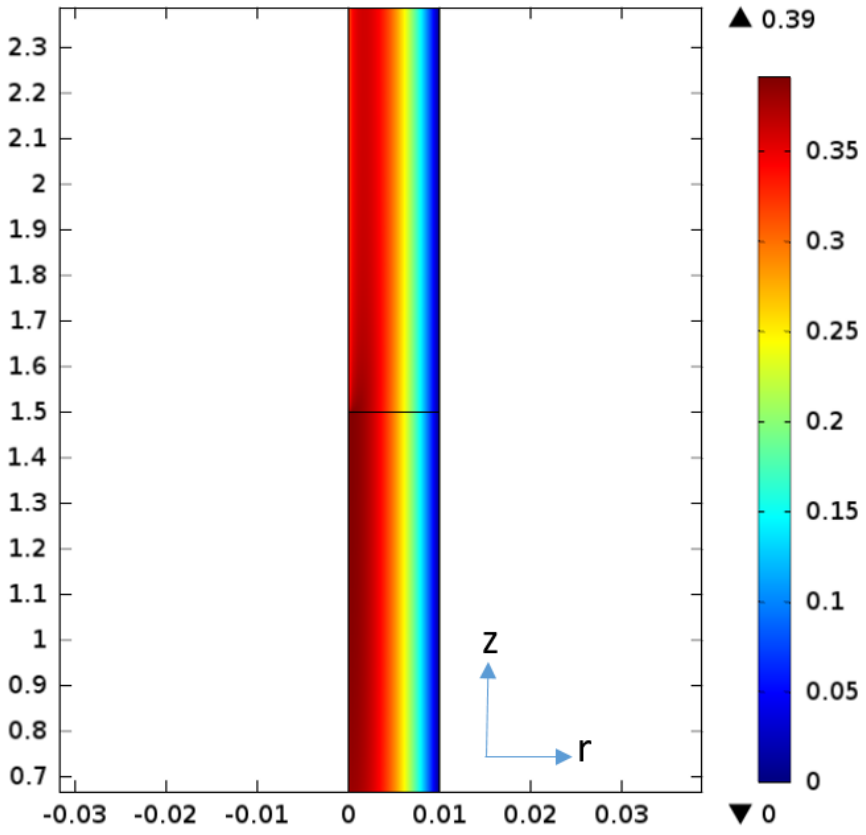

Figure 3.13. Velocity Magnitude Contour Plot for Re=800 and $I_0 = 100$

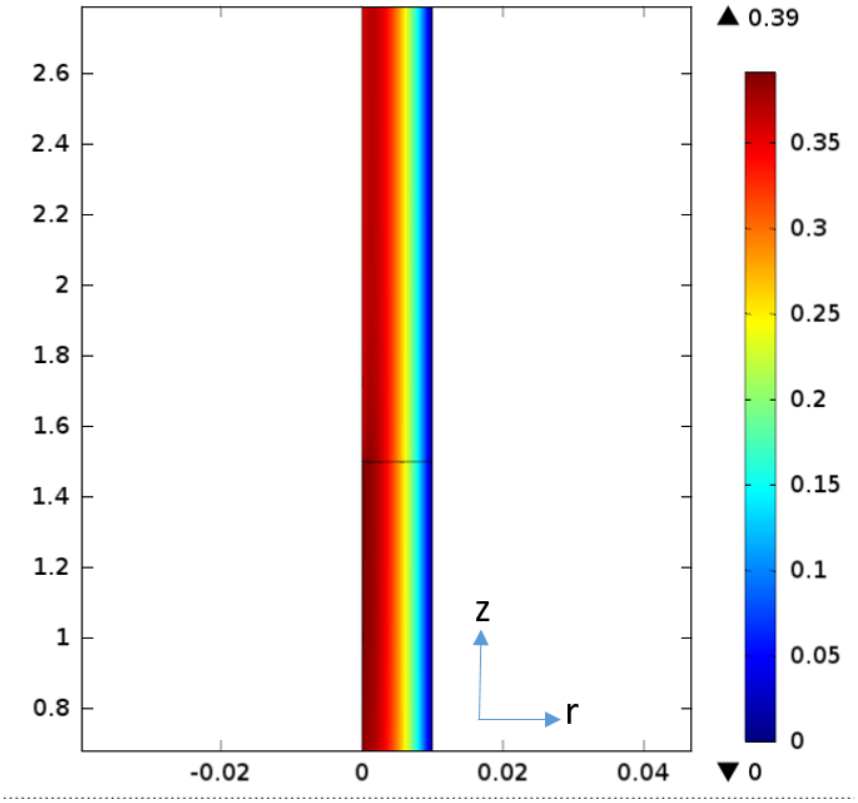

Figure 3.14. Velocity Magnitude Contour Plot for Re=800 and $I_0 = 75$

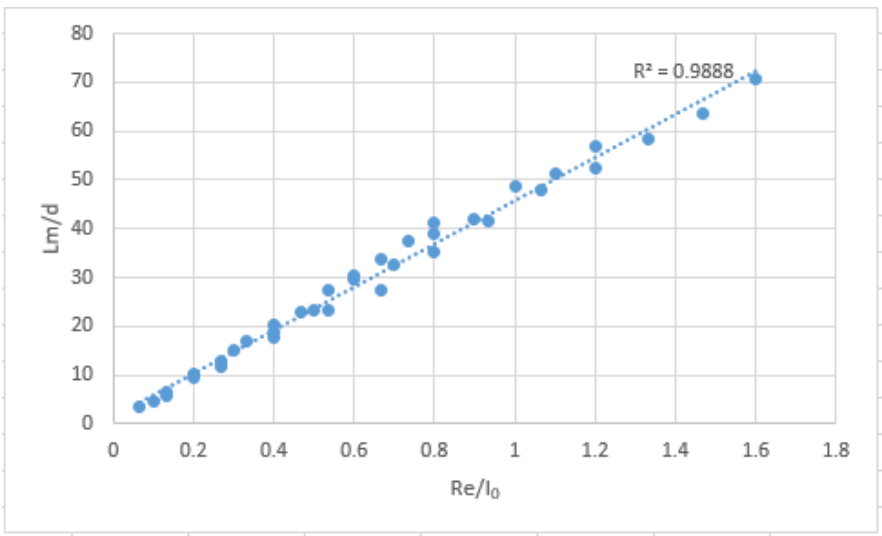

Figure 3.15. Distribution of Magnetic Entrance Length for Different Reynolds Numbers and non-dimensional electric current

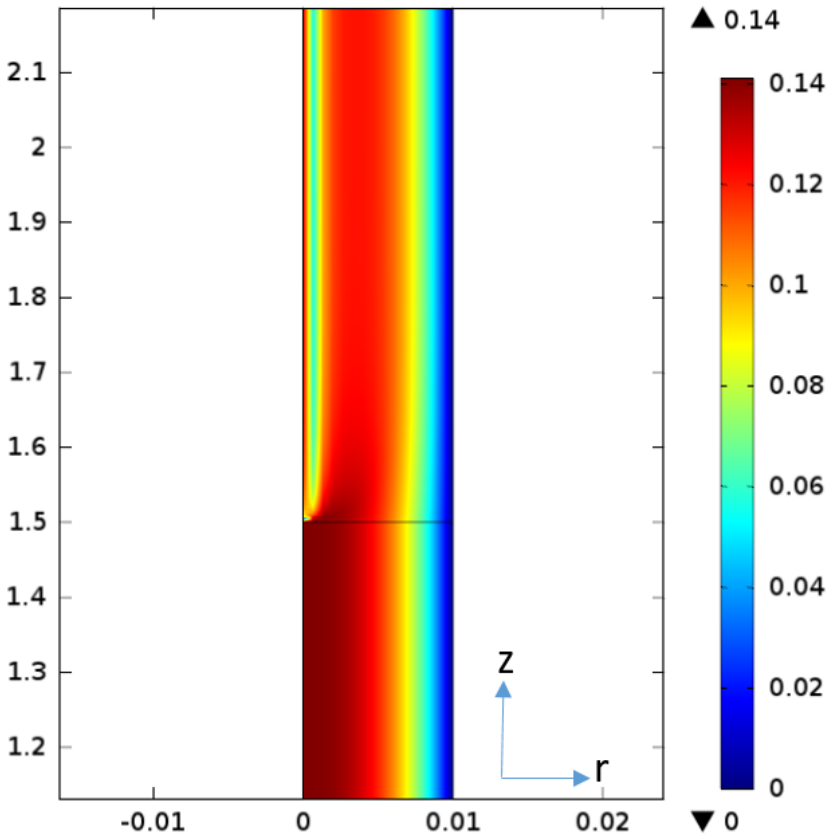

Figure 3.16. Velocity Magnitude Contour Plot for $Re = 200$, $n = 0.6$ and $I_0 = 150$

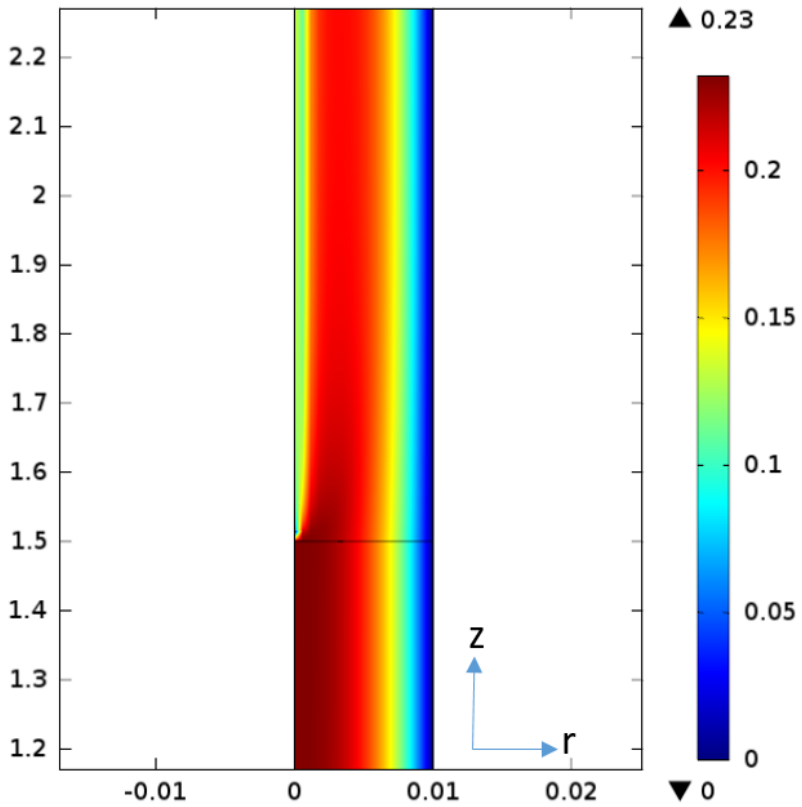

Figure 3.17. Velocity Magnitude Contour Plot for $Re = 400$, $n = 0.6$ and $I_0 = 150$

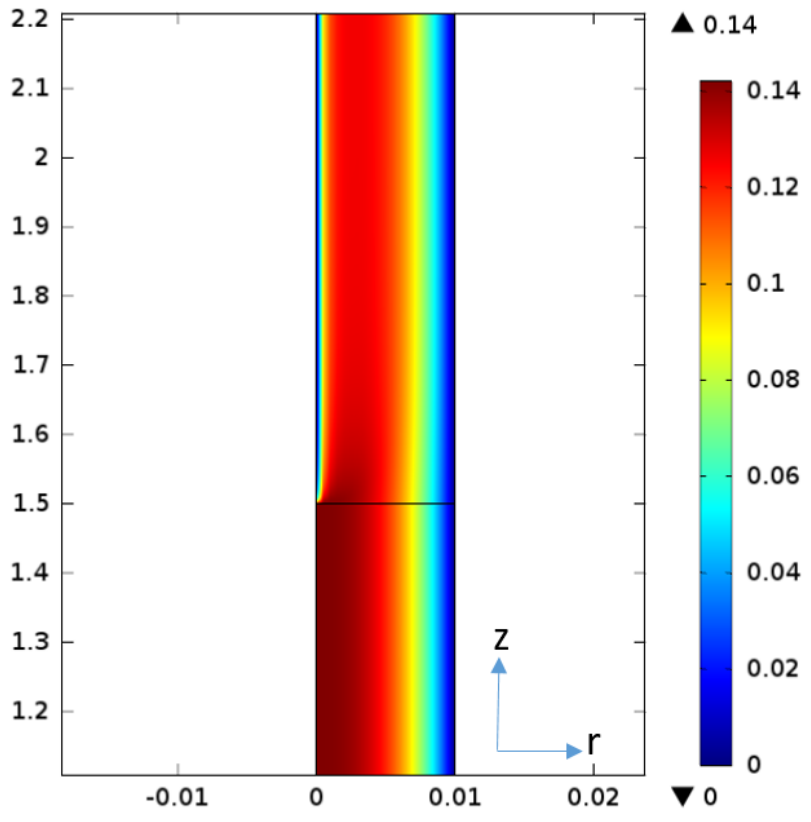

Figure 3.18. Velocity Magnitude Contour Plot for $Re = 200$, $n = 0.6$ and $I_0 = 100$

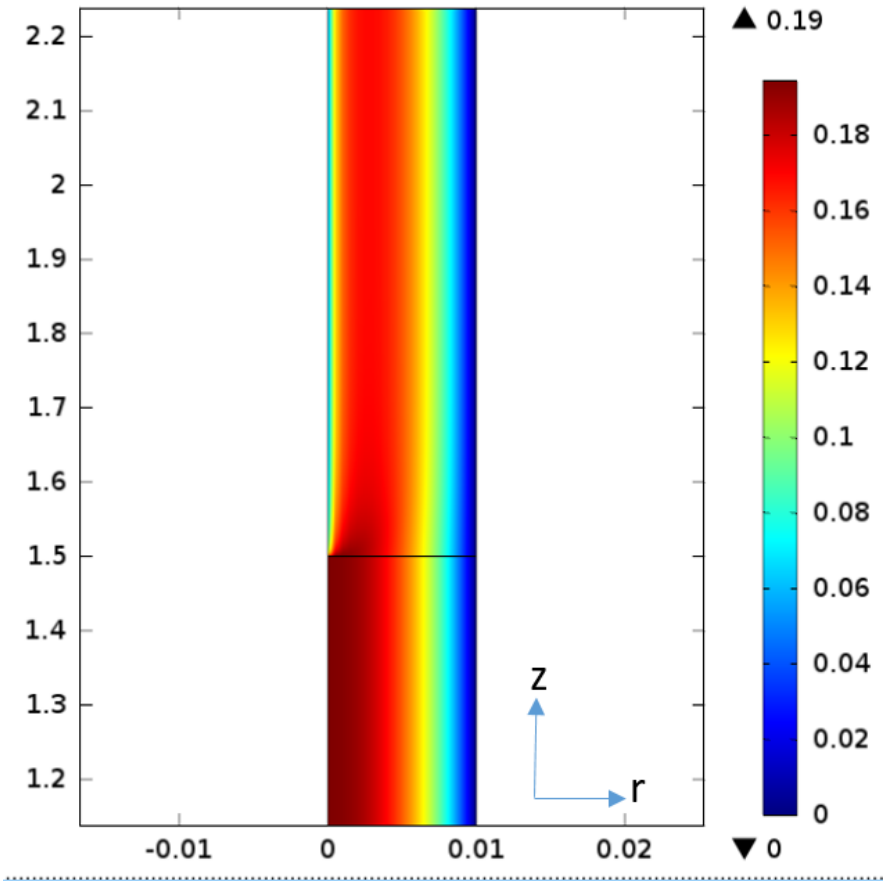

Figure 3.19. Velocity Magnitude Contour Plot for $Re = 200$, $n = 0.8$ and $I_0 = 150$

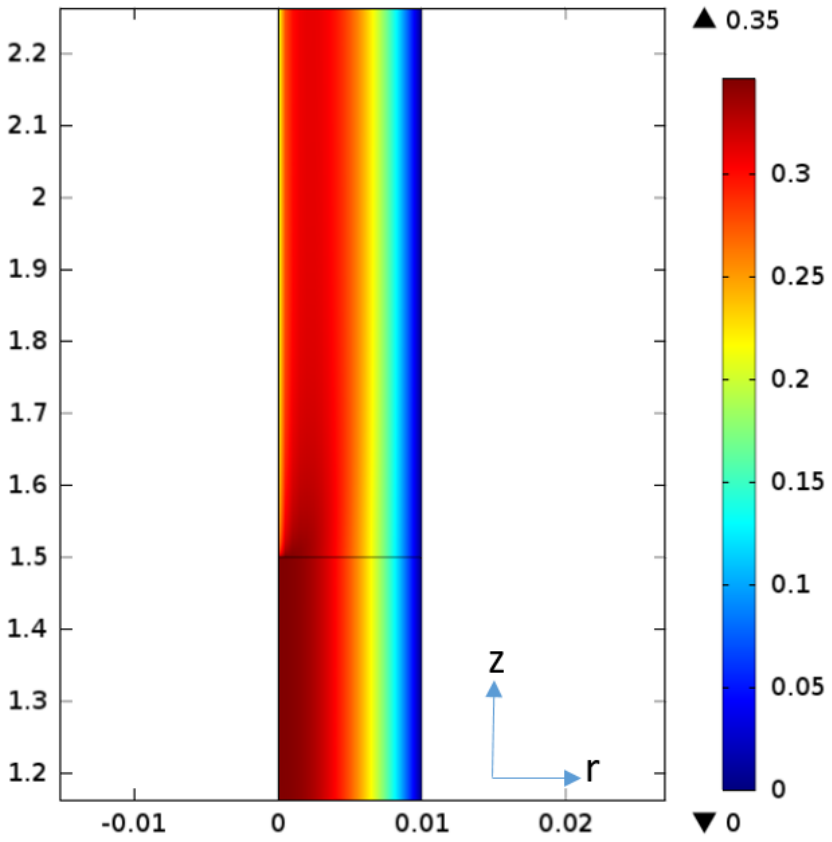

Figure 3.20. Velocity Magnitude Contour Plot for $Re = 400$, $n = 0.8$ and $I_0 = 150$

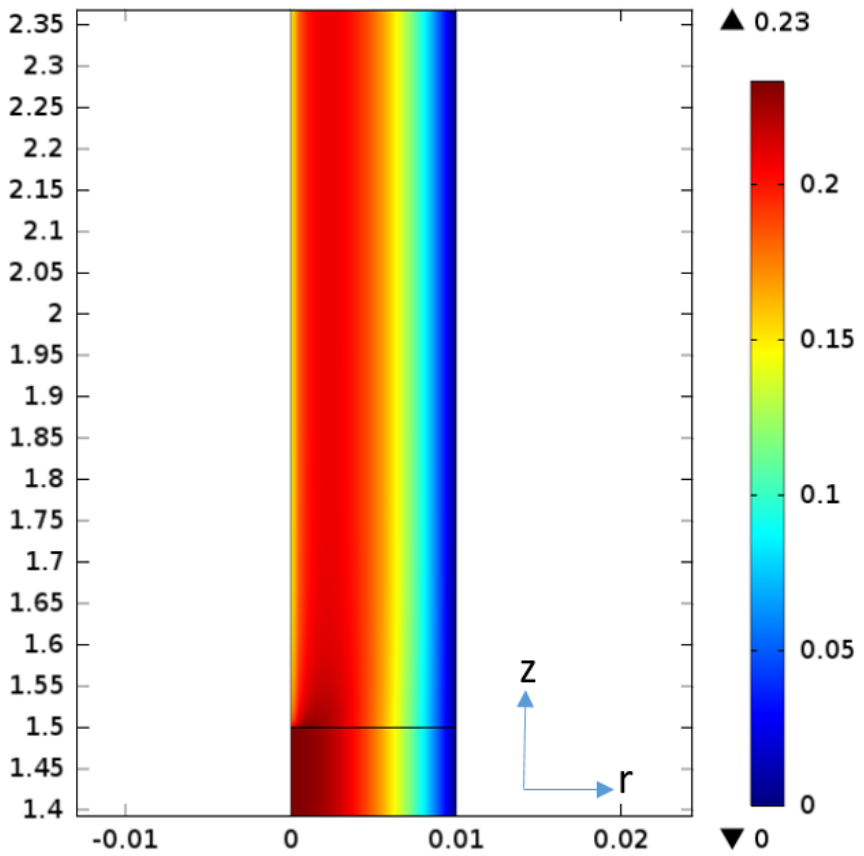

Figure 3.21. Velocity Magnitude Contour Plot for $Re = 200$, $n = 0.9$ and $I_0 = 150$

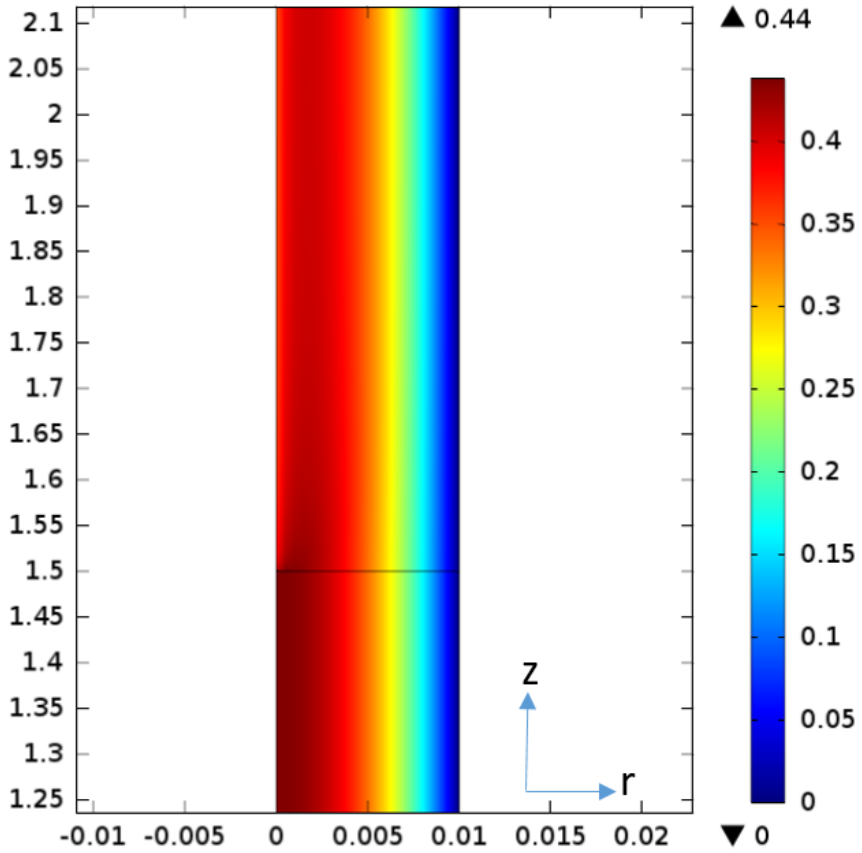

Figure 3.22. Velocity Magnitude Contour Plot for $Re = 400$, $n = 0.9$ and $I_0 = 150$

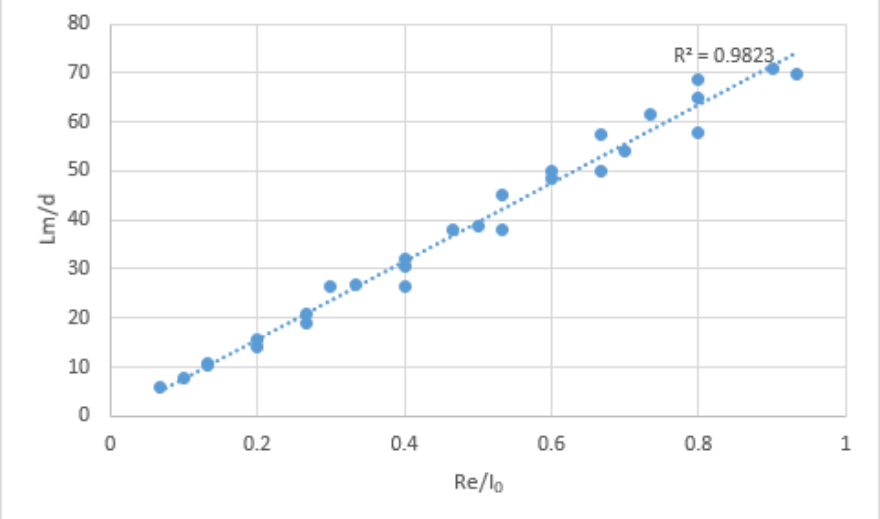

Figure 3.23. Distribution of Magnetic Entrance Length for Different Reynolds Numbers and non-dimensional current for $n = 0.6$

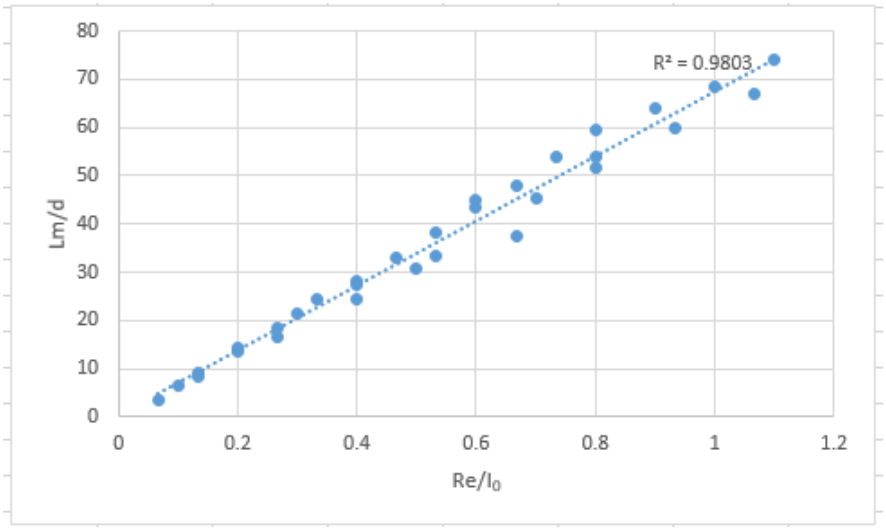

Figure 3.24. Distribution of Magnetic Entrance Length for Different Reynolds Numbers and non-dimensional current for $n = 0.7$

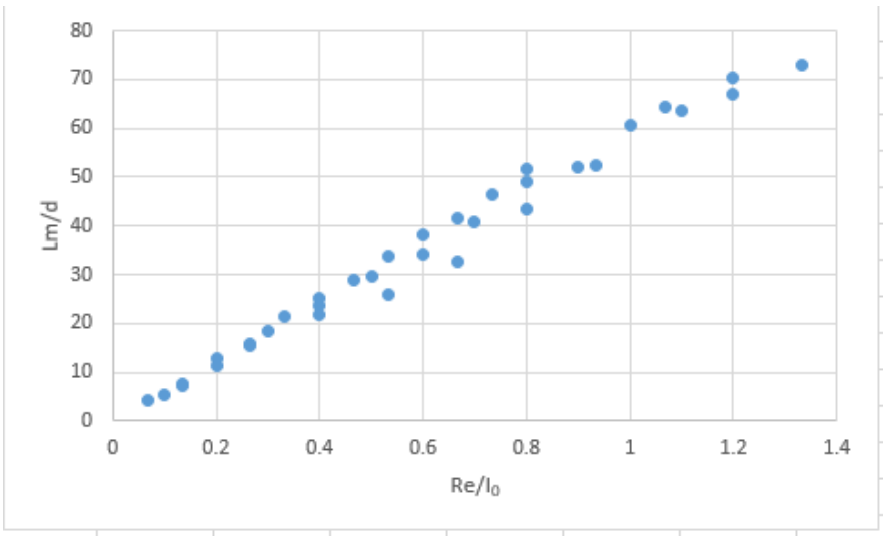

Figure 3.25. Distribution of Magnetic Entrance Length for Different Reynolds Numbers and non-dimensional current for $n = 0.8$

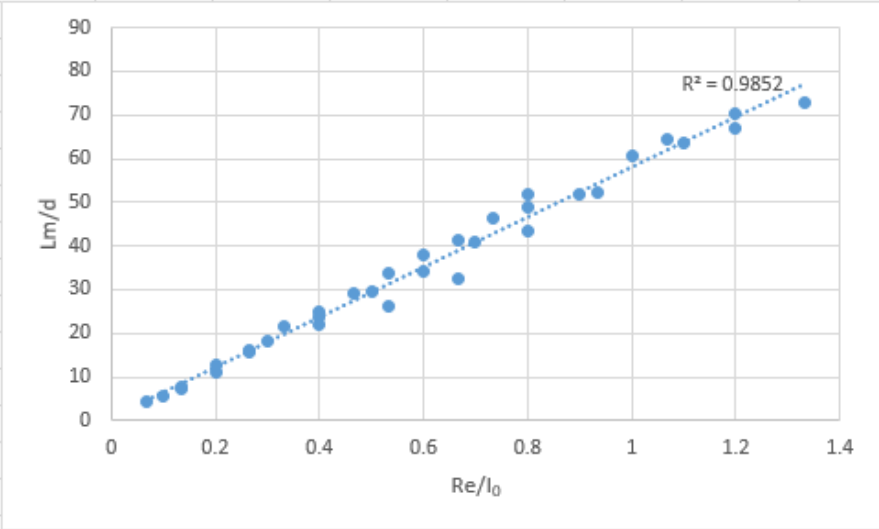

Figure 3.26. Distribution of Magnetic Entrance Length for Different Reynolds Numbers and non-dimensional current for $n = 0.9$

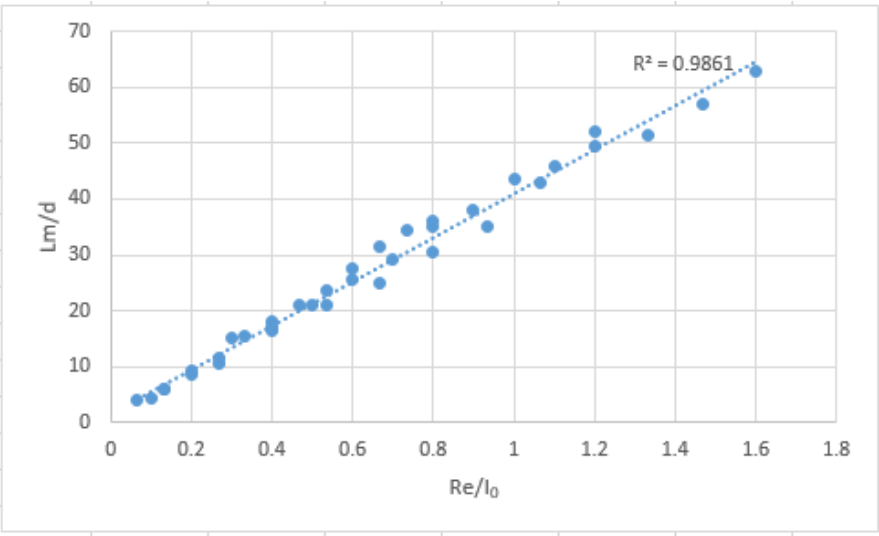

Figure 3.27. Distribution of Magnetic Entrance Length for Different Reynolds Numbers and non-dimensional current for $n = 1.1$

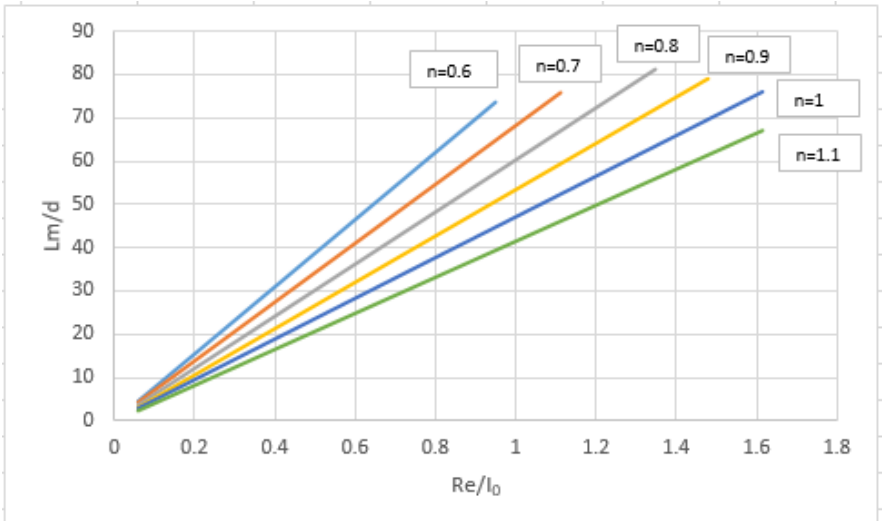

Figure 3.28. Distribution of Magnetic Entrance Length for Different Reynolds Numbers and non-dimensional current for all power law indices and Magnetic Flux Values

Figures from 3.18 to 3.22 reveal the velocity magnitude contour plots for power law ferro fluids for different power law indices, Reynolds numbers and non-dimensional currents. Similar to Newtonian ferro fluid modelling the results are directly proportional with the Reynolds number. With increasing Reynolds number the magnetic entrance length L_m also increases and it takes the ferro fluid a larger distance to develop the velocity profile fully. Therefore the velocity magnitude contour plot for power law index 0.6, Reynolds Number 200 for non-dimensional current of 150 reveals a more visible color change than the contour plot for power law index 0.6, Reynolds Number 400 for non-dimensional electric current of 75.

The results reveal that for shear thinning ferro fluids, where the power law index is smaller than one, the magnetic entrance length L_m is inversely proportional with the power law index of the ferro fluid and with increasing n leads to a decrease in the magnetic entrance length. The more Newtonian the fluid behaves, the sooner the velocity profile develops in the pipe. Therefore the velocity magnitude contour plot

for power law index 0.6, Reynolds Number 200 for a non-dimensional electric current of 150 reveals a more visible color change than the contour plot for power law index 0.9, Reynolds Number 200 for a non-dimensional electric current of 100. For shear thickening ferro fluids, where the power law index is larger than one, no difference is observed and the results revealed an inverse relationship between the power law index and the magnetic entrance length too.

Similar to the Newtonian ferro fluid modelling case a linear relationship between the magnetic entrance length, Reynolds number, power law index and non-dimensional current is observed. Figures from 3.23 to 3.28 reveal the distribution of the magnetic entrance length data for each power law index. Results revealed linear plots similar to Newtonian fluid case. The magnetic entrance length equation for the Newtonian fluid case can be modified to determine the effect of the power law index on magnetic entrance length. Equation (3.9) gives the generalized magnetic entrance length formula for both Newtonian and non-Newtonian fluids as:

$$\frac{L_m}{d} = 0.1637 \quad 0.325^n \quad \frac{Re}{I_0} \tag{3.8}$$

where n is the power law index of the ferro fluid. If it is taken as 1 then it is a Newtonian fluid. For each power law index the entrance length, Reynolds number and the non-dimensional current are linearly proportional and the power law index shifts the distribution line.

3.1.3. Friction Factor for Newtonian Ferro Fluid

As it is mentioned before friction is the second parameter studied in this work for both Newtonian and power law ferro fluid. First the analyses are conducted for Newtonian ferro fluid. Equation (3.5) reveals the rate of deformation for two dimensional axi-symmetric pipe flow and Equation (3.6) reveals the friction factor. Combining both of these equations the friction factor for Newtonian fluid flow in a two dimensional axis-

symmetric pipe is given as:

$$c_f = \frac{\mu \frac{\partial w}{\partial r}}{0.5 \rho U_\infty^2} \tag{3.9}$$

Equation (3.6) is also known as the Fanning friction factor. For a laminar circular pipe flow the Fanning friction factor is also given as:

$$c_f = \frac{16}{Re} \tag{3.10}$$

In the analyses, when the fully developed fluid enters to the magnetic region of the pipe a similar process takes place. Due to the magnetic effects the velocity profile undergoes a change and re-develops. During this redevelopment the friction factor value also redevelops itself before reaching to its constant value. Figure 3.29 shows the change of the friction factor in the magnetic region of the pipe for Reynolds number of 100 and for non-dimensional current of $I_0 = 150$.

The same definition of the friction factor is used for the magnetic region of the pipe as well. Results revealed that with increasing Reynolds number the friction factor is less affected in the magnetic region of the pipe. Figure 3.30 shows the change of the friction factor in the magnetic region of the pipe for Reynolds number 400 and for non-dimensional current of $I_0 = 150$. When Figures 3.29 and 3.30 are compared with each other it can be seen that under the same magnetic effects with increasing Reynolds number the effect of the induced magnetic field on friction factor decreases.

Results also revealed that the friction factor and the non-dimensional electric current are directly proportional. Increasing non-dimensional electric current brings the stabilized friction factor value to a larger value. Comparing Figures 3.28 and 3.31 with each other the direct proportionality of the magnetic effects and the friction factor can be seen. The results of the friction factor is determined for Reynolds numbers from 100 to 1200 under non-dimensional currents of $I_0 = 75$, $I_0 = 100$ and $I_0 = 150$

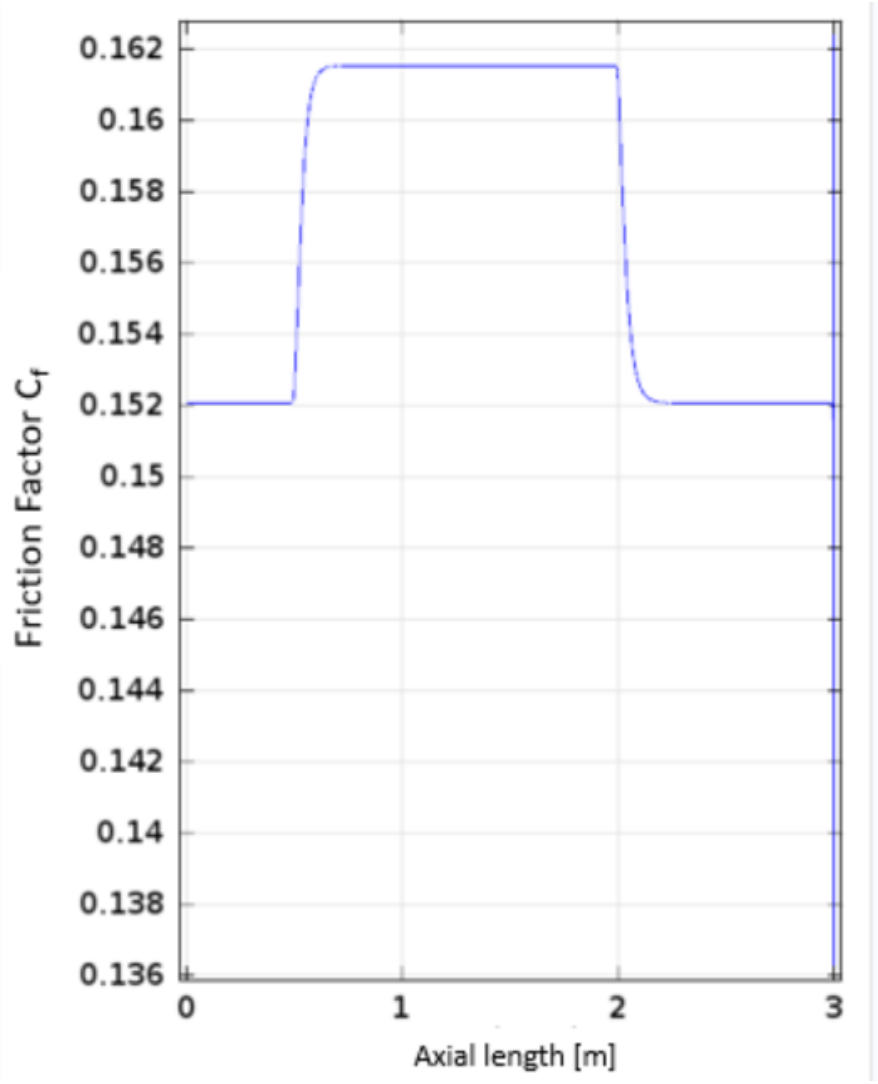

Figure 3.29. Friction factor along the pipe at $Re = 200$ and $I_0 = 150$

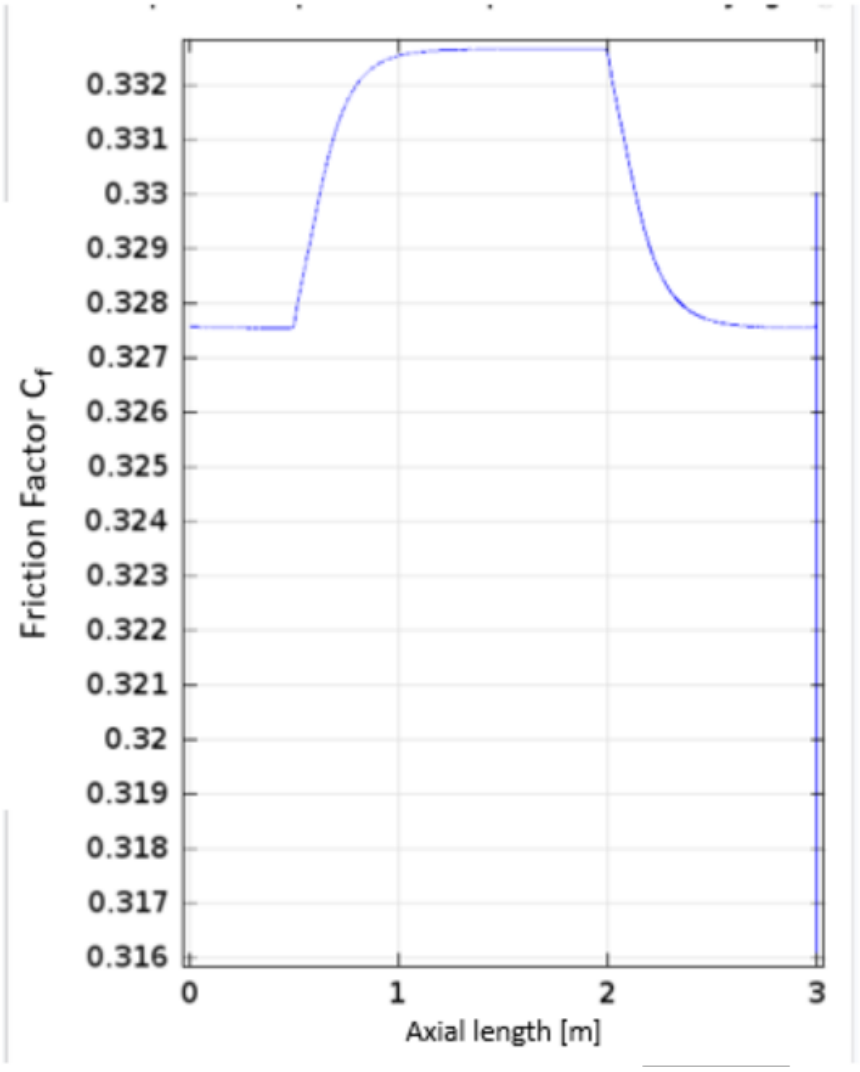

Figure 3.30. Friction factor along the pipe at $Re = 400$ and $I_0 = 150$

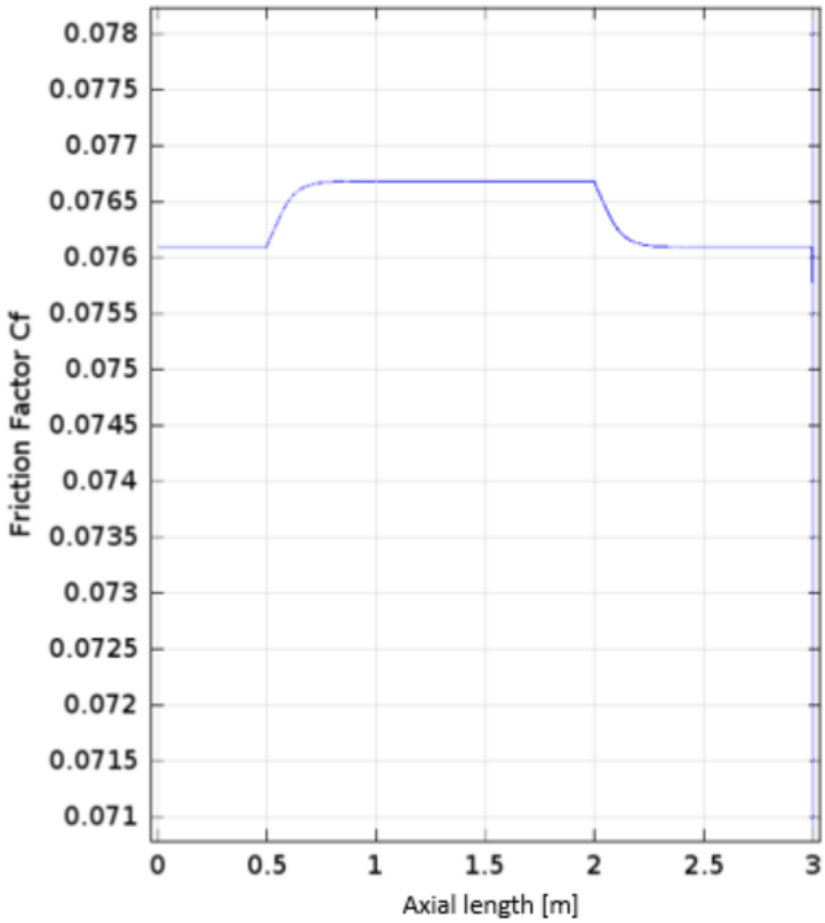

Figure 3.31. Friction factor along the pipe at $Re = 200$ and $I_0 = 75$

T. Figure 3.32 reveals the distribution of the friction coefficient Reynolds number and non-dimensional current for the Newtonian ferro fluid. Results are plotted for power law index $n = 1$ for the given non-dimensional currents. The friction factor is given as:

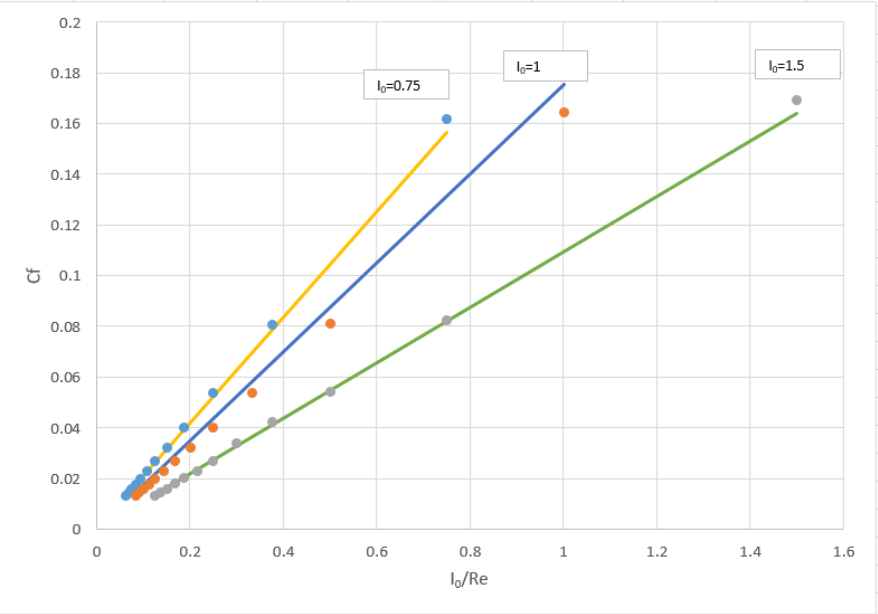

Figure 3.32. Friction Factor Values for $I_0 = 150$, $I_0 = 100$ and $I_0 = 75$

$$C_f = (-0.13243\frac{I_0}{100} + 0.308)\frac{I_0}{Re} \tag{3.11}$$

X axis represents the ratio of the Reynolds number to non-dimensional current. Just like the magnetic entrance length, compared to Malekzadeh [5]'s results a similar relationship observed and the trend is the same. With increasing magnetic effects the value of the friction factor increases. The difference is that Malekzadeh [5] uses electrically conducting fluid and the fluid in this study is ferro fluid therefore the trends are the same but values differ. In addition to this Weier *et al.* [10] also revealed an increasing friction factor with increasing magnetic field. If one of the curves is taken as a reference it can be seen that the non-dimensional current shifts the friction factor curve and is directly proportional with the friction factor. On the other hand Reynolds

number does not create a curve shift but affects the value of the friction factor along the curve in an inverse proportional way.

3.1.4. Friction Factor for Power Law Ferro Fluid

In order to study the effect of the induced magnetic field on friction factor for non- Newtonian ferro fluid the analyses are conducted for power law indices of $n = 0.6, 0.7, 0.8, 0.9, 1.1$ and 1.2 for power law Reynolds numbers from 100 to 1200. Similar to the Newtonian ferro fluid case, the power law ferro fluid develops itself and the friction factor converges to a constant value. This is related to the development of the velocity profile of the ferro fluid. When the power law ferro fluid enters to the magnetic region of the pipe the velocity profile redevelops and so does the friction factor. Similar to the case of the Newtonian fero fluid the friction factor value starts to increase and converges to a certain value along the magnetic region of the pipe.

Figure 3.33 reveals the friction factor value along the pipe for power law index $n = 0.6$, at $I_0 = 150$ for $Re = 100$. It reveals the effect of the induced magnetic field when the power law ferro fluid enters to the magnetic portion of the pipe. The induced magnetic field increases the value of the friction factor along the pipe.

Similar to the Newtonian ferro fluid modeling, the friction factor and the induced magnetic field are directly proportional. Figure 3.34 reveals the friction factor value along the pipe for power law index $n = 0.6$, at $I_0 = 75$ for $Re = 100$. Comparing Figure 3.33 with Figure 3.34 it can be seen that the induced magnetic field is directly proportional with the friction factor for power law ferro fluid as well.

Similar to the Newtonian ferro fluid modeling, the friction factor and the Reynolds number are inversely proportional. With increasing Reynolds number the effect of the induced magnetic field on the friction factor decreases. As the ferro fluid enters to the magnetic portion of the pipe, the friction factor increase becomes smaller with increasing Reynolds number. Figure 3.34 reveals the friction factor value along the pipe for power law index $n = 0.6$, at $I_0 = 150$ for $Re = 100$. Comparing Figure 3.34

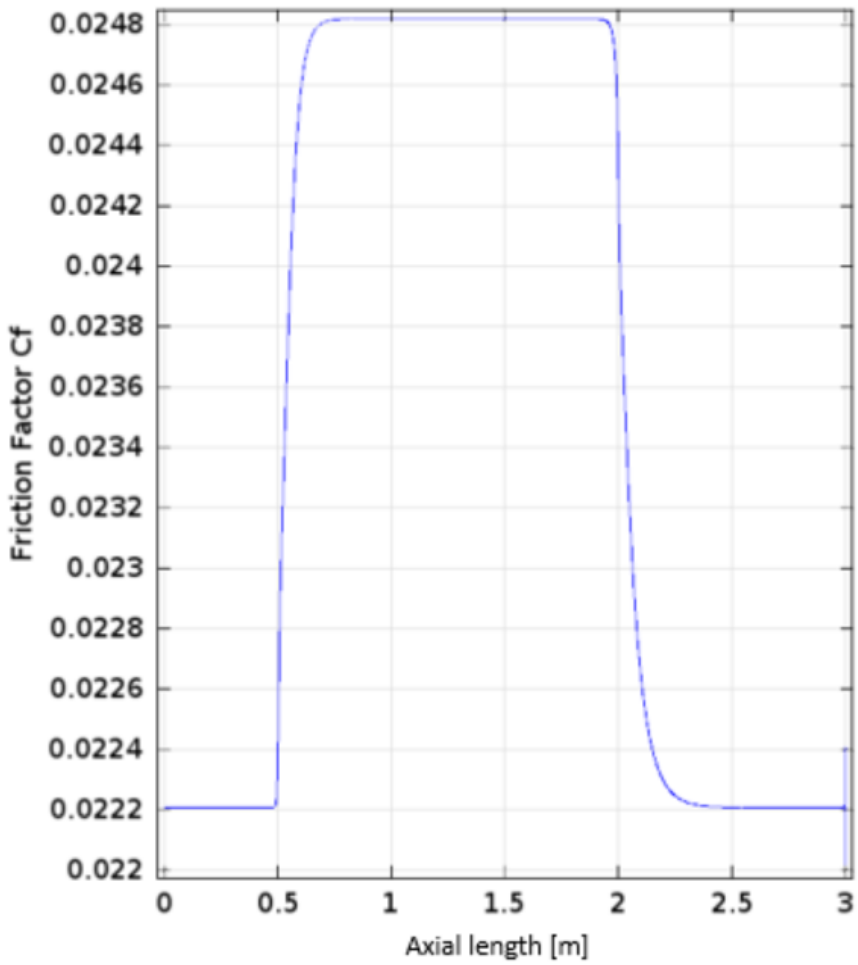

Figure 3.33. Friction Factor Along the Pipe at $I_0 = 150$ for $Re = 100$

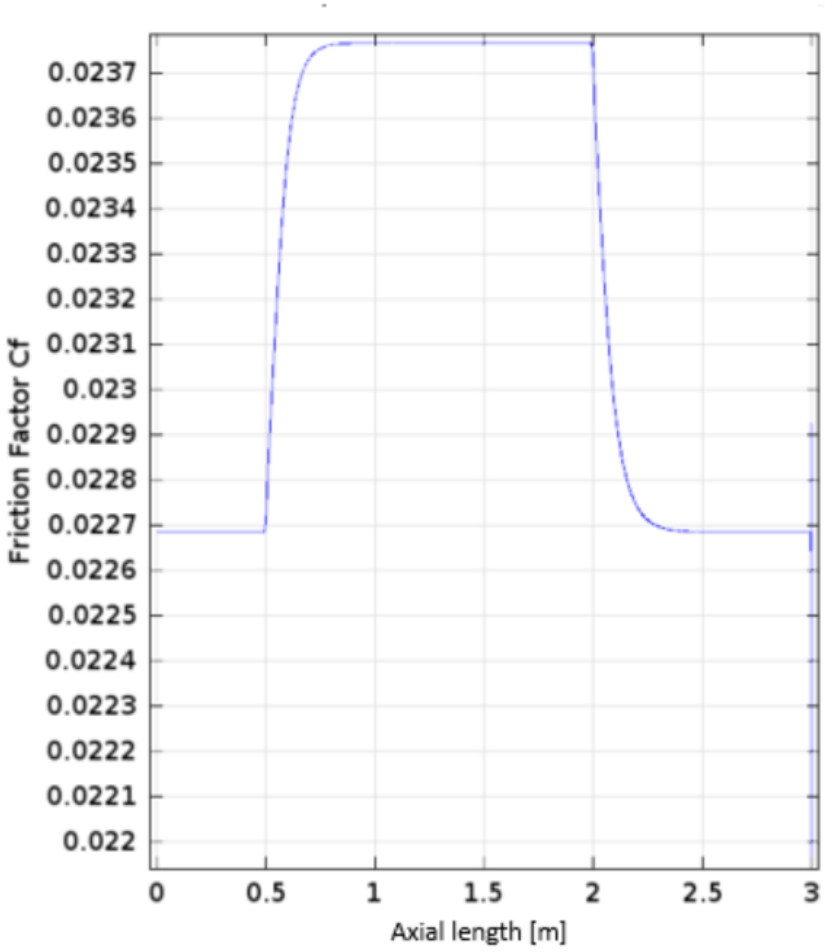

Figure 3.34. Friction Factor Along the Pipe at $I_0 = 75$ for $Re = 100$

with 3.32 the decreasing effect of the Reynolds number on friction factor in the presence of an induced magnetic field for a power law ferro fluid can be seen.

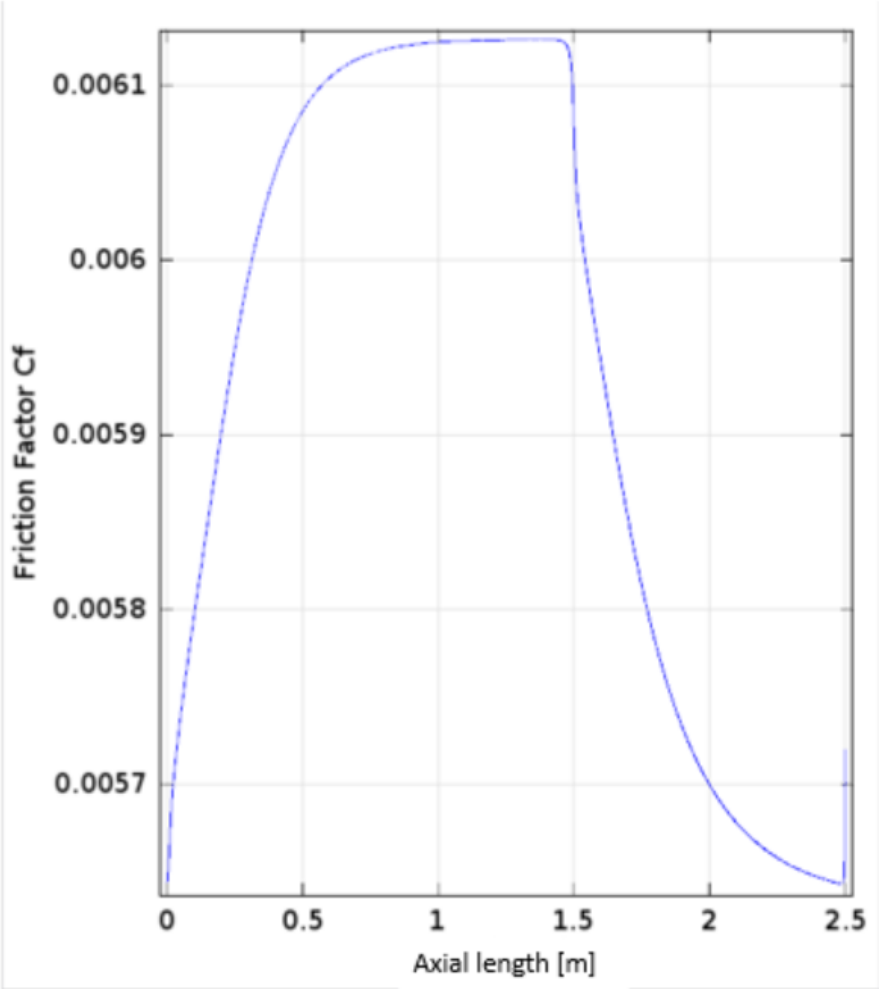

Figure 3.35. Friction Factor Along the Pipe at $I_0 = 75$ for $Re = 100$

In the presence of a constant induced magnetic field the power law index n has an increasing effect on the friction factor. Figure 3.39 and 3.40 reveal the friction factor value along the pipe for power law index $n = 0.9$ and $n = 1.1$ respectively at $I_0 = 150$ for $Re = 100$. Comparing Figures 3.39 and 3.40 with 3.33 it can be seen that the power law index and the friction factor are directly proportional. For the same Reynolds number in the presence of the same magnetic field the friction factor increases with power law index. However this is not coming from the magnitude of the induced magnetic field but from the nature of the ferro fluid itself. With increasing shear thickening behavior

higher viscous effects near the wall are seen and this results in higher shear rates. As a result a higher friction factor is observed for shear thickening fluids. Although the value of the friction factor increases with the power law index the percent increase of the magnetic field with the power law index are inversely proportional. This means that the induced magnetic field has a larger effect on the ferro fluid as it behaves more shear thinning. Equation (3.12) and (3.13) combine the effect of the power law index with Equation (3.11) for $n \leq 1$ and $n > 1$ respectively, which is the friction factor for the Newtonian ferro fluid, and gives a generalized relationship as:

$$C_f = (-0.13243\frac{I_0}{100} + 0.308)(2.1404n - 1.1358)\frac{I_0}{Re} \tag{3.12}$$

$$C_f = (-0.13243\frac{I_0}{100} + 0.308)(0.0187n + 0.1644)\frac{I_0}{Re} \tag{3.13}$$

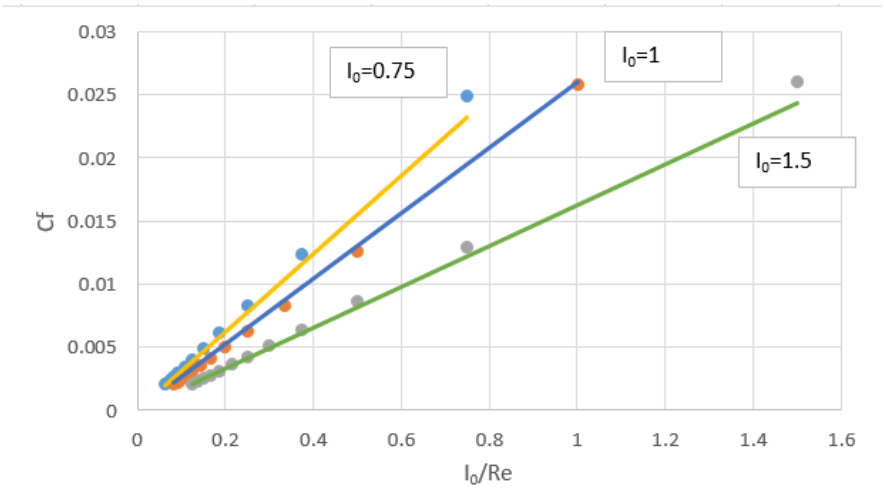

Figure 3.36. Cf vs N/Re for $n = 0.6$ at $I_0 = 150$ $I_0 = 100$ $I_0 = 75$

It is important to mention that the effect of n decreases, which is seen in the slope contributed by power law index. This is because as the fluid becomes shear thickening viscous effects on the wall increase significantly and as it becomes shear thickening the

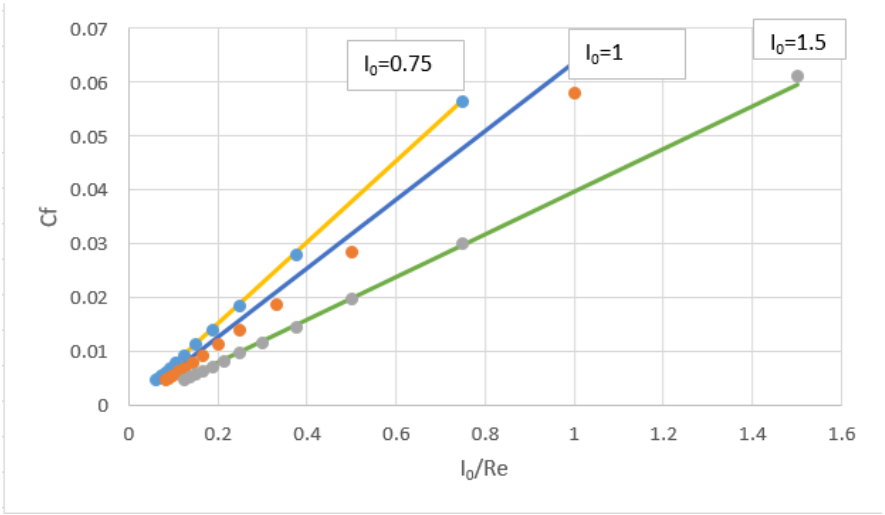

Figure 3.37. Cf vs N/Re for $n = 0.7$ at $I_0 = 150$ $I_0 = 100$ $I_0 = 75$

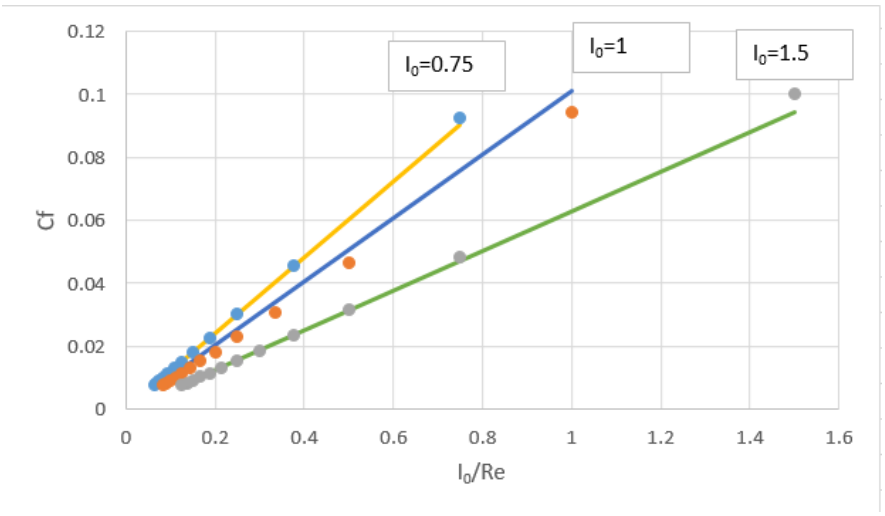

Figure 3.38. Cf vs N/Re for $n = 0.8$ at $I_0 = 150$ $I_0 = 100$ $I_0 = 75$

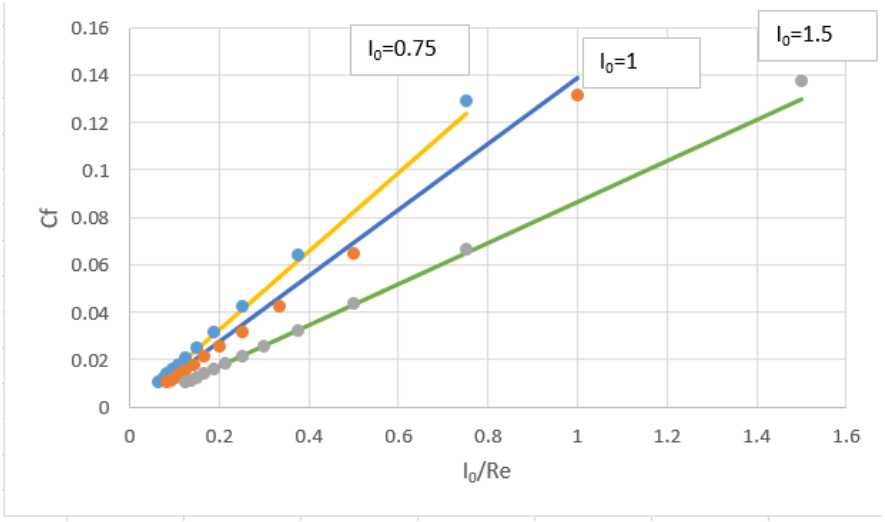

Figure 3.39. Cf vs N/Re for $n = 0.9$ at $I_0 = 150$ $I_0 = 100$ $I_0 = 75$

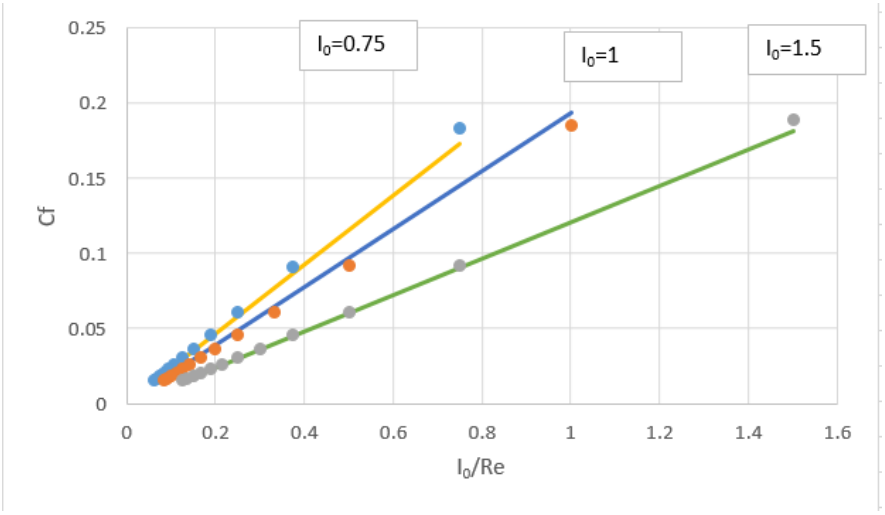

Figure 3.40. Cf vs N/Re for $n = 1.1$ at $I_0 = 150$ $I_0 = 100$ $I_0 = 75$

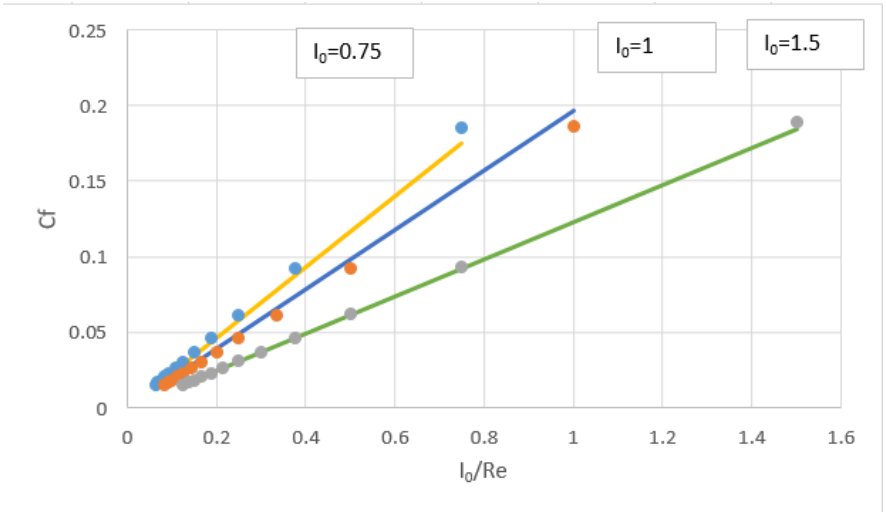

Figure 3.41. Cf vs N/Re for $n = 1.2$ at $I_0 = 150$ $I_0 = 100$ $I_0 = 75$

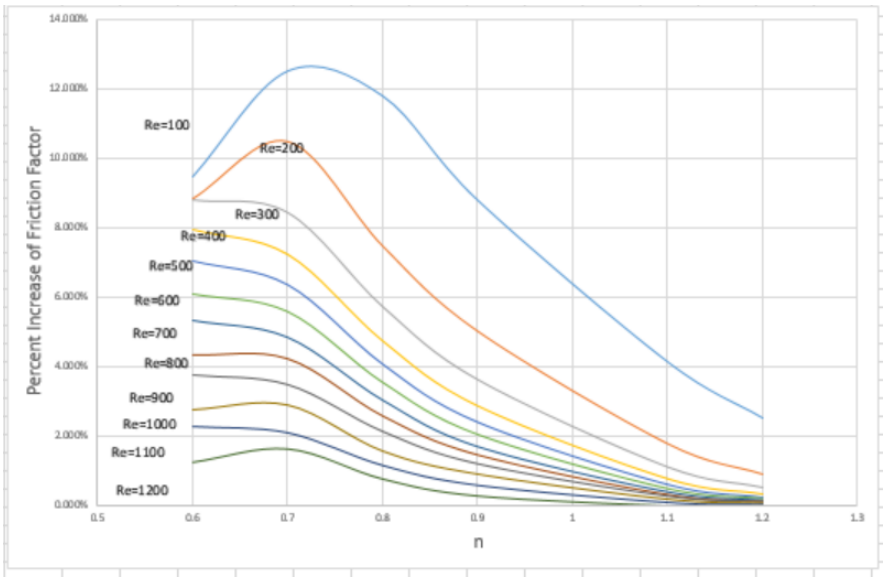

Figure 3.42. Percent Increase of Friction Factor for Power Law Indices at Constant Reynolds Numbers

viscous effects increase but do not increase as high as shear thinning fluid which has a larger margin of increase compared to a shear thickening fluid as the viscous effects are less dominant when the power law index is low. Figure 3.42 reveals the percent increase of the friction factor vs. the power law index for constant Reynolds numbers. Each line represent the Reynolds number from $Re = 100$ to $Re = 1200$. Results reveal that with increasing Reynolds number the percent increase of the friction factor reduces. This is because the inertia effects become more dominant than the viscous effects. However each constant Reynolds number line has a parabolic form and makes a peak at $n = 0.7$. Although the magnitude of the friction factor is higher as the ferro fluid becomes more shear thickening, the percent increase of the friction factor is higher as the fluid becomes shear thinning. As it is mentioned before the friction factor and the power law index under the constant magnetic field are inversely proportional therefore with increasing power law index larger friction factor values are observed. This is coming from the rheological behavior of the fluid itself. However Figure 3.42 shows that the percent increase is larger when the fluid becomes more shear thinning therefore it can be concluded that the magnetic field has a larger effect on the fluid as ferro fluid becomes more shear thinning but the rheological behavior of the fluid has also an impact on the parameters. Therefore a larger value of friction factor is observed as it becomes shear thickening but a larger percent increase is observed as it becomes more shear thinning. A similar phenomena is observed under the oscillating magnetic field where it is easy to develop vortices with a given oscillating magnetic field as the fluid becomes more shear thinning. This is very important to distinguish the difference between the rheological behavior of the fluid and the influence of the magnetic field and their relationship.

3.1.5. Effect of the Induced Magnetic Field on Velocity Profile for Newtonian and Power Law Index Ferro Fluid

Figures 3.43 to 3.48 reveal the comparison of the fully developed velocity profile with fully developed velocity profile under the effect of constant magnetic field for Reynolds 100, 200 and 300. Results reveal that when a constant magnetic field is

applied to a ferro fluid, the velocity profile becomes flatter compared to the case with no induced magnetic field. The effect of the induced magnetic field on the flatness of the velocity profile is inversely proportional with the Reynolds number. As it is seen in the Figures 3.43 to 3.48 the velocity curve becomes similar to the case with no induced magnetic field. When the Reynolds number is low the viscous effects become more dominant whereas with increasing Reynolds number the inertia effects become significant. Due to this the magnetic body force is more effective at low Reynolds numbers and therefore the velocity profile becomes less flatter when the Reynolds number increases. The flatness of the velocity profile, which indicates the influence of the induced magnetic field on ferro fluid, is directly proportional with the magnetic field. Figure 3.47 reveal the comparison of the velocity profiles at Reynolds 100 and 200 for the given magnetic flux values. It can be seen that the velocity profile is flatter with increasing magnetic flux density. Equation (3.1) reveals that the non-dimensional electric current is directly proportional with the magnetic flux due to this the magnetic body force increases with the magnetic field therefore the direct relationship between the velocity profile flatness and magnetic field can be easily concluded.

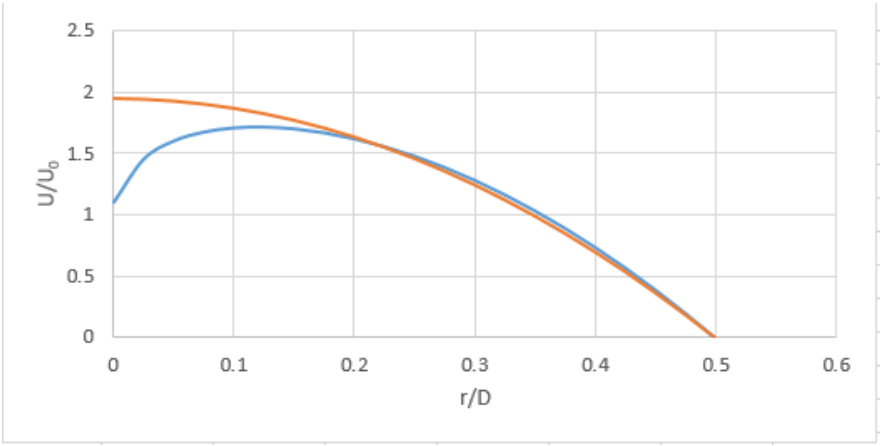

Figure 3.43. Velocity Profile Comparison at $Re = 100$ at $I_0 = 150$

The effect of the induced magnetic field on for power law ferro fluid is studied as well. Similar to the Newtonian ferro fluid case the effect of the induced magnetic field on the velocity profile is higher at low Reynolds number. As it is mentioned before this

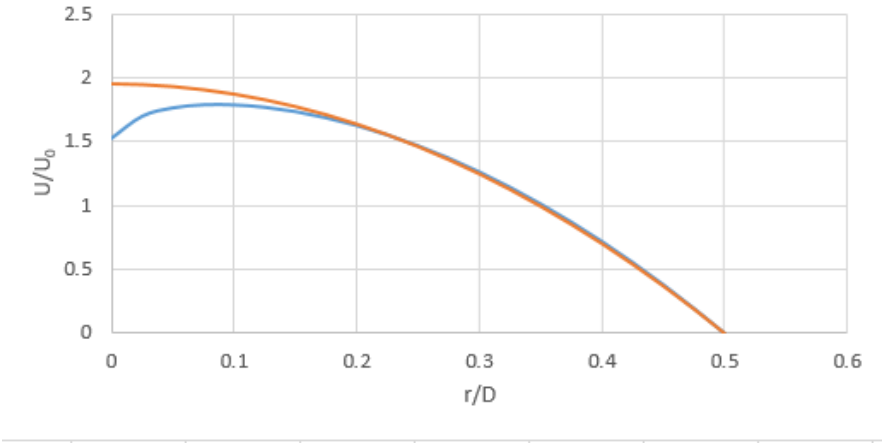

Figure 3.44. Velocity Profile Comparison at $Re = 200$ at $I_0 = 150$

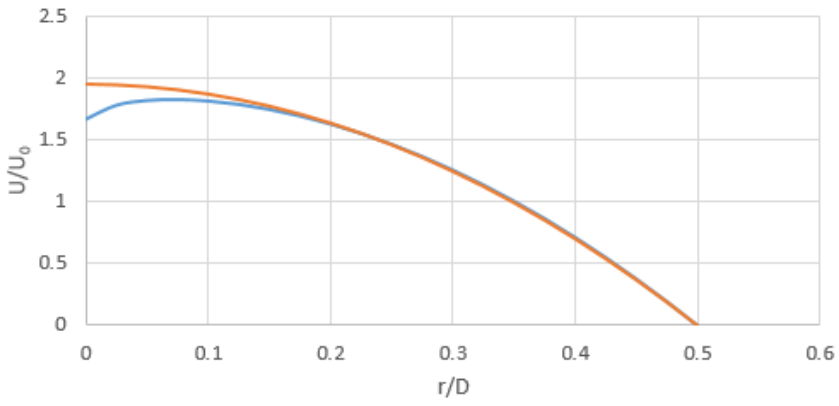

Figure 3.45. Velocity Profile Comparison at $Re = 300$ at $I_0 = 150$

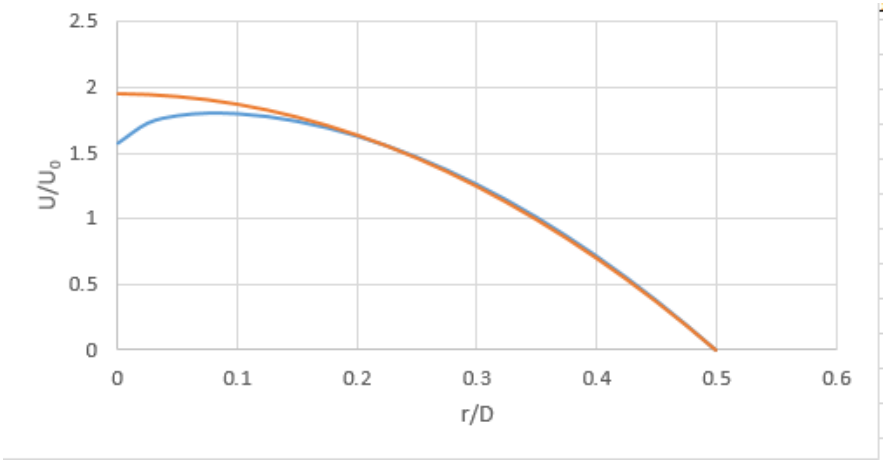

Figure 3.46. Velocity Profile Comparison at $Re = 100$ at $I_0 = 100$

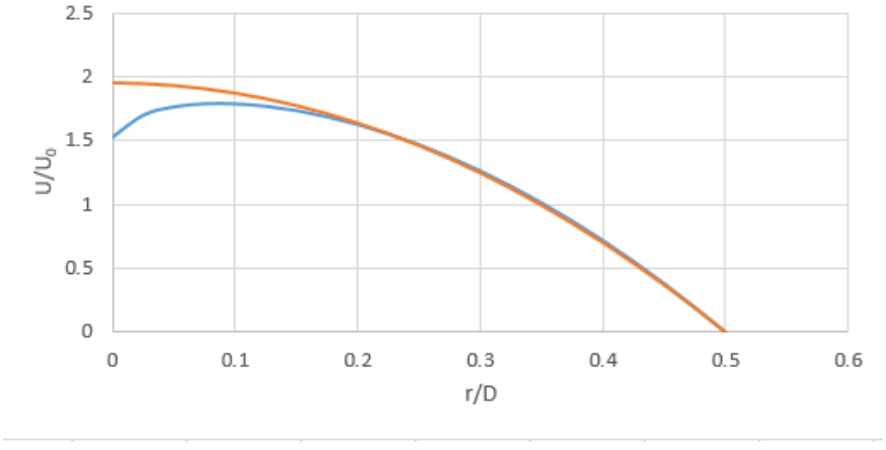

Figure 3.47. Velocity Profile Comparison at $Re = 200$ at $I_0 = 100$

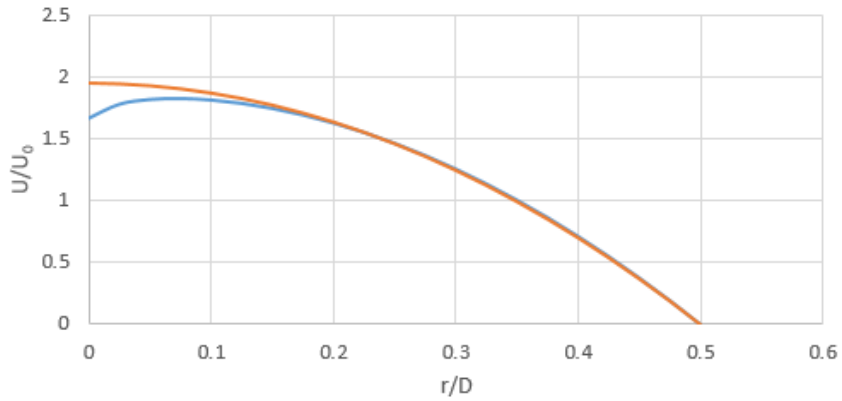

Figure 3.48. Velocity Profile Comparison at $Re = 300$ at $I_0 = 100$

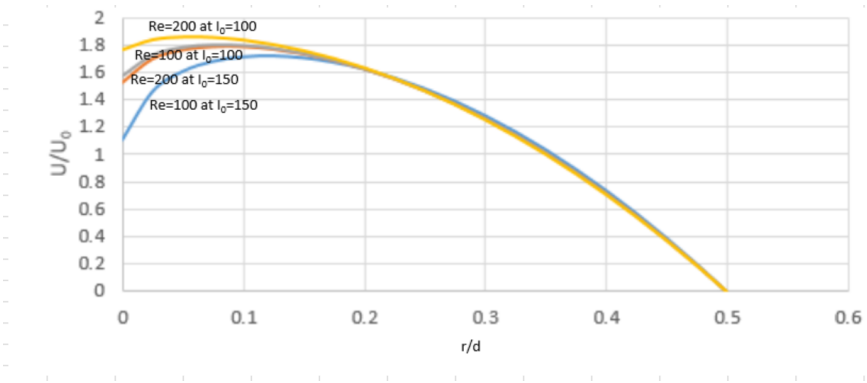

Figure 3.49. Velocity Profile Comparison for $Re = 100$ and 200 at $I_0 = 100$ and $I_0 = 150$

is due to the decreasing effect of the inertial forces with decreasing Reynolds number. With decreasing Reynolds number the velocity profile becomes flatter and this flatness indicates the effect of the magnetic force on the velocity profile.

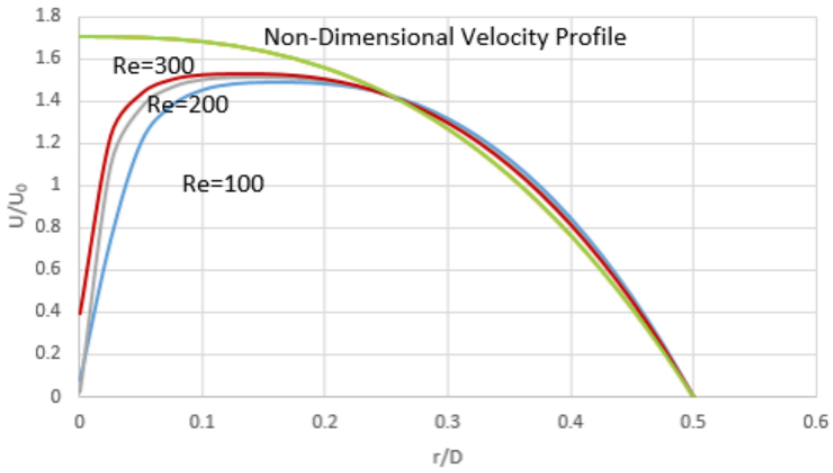

Figure 3.50. Magnetic Velocity Profile Comparison for $Re = 100$, 200 and 300 vs. Velocity Profile without applied magnetic force for n=0.6 at $I_0 = 100$

It is important to mention that the results for both Newtonian and power law ferro fluids are plotted up to Reynolds 300 as the Reynolds number increases the inertia forces start to become more effective and the influence of the induced magnetic field on velocity profile decreases. Figures from 3.48 to 3.59 reveal the non-dimensional magnetic velocity profile and the non-dimensional velocity profile without any magnetic force. As the velocity profile is non-dimensionalized with the inlet velocity U_∞ for each case, the velocity profile without any magnetic field is the same for each Reynolds number case. Results reveal the decreasing effect of the magnetic field on the velocity profile. Results also reveal that there is almost no difference between the magnetic velocity profile and the velocity profile without any applied magnetic force. In order to observe the effect of the induced magnetic field at higher Reynolds numbers the magnitude of the magnetic field should be increased. In addition, the induced magnetic field has also an increasing effect on the flatness of the velocity profile as the magnetic force is directly proportional with the induced magnetic field. Similar to the Reynolds

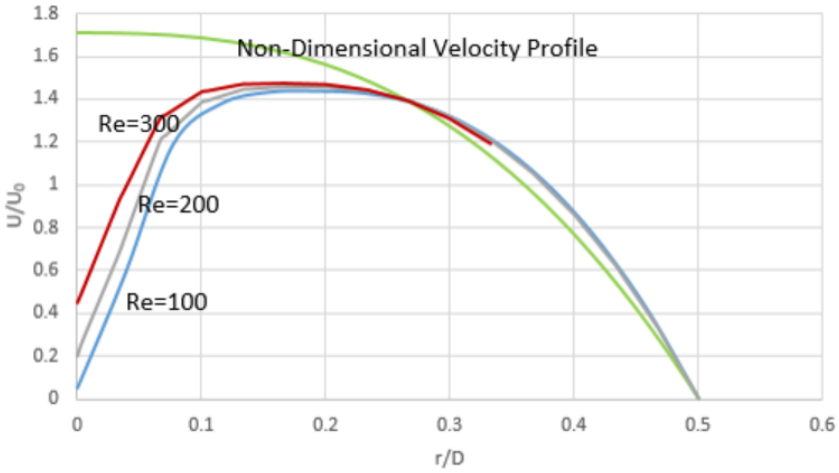

Figure 3.51. Magnetic Velocity Profile Comparison for $Re = 100$, 200 and 300 vs. Velocity Profile without applied magnetic force for n=0.6 at $I_0 = 150$.

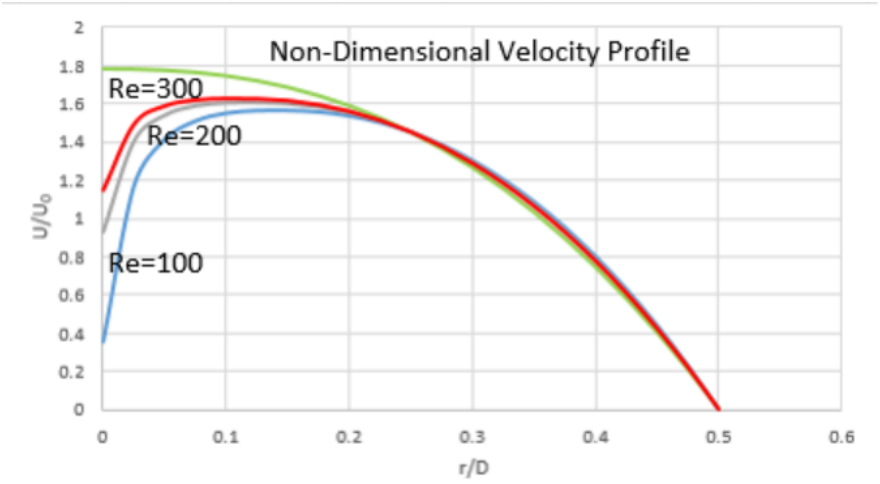

Figure 3.52. Magnetic Velocity Profile Comparison for $Re = 100$, 200 and 300 vs.Velocity Profile without applied magnetic force for n=0.7 at $I_0 = 100$.

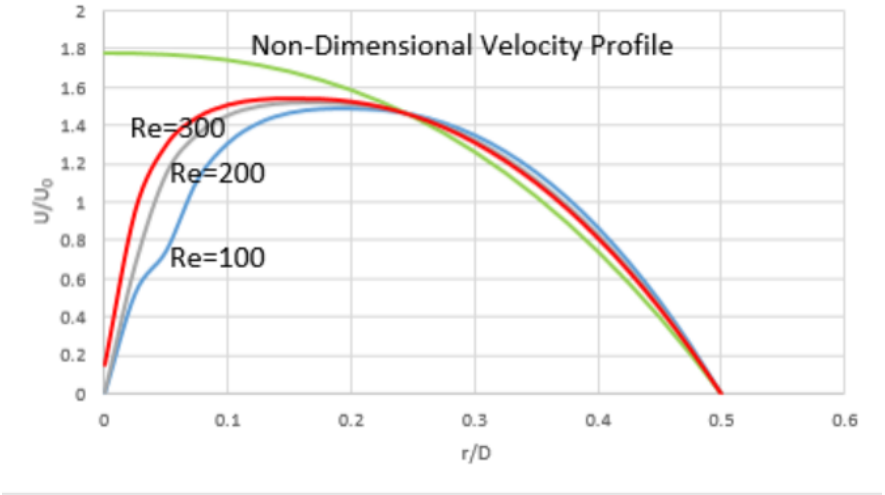

Figure 3.53. Magnetic Velocity Profile Comparison for $Re = 100$, 200 and 300 vs. Velocity Profile without applied magnetic force for n=0.7 at $I_0 = 150$.

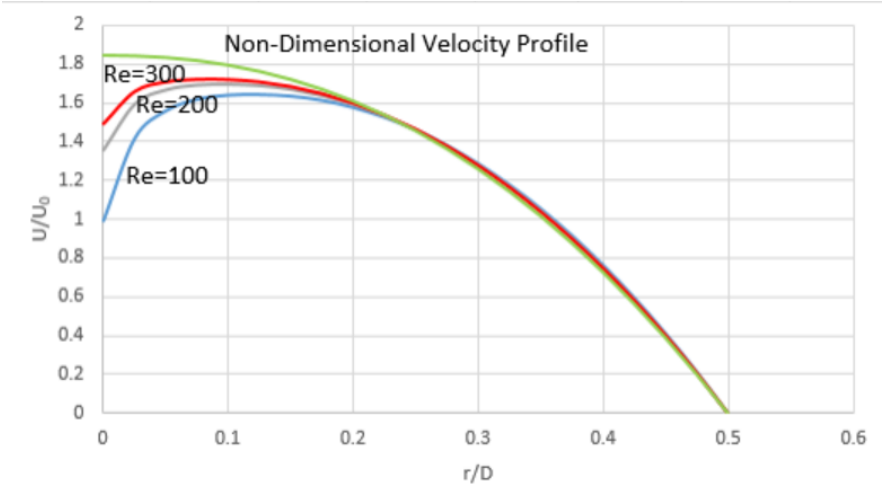

Figure 3.54. Magnetic Velocity Profile Comparison for $Re = 100$, 200 and 300 vs. Velocity Profile without applied magnetic force for n=0.8 at $I_0 = 100$.

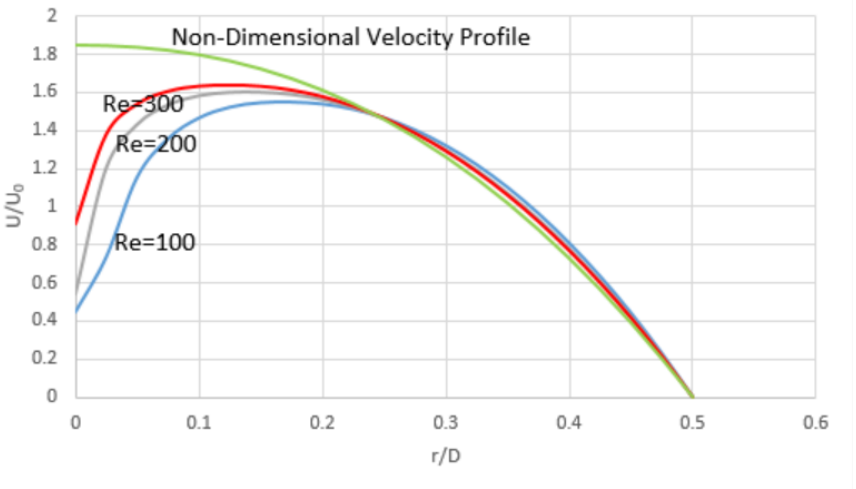

Figure 3.55. Magnetic Velocity Profile Comparison for $Re = 100$, 200 and 300 vs. Velocity Profile without applied magnetic force for n=0.8 at $I_0 = 150$.

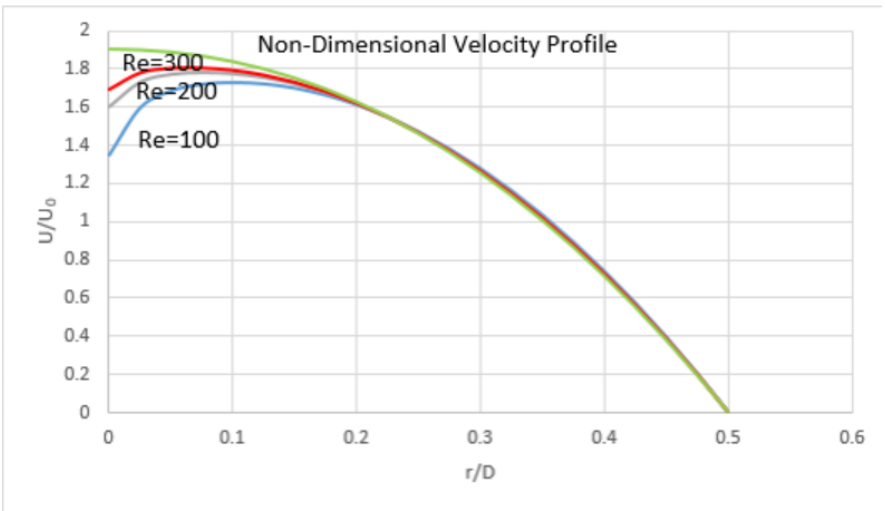

Figure 3.56. Magnetic Velocity Profile Comparison for $Re = 100$, 200 and 300 vs. Velocity Profile without applied magnetic force for n=0.9 at $I_0 = 100$.

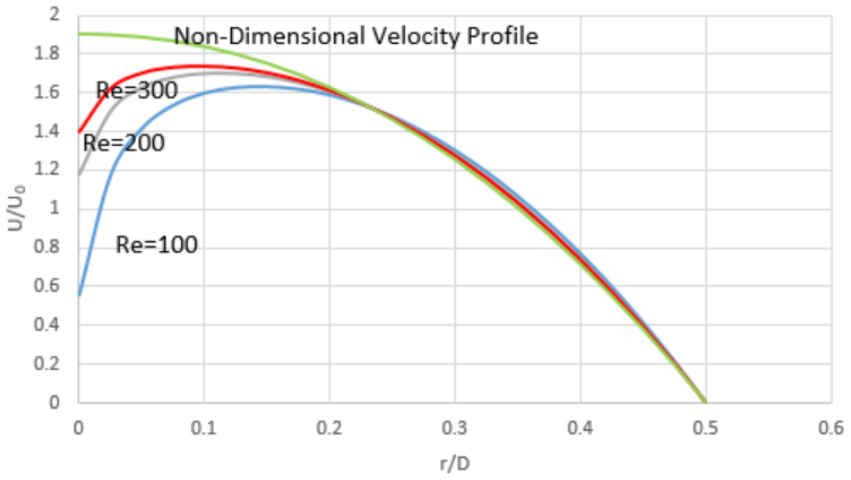

Figure 3.57. Magnetic Velocity Profile Comparison for $Re = 100$, 200 and 300 vs. Velocity Profile without applied magnetic force for n=0.9 at $I_0 = 150$.

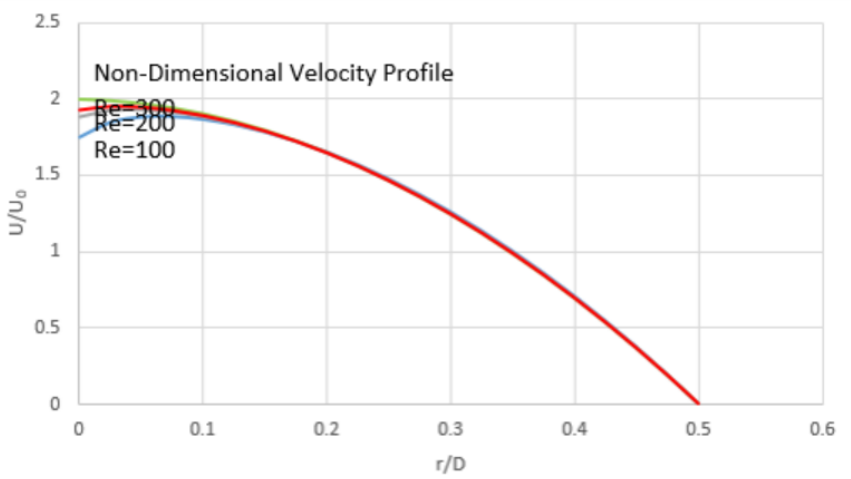

Figure 3.58. Magnetic Velocity Profile Comparison for $Re = 100$, 200 and 300 vs. Velocity Profile without applied magnetic force for n=1.1 at $I_0 = 100$.

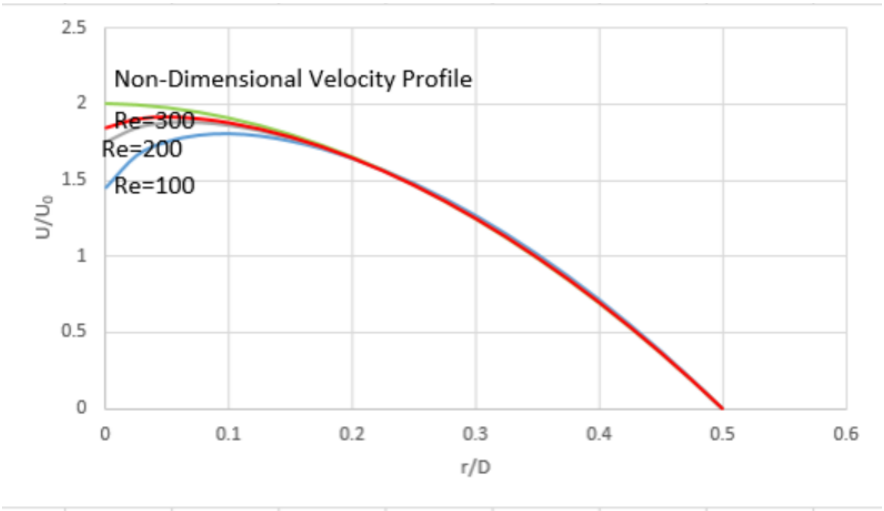

Figure 3.59. Magnetic Velocity Profile Comparison for $Re = 100$, 200 and 300 vs. Velocity Profile without applied magnetic force for n=1.1 at $I_0 = 150$.

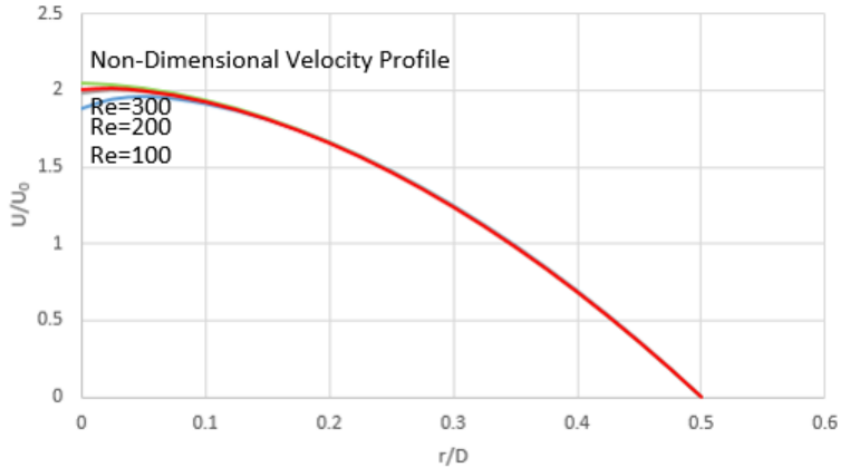

Figure 3.60. Magnetic Velocity Profile Comparison for $Re = 100$, 200 and 300 vs. Velocity Profile without applied magnetic force for n=1.2 at $I_0 = 100$.

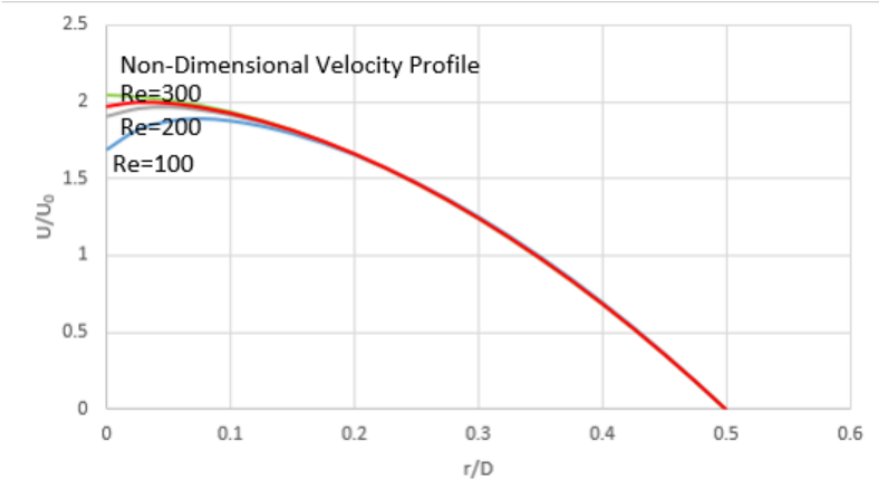

Figure 3.61. Magnetic Velocity Profile Comparison for $Re = 100$, 200 and 300 vs. Velocity Profile without applied magnetic force for n=1.2 at $I_0 = 150$.

number, in order to obtain the effect of the induced magnetic field on low magnetic field values the Reynolds number should be decreased. At low magnetic field values the magnetic velocity profile is very close to the magnetic velocity profile without applied magnetic force. Comparing the power law ferro fluid results with the Newtonian case, which is actually a power law fluid with index 1, it can be concluded that the power law index and the effect of the induced magnetic field on the velocity are inversely proportional. As the ferro fluid becomes more shear thinning the velocity becomes flatter and as the ferro fluid becomes more shear thickening the velocity becomes close to the velocity profile under no magnetic effects. The magnetic velocity profile is inversely proportional with the power law index. As the ferro fluid becomes more shear thinning the magnetic effects on the ferro fluid increase and the velocity profile becomes flatter for low power law indices. Malekzadeh [5] *et al.* also revealed that the velocity profile under magnetic effects take a flatter form for electrically conducting fluid. Although the nature of the fluid used in this study is different the trend and the behavior is the same. In addition Sheikholeslami *et al.* [7] and Weier *et al.* [10] also reveals a suppressed velocity profile which are similar to the trends observed in this study.

3.2. Oscillating Magnetic Field Cases

The second part of this work, as it is mentioned before, is conducted for a oscillating magnetic field for both Newtonian and power law ferro fluid. The induced magnetic field changes oscillating along the axis of the pipe. Equation (2.1) reveals the magnetic flux density induced by the current carrying conductor. It can be seen that the magnitude of the magnetic flux and the magnetic field depends on the radius around the conductor. If the current carrying wire is in the form of a straight line along the axis of the pipe then the value of the magnetic field along the pipe will be the same for all radii. If the current carrying conductor has a certain curvature along the pipe, then the value of the magnetic field along the axis will not be the same for all radii as the radius of the circle around the current carrying conductor will change through the axis. If the current carrying conductor follows a oscillating path then a oscillating path can be obtained along the axis of the pipe. By altering the path of that the current carrying conductor follows linearly increasing decreasing or parabolic changing magnetic fields can be created. The analyses are conducted for power law indices $n = 0.75$, $n = 0.85$, Newtonian ferro fluid $n = 1$ and for Reynolds numbers of $Re = 100$, 200 and 300. Figure 3.62 reveals an example to the distribution of the magnetic field along the magnetic portion of the pipe at $Re = 100$, for Newtonian ferro fluid at non-dimensional current of 150. It is important to mention that as the path followed by the current carrying conductor is in oscillating form, the values of the magnetic field or magnetic flux may be confusing. To avoid this the value of the current to create the magnetic field will be mentioned.

To understand the effect of the oscillating oscillating magnetic field on the ferro fluid the definition of the vorticity is crucial. Equation (3.11) defines the vorticity as:

$$curl \quad \vec{V} = 2\overrightarrow{\omega} \tag{3.14}$$

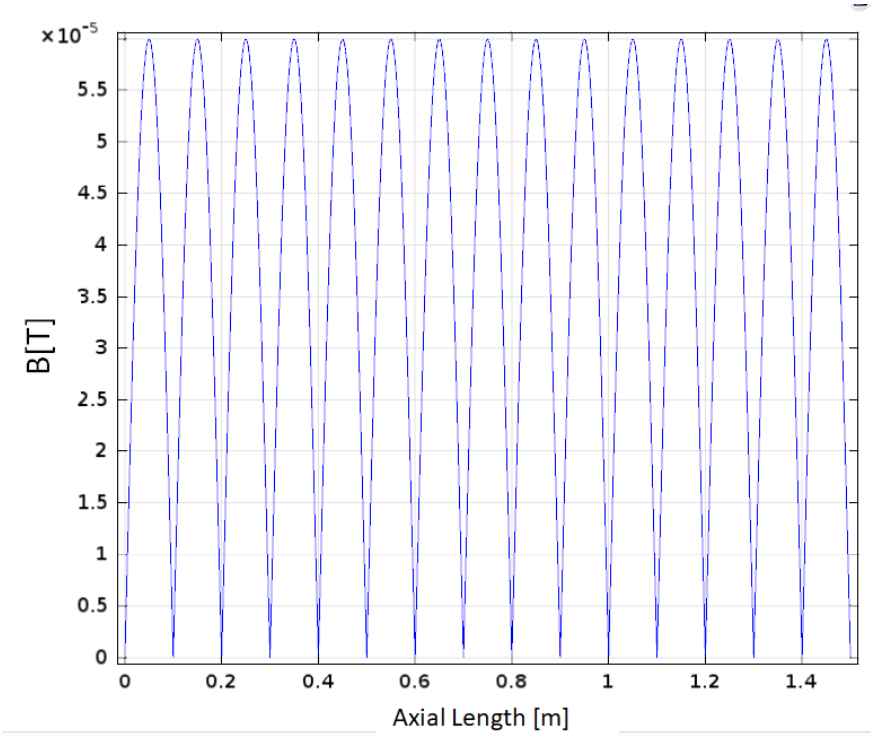

Figure 3.62. Distribution of the magnetic field along the magnetic portion of the pipe at $Re = 100$, for Newtonian ferro fluid at non-dimensional current of $I_0 = 300$

where $curl \quad \vec{V}$ is defined as the vorticity vector and ω is the angular velocity vector. Physically the vorticity is a measure of rotation of a fluid particle. Since the flow is two dimensional, the vorticity vector has only the tangential (θ) component. Under the effect of the constant magnetic field, when the ferro fluid enters to the magnetic portion of the pipe, the vorticity develops and converges to a certain value. Figure 3.63 reveals the distribution of the θ component of the vorticity vector along the centerline of the pipe for constant magnetic field created by non- dimensional current of 150 current at Reynolds number 100 for Newtonian ferro fluid. Figure 3.64 reveals the vorticity at the same Reynolds number for Newtonian ferro fluid under oscillating magnetic field at non-dimensional current 150. Figure 3.64 shows that the shape of the curve is influenced by the distribution of the magnetic field. Vorticity curve has the same peaks and the oscillating shape of the magnetic field. In addition, comparing Figure 3.63 with 3.64 it can be concluded that the oscillating magnetic field creates higher peaks of the vorticity. The peak value of the vorticity created by the oscillating magnetic field is higher than the peak value of the vorticity created by the constant magnetic field along the center line of the pipe. The difference decreases radially along the pipe because the radius around the current carrying conductor increases but the oscillating magnetic field still creates higher vortices compared to constant magnetic field both created by the same amount of current. It can be concluded that when both magnetic fields are created by the same amount of current the oscillating magnetic field creates a larger peak vorticity value compared to the constant magnetic field. Although the vorticity follows the shape of the applied magnetic field, which is a oscillating wave, in addition to the peak values the average vorticity value is still higher for oscillating magnetic field.

Oscillating magnetic field creates higher and oscillating vortices for the ferro fluid along the pipe. In order to obtain the effect of the oscillating magnetic field stream lines along the pipe are generated. Figure 3.65 reveals the distribution of the stream lines along the magnetic portion of the pipe for Newtonian ferro fluid at Reynolds 50. The distribution of the magnetic field along the pipe is given by the Equation (3.12):

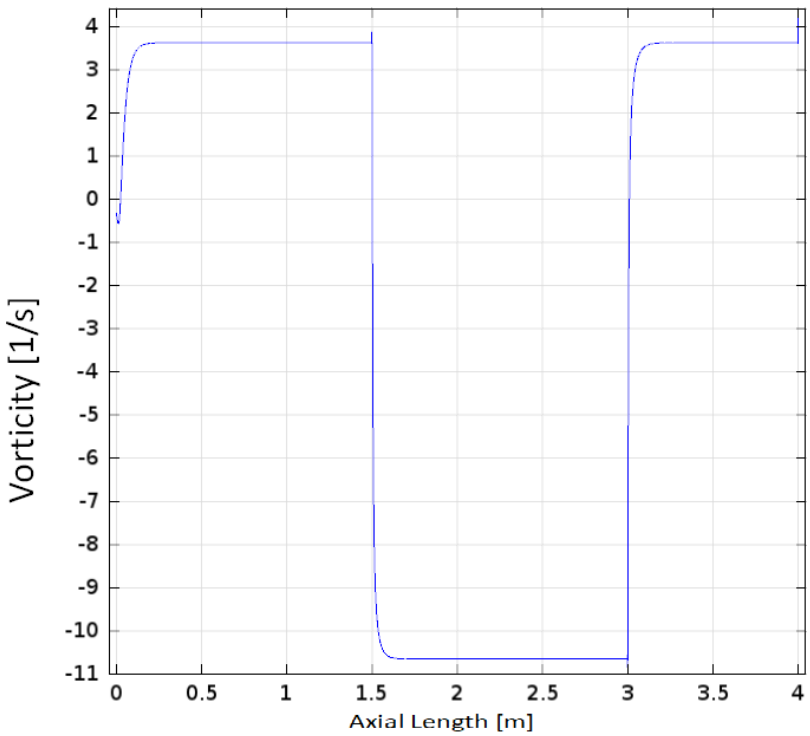

Figure 3.63. Distribution of the vorticity along the centerline of the pipe for constant magnetic field at non- dimensional current of $I_0 = 150$ at $Re = 100$ for $n = 1$

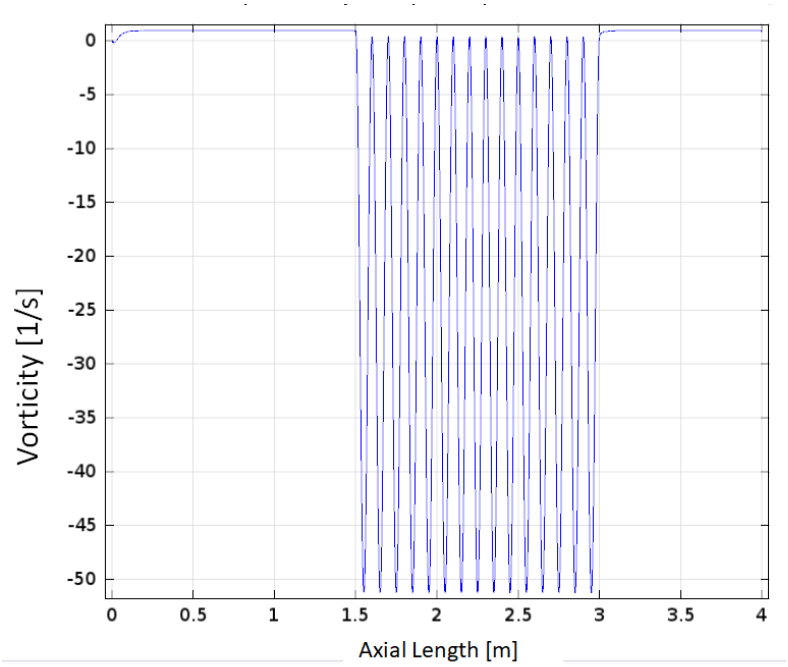

Figure 3.64. Distribution of the vorticity along the centerline of the pipe for oscillating magnetic field at non-dimensional current of $I_0 = 150$ at $Re = 100$ for $n = 1$

$$H = I_0 sin(A\bar{z})\frac{1}{2\pi r} \tag{3.15}$$

where $\bar{z}$ is the non-dimensional length of the magnetic portion of the pipe, A is the frequency of the sinus wave and I is the current which is $3A$ for the case of Figure 3.65. Magnetic field has a frequency of 10π which creates 10 peaks of the magnetic field along the pipe. By changing this, the sinus wave can be altered along the pipe. It can be seen in Figure 3.65 that the stream lines follow a similar pattern to the magnetic field distribution. The magnetic portion of the pipe is $1.5m$ long and the frequency of the sinus wave is 10π per meter therefore the magnetic field makes 15 peaks along the pipe. As it is mentioned before oscillating magnetic field causes vortices along the pipe so vortices are obtained and 10 vorticity field per meter are observed along the magnitude portion of the pipe.

As it is mentioned before the Reynolds number and the magnetic effects are inversely proportional. Figures from 3.65 to 3.68 reveal the distribution of the stream lines along the magnetic portion of the pipe for Newtonian ferro fluid for Reynolds 50, 100, 200 and 300 for oscillating magnetic field with frequency 10π created by non- dimensional current of $I = 300$. Comparing these figures with each other it can be seen that the vortices start to diminish with increasing Reynolds number. When Reynolds number is 100 vortices start to become very small and they diminish as Reynolds number increases. In addition stream lines start to take more straight forms with increasing Reynolds number especially when it increases from 200 to 300. This is because with increasing Reynolds number inertia effects start to dominate and the influence of the magnetic force decreases.

The influence of the oscillating magnetic field on the ferro fluid is similar to the constant magnetic field case, with increasing non-dimensional electric current the effect of the magnetic force on the ferro fluid increases. The difference is that when the oscillating magnetic field is large enough it creates vortices within the ferro fluid

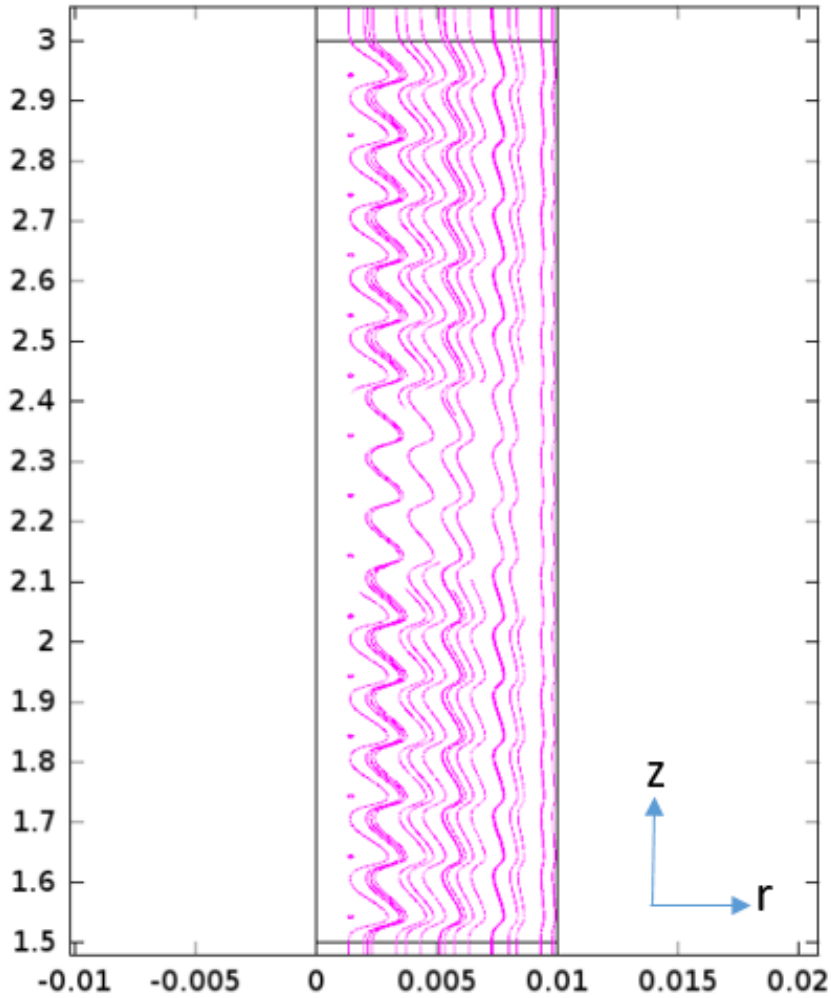

Figure 3.65. Distribution of the stream lines along the magnetic portion of the pipe for Newtonian ferro fluid at $Re = 50$ at oscillating magnetic field created by non-dimensional current of $I_0 = 300$ with frequency 10π

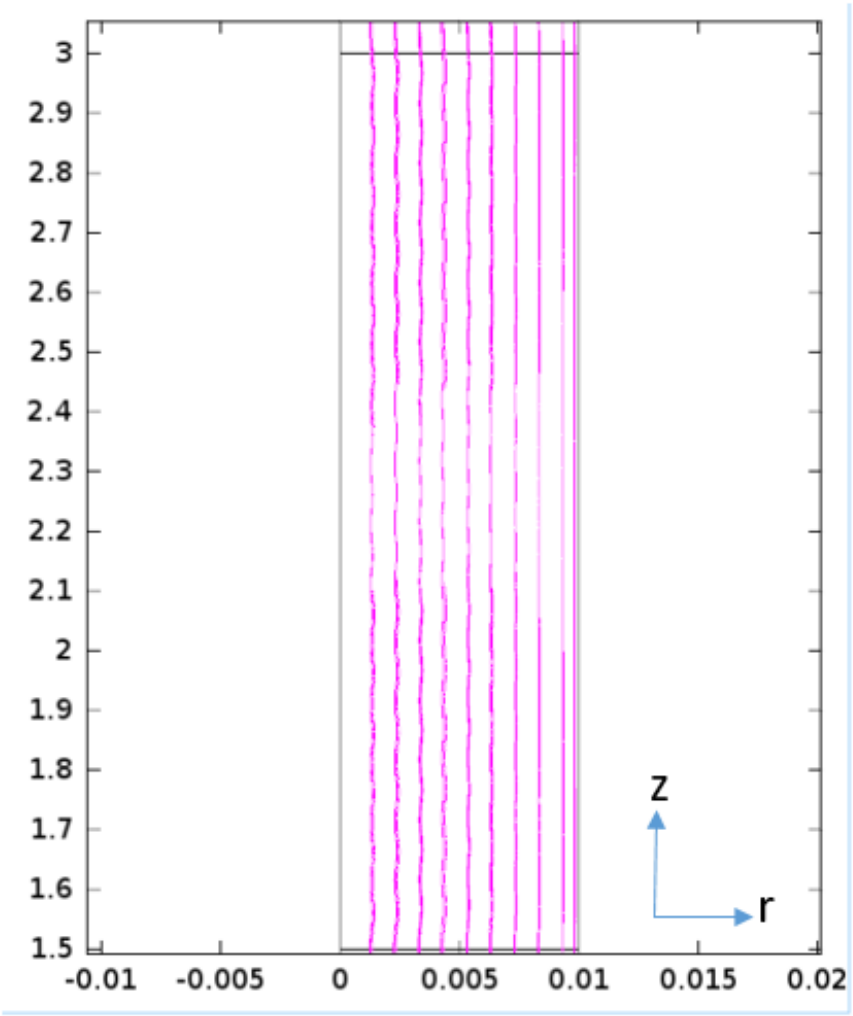

Figure 3.66. Distribution of the stream lines along the magnetic portion of the pipe for Newtonian ferro fluid at $Re = 100$ at oscillating magnetic field created by non dimensional current of $I_0 = 300$ with frequency 10π

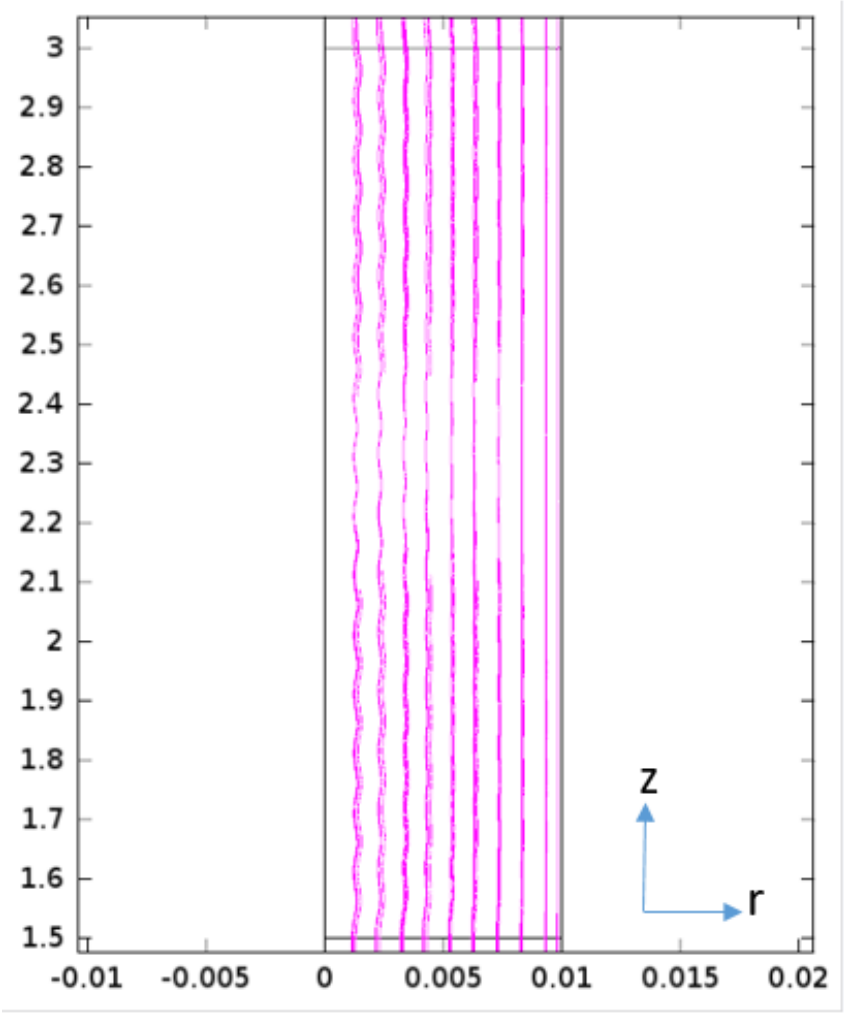

Figure 3.67. Distribution of the stream lines along the magnetic portion of the pipe for Newtonian ferro fluid at $Re = 200$ at oscillating magnetic field created by non-dimensional current of $I_0 = 300$ with frequency 10π

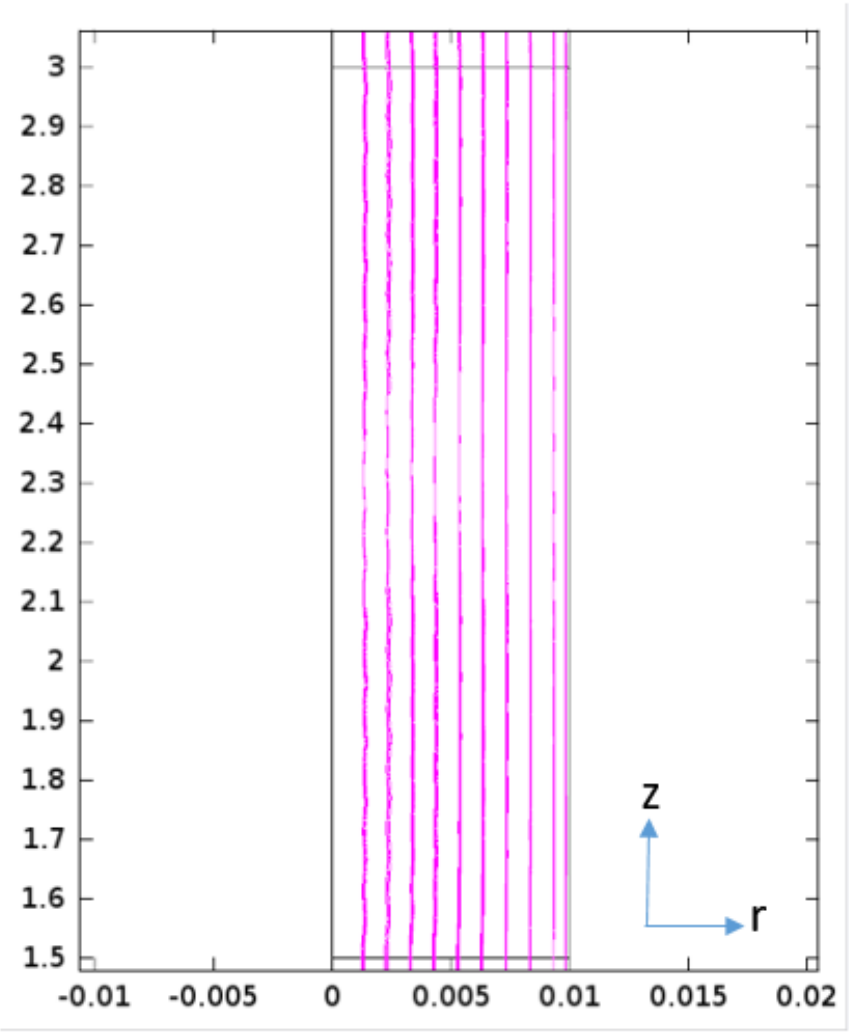

Figure 3.68. Distribution of the stream lines along the magnetic portion of the pipe for Newtonian ferro fluid at $Re = 300$ at oscillating magnetic field created by non-dimensional current of $I_0 = 300$ with frequency 10π

and even if it has a moderate value it creates wavy stream lines along the magnetic portion of the pipe. The size and amount of the vortices increase with increasing magnetic field. Figures from 3.69 to 3.72 reveal the stream lines for Newtonian ferro fluid at $Re = 50$ for magnetic fields created with frequency 10π by non dimensional currents of $I_0 = 75, 150, 300$ and 600 of current. When $I_0 = 75$ the stream lines start to take a wavy shape but still in the form as if a constant magnetic field is applied. When I_0 increases to 150 stream lines start to take a wavy shape and small vortices develop. It can be said that the magnetic effects start to become dominant. When I_0 increases to 300 the magnetic effects become clear and in addition to this the effect of the oscillating magnetic field becomes visible as vortices start to occur in the ferro fluid and the pattern of the vortices follow the distribution of the magnetic field along the pipe. Finally when I_0 increases to 600 the magnetic dominance becomes obvious and larger vortices are obtained in the ferro fluid. Therefore it can be concluded that with increasing non-dimensional electric current the influence of the oscillating magnetic field becomes larger and the obvious proof of this are the vortices occurring within the ferro fluid. Solis and Martin [6] created vortices by using tri axial magnetic field. In this case instead of a tri-axial ac-ac- dc field a oscillating oscillating magnetic field is created and vortices are developed within the fluid. Variation of the magnetic field as it is achieved by an ac-ac-dc tri-axial magnetic field like in Solis and Martin [6]'s study or as it is achieved by oscillating variation along the pipe can create vortices when the gradient and the magnitude of the magnetic field is high enough.

As mentioned before the distribution of the oscillating magnetic field has an impact on the vortices pattern along the magnetic portion of the pipe. The distribution of the magnetic field is conducted by changing the frequency of the magnetic field. Figures 3.73 and 3.74 reveal the distribution of the oscillating magnetic flux density, which corresponds to the magnetic field when divided by vacuum permeability, with frequencies of 10π and 3π created by 600 of non-dimensional current and Figures 3.75 and 3.76 reveal the distribution of the stream lines under these oscillating magnetic fields. Comparing Figures 3.75 with 3.76 it can be seen that the vortices pattern is related to the number of the peaks of the oscillating magnetic field and the shape of the magnetic field directly impacts the flow.

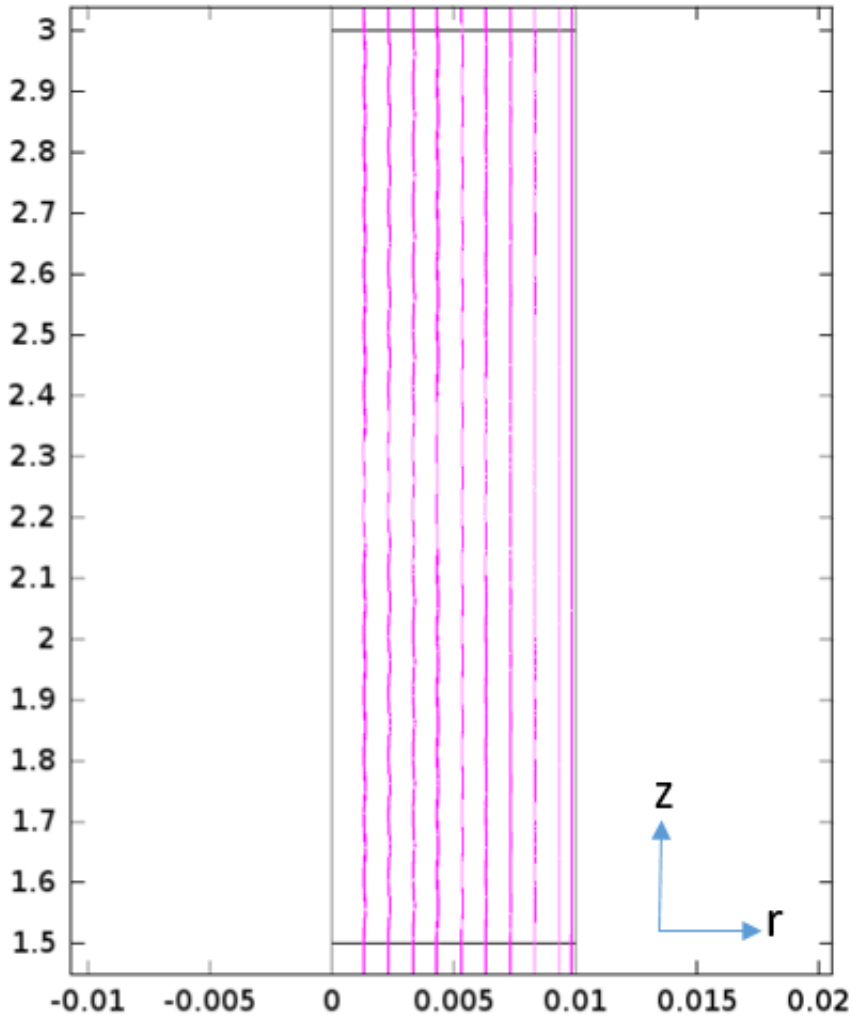

Figure 3.69. Distribution of the stream lines along the magnetic portion of the pipe for Newtonian ferro fluid at $Re = 50$ at oscillating magnetic field created by non-dimensional current $I_0 = 75$ with frequency 10π

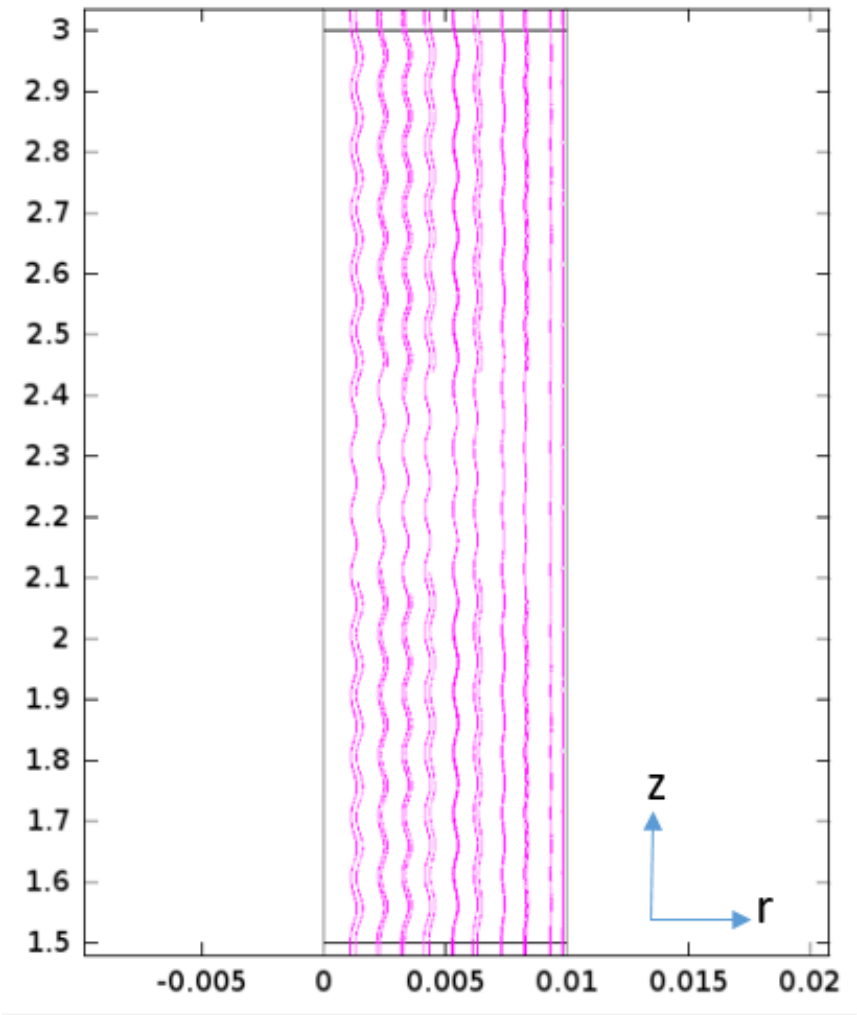

Figure 3.70. Distribution of the stream lines along the magnetic portion of the pipe for Newtonian ferro fluid at $Re = 50$ at oscillating magnetic field created by non-dimensional current of $I_0 = 150$ with frequency 10π

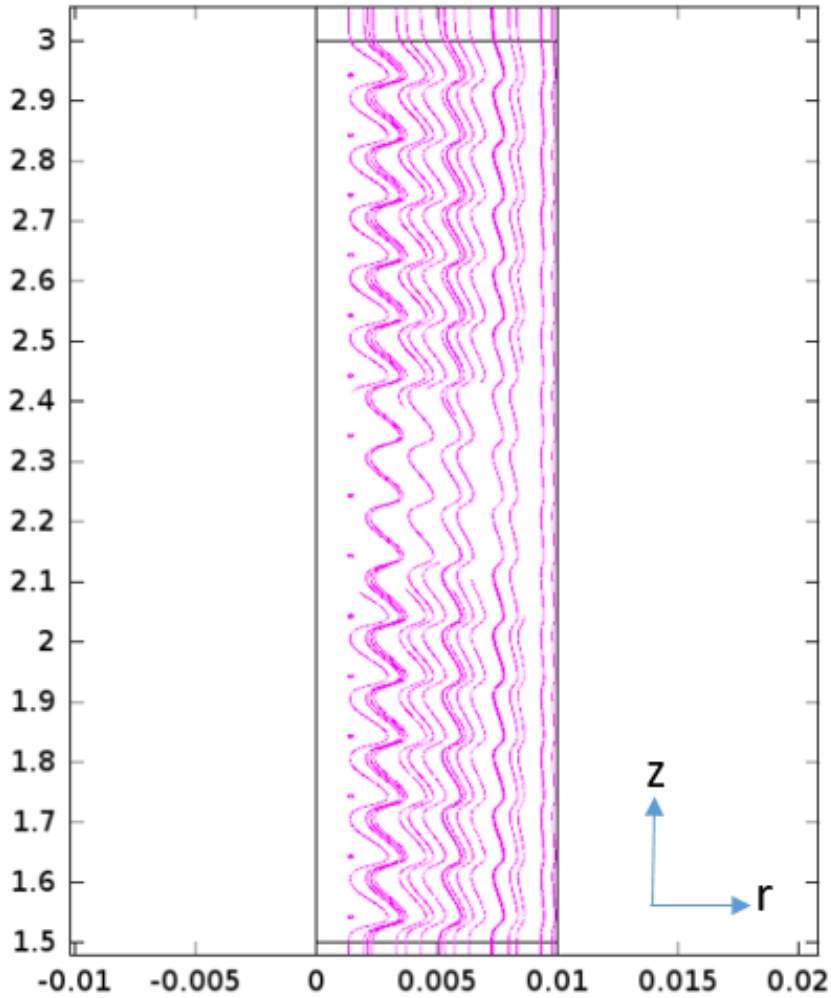

Figure 3.71. Distribution of the stream lines along the magnetic portion of the pipe for Newtonian ferro fluid at $Re = 50$ at oscillating magnetic field created by non-dimensional current of $I_0 = 300$ with frequency 10π

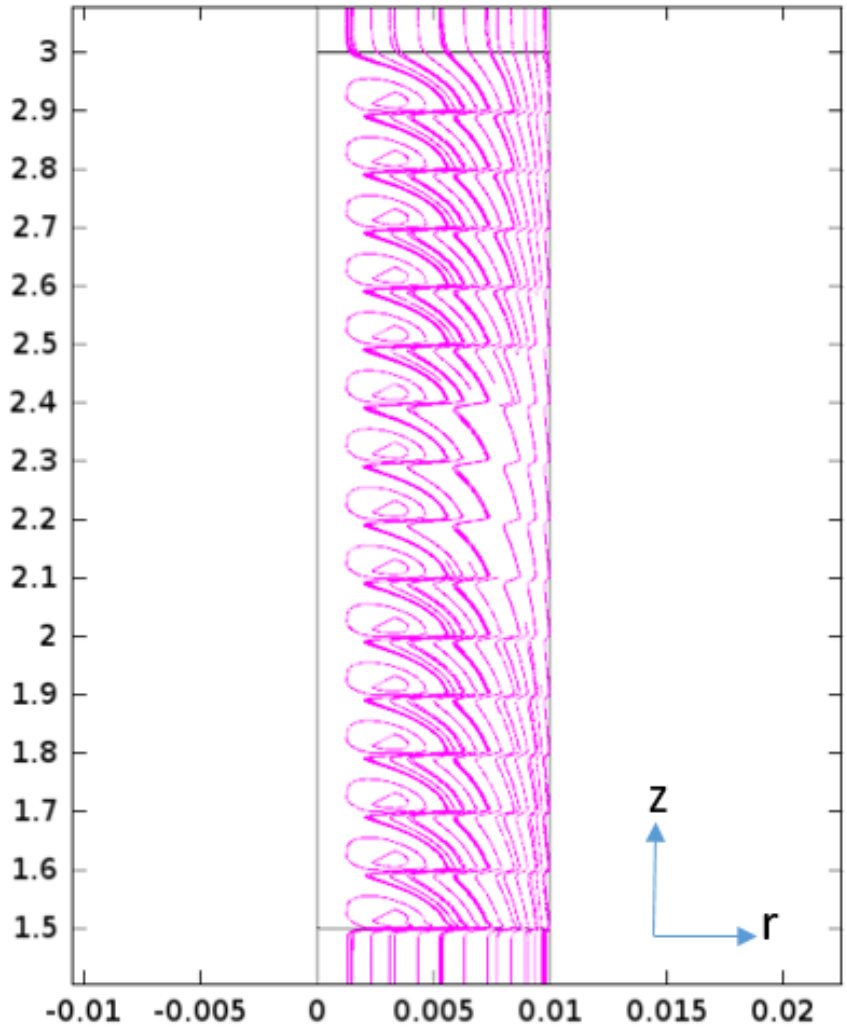

Figure 3.72. Distribution of the stream lines along the magnetic portion of the pipe for Newtonian ferro fluid at $Re = 50$ at oscillating magnetic field created by non-dimensional current $I_0 = 600$ with frequency 10π

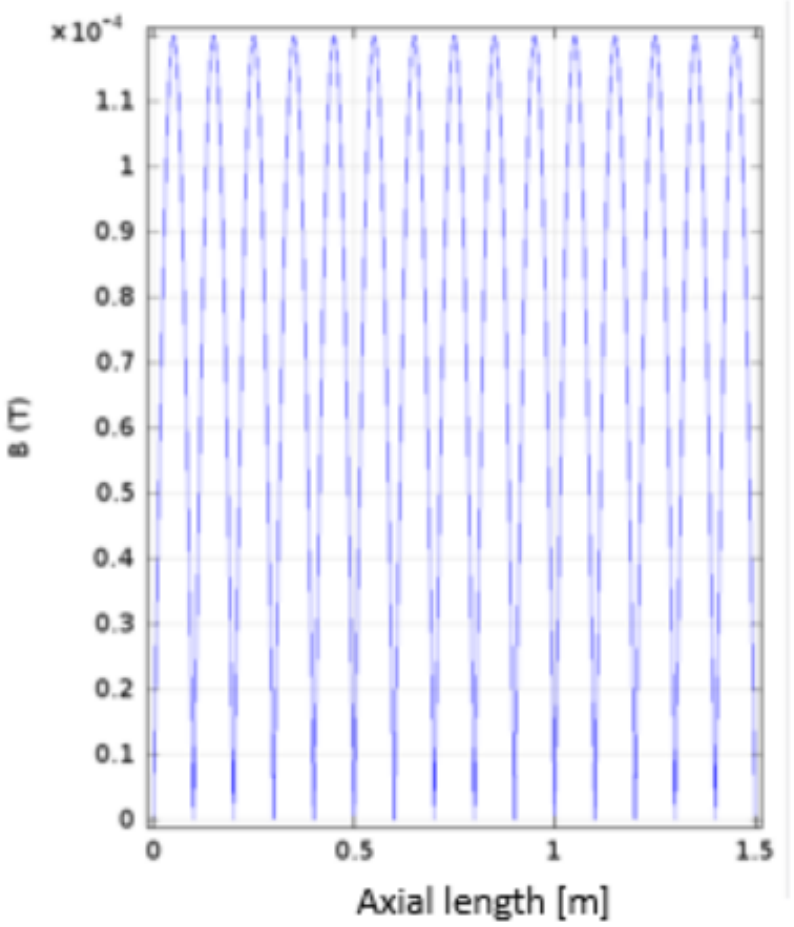

Figure 3.73. Distribution of the stream lines along the magnetic portion of the pipe for Newtonian ferro fluid at $Re = 50$ at oscillating magnetic field created by $I_0 = 600$ with frequency 10π

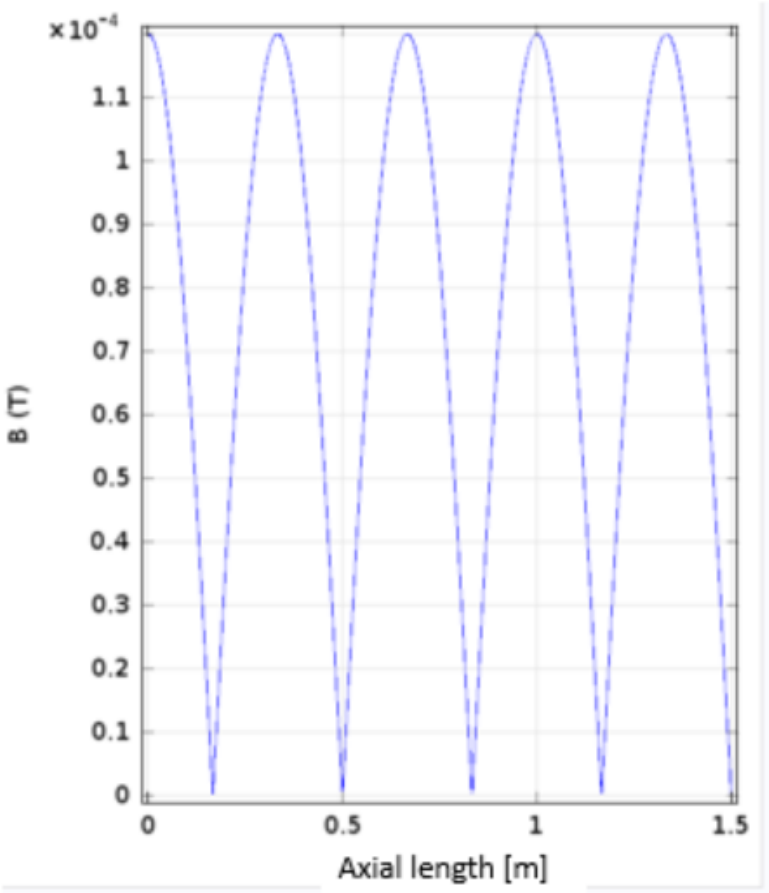

Figure 3.74. Distribution of the magnetic flux density created by $I_0 = 600$ with frequency 3π at $Re = 50$

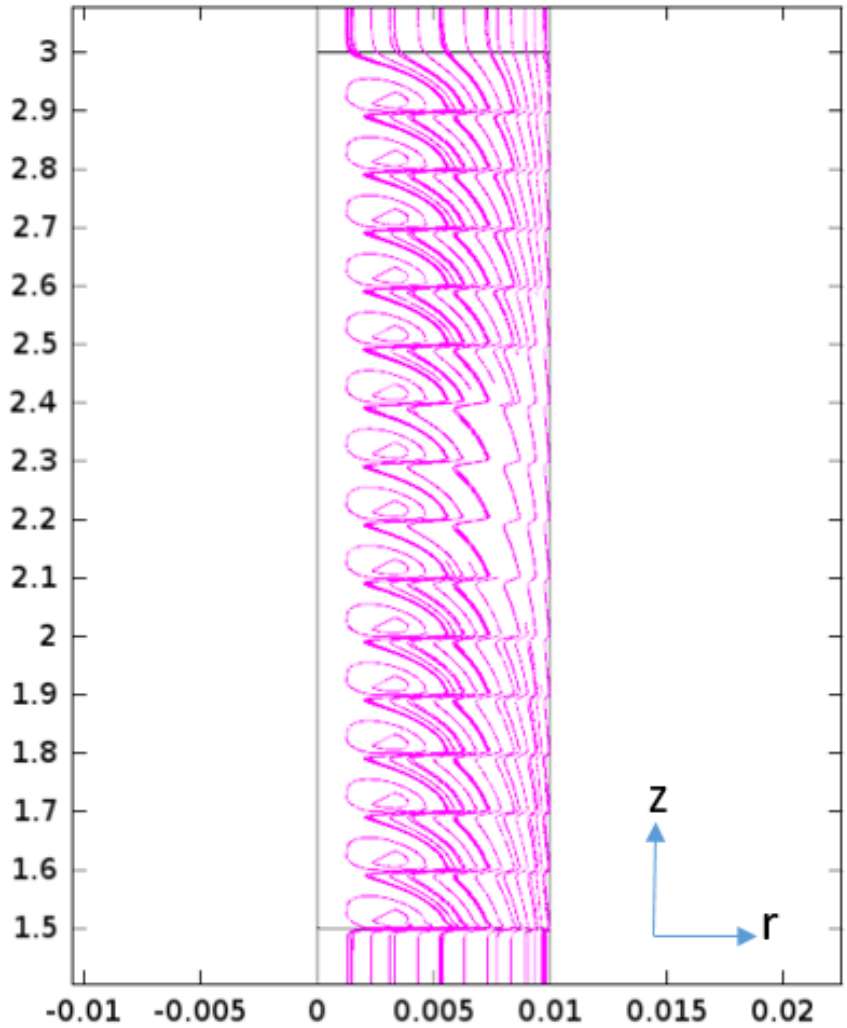

Figure 3.75. Distribution of the magnetic flux density created by $I_0 = 600$ with frequency 10π at $Re = 50$

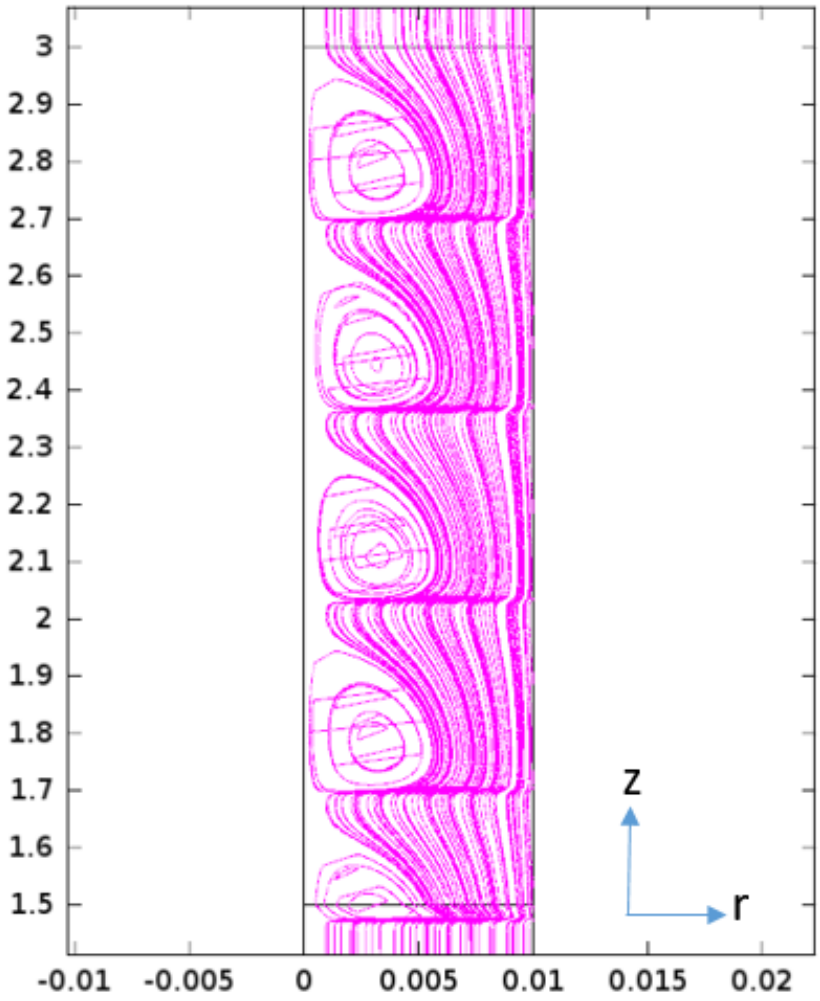

Figure 3.76. Distribution of the magnetic flux density created by $I_0 = 600$ with frequency 3π at $Re = 50$

Similar to the Newtonian fluid the power law ferro fluid stream line pattern is related to the oscillating magnetic field shape. Figure 3.77 reveal the stream lines for $n = 0.85$ at $Re = 200$ with oscillating magnetic field created by $I_0 = 300$ with frequency 10π. As it is seen in Figure 3.77 the stream line distortions are related and the stream lines have the shape of the oscillating magnetic field. Therefore it can be concluded that the oscillating magnetic field shape has the same influence on the stream lines of power law fluids.

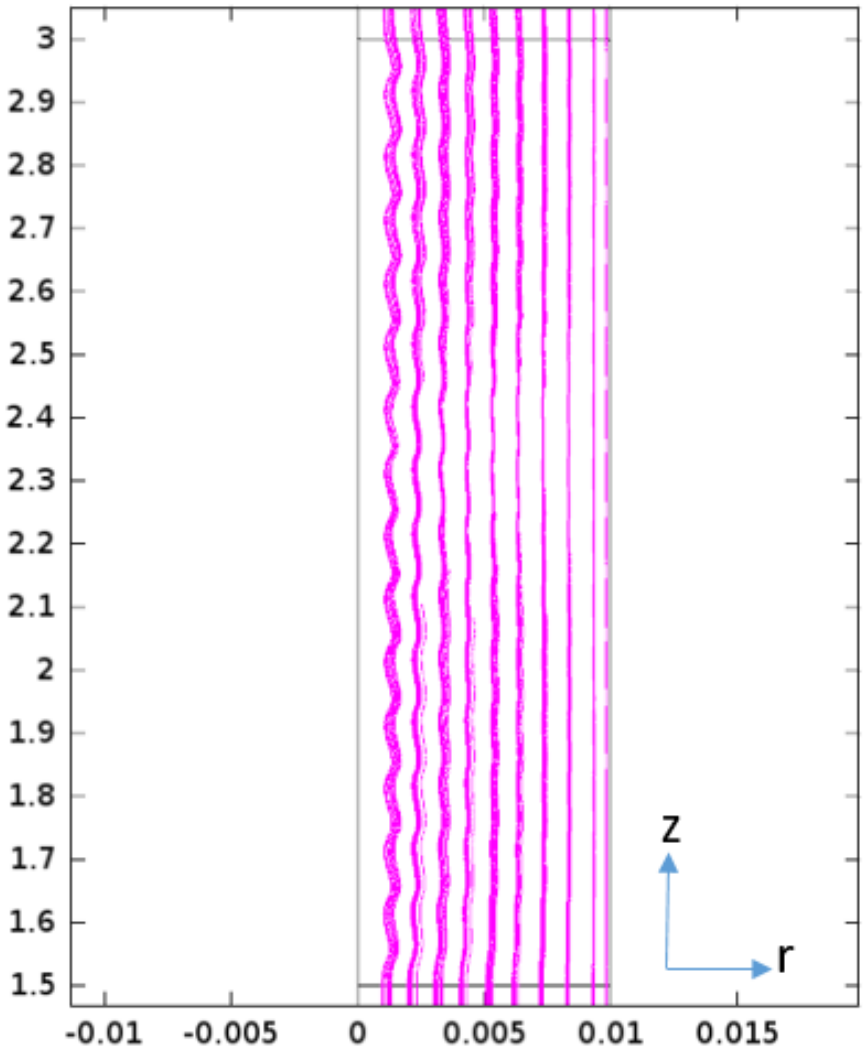

Figure 3.77. Distribution of the Stream Lines created by $I_0 = 300$ with frequency 3π at $Re = 200$ for $n = 0.85$

The influence of the Reynolds number on power law ferro fluids under oscillating magnetic field is similar to the Newtonian ferro fluids. With increasing Reynolds number non-dimensional electric current and therefore magnetic effects decrease. Figures from 3.78 to 3.81 reveal the stream lines for $n = 1$ at a magnetic field created by $I_0 = 300$ with frequency of 10π for Reynolds 50, 100, 200 and 300 respectively. The size of the vortices occurring in the magnetic portion of the pipe reveal that with increasing Reynolds number the size of the vortices decreases. With increasing Reynolds number the inertia effects start to dominate which reduces the influence of the magnetic force on the ferro fluid causing smaller vortices occur during the flow.

As it is with the Newtonian fluids with the increasing non-dimensional electric current the ferro fluid undergoes a larger magnetic force. With the increasing non-dimensional electric current the magnetic forces start to become more dominant and the effect can be obtained on the stream lines. Figures from 3.82 to 3.84 reveal the stream lines for $n = 0.85$ at Reynolds 50 with oscillating magnetic fields created with frequency 10π by $I_0 = 75A$, $I_0 = 150$ and $I_0 = 300$ respectively. When the oscillating magnetic field is the smallest it is seen that the stream lines start to distort. With increasing magnetic effects stream lines start to take a wavy form and formation of the small vortices become visible. When the oscillating magnetic field increases further larger and visible vortices, which have the pattern of the induced oscillating magnetic field, starts to develop in the magnetic portion of the pipe. Therefore it can be concluded that the non-dimensional electric current and the vortices formation under oscillating magnetic field are directly proportional like in the Newtonian fluid case.

In order to study the effect of the power law index on ferro fluid under oscillating magnetic field analyses are conducted for power law indices $n = 0.75$, 0.85, 1 and 1.1. Figures from 3.85 to 3.88 reveal the stream lines for Reynolds 100 at oscillating magnetic field created by $I_0 = 300$ with frequency 10π for the given power law indices respectively. As it is mentioned before when the power law index is lower than 1 it behaves as a shear thinning fluid and when it is higher than 1 it behaves as a shear thickening fluid. Streamlines reveal that when the fluid is shear thinning the effect of

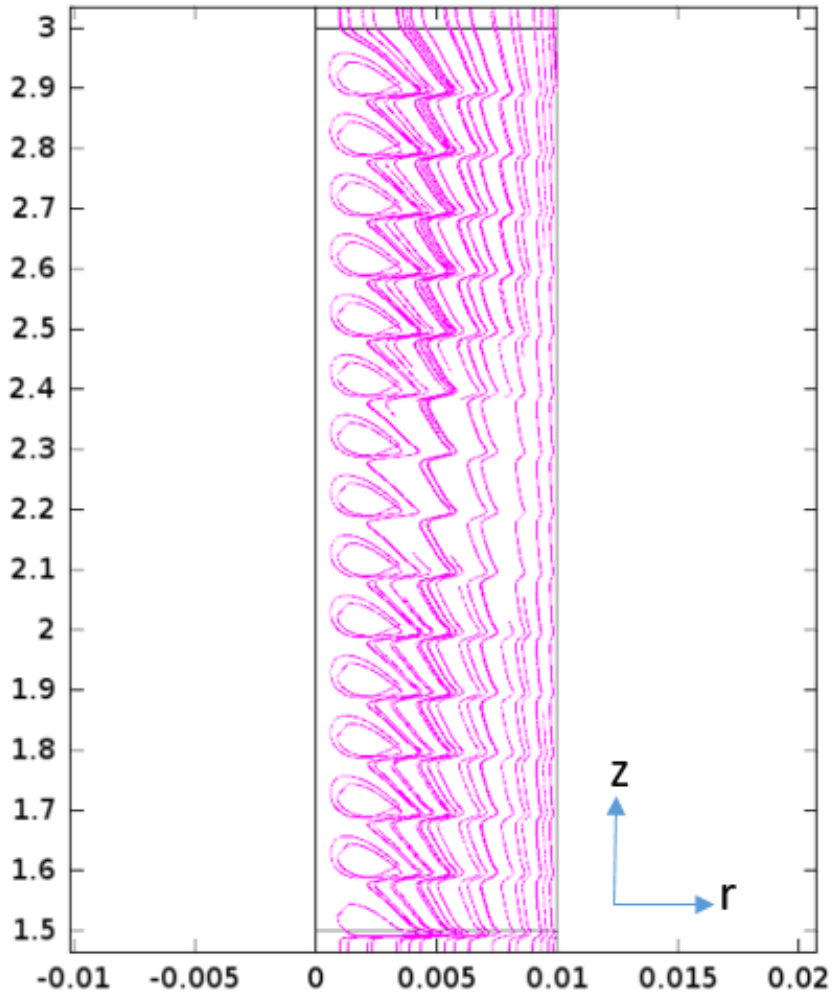

Figure 3.78. Distribution of the Stream Lines created by $I_0 = 300$ with frequency 10π at $Re = 50$ for $n = 0.75$

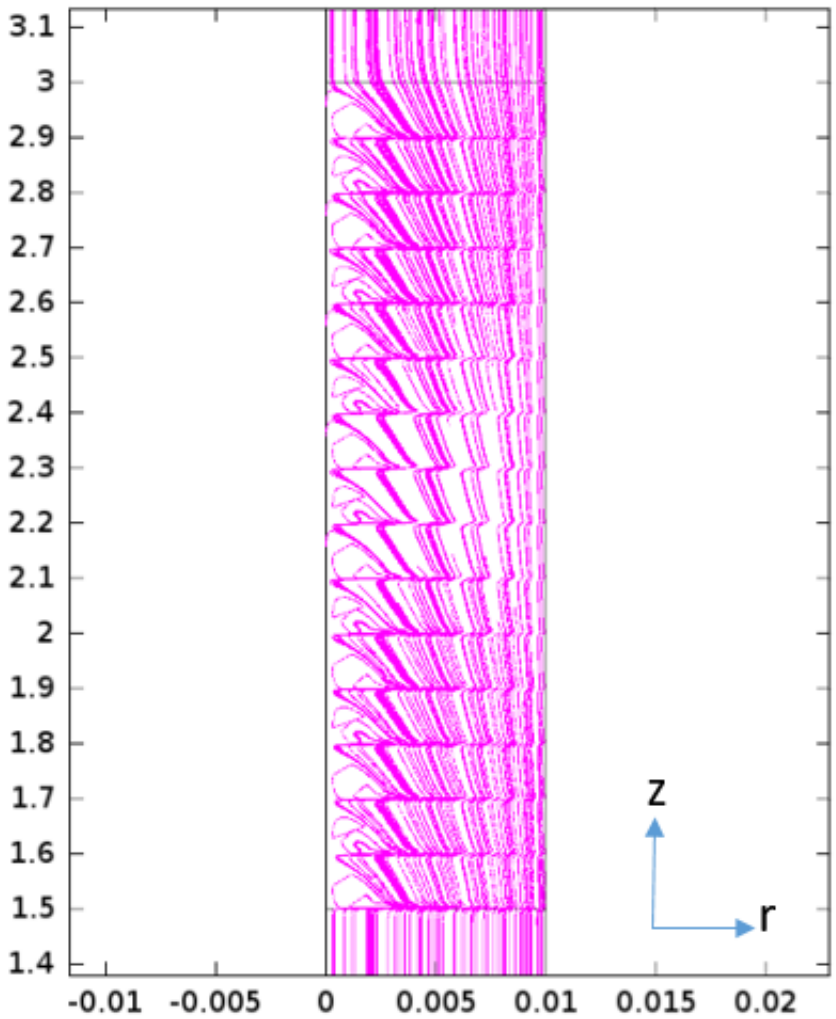

Figure 3.79. Distribution of the Stream Lines created by $I_0 = 300$ with frequency 10π at $Re = 50$ for $n = 0.75$

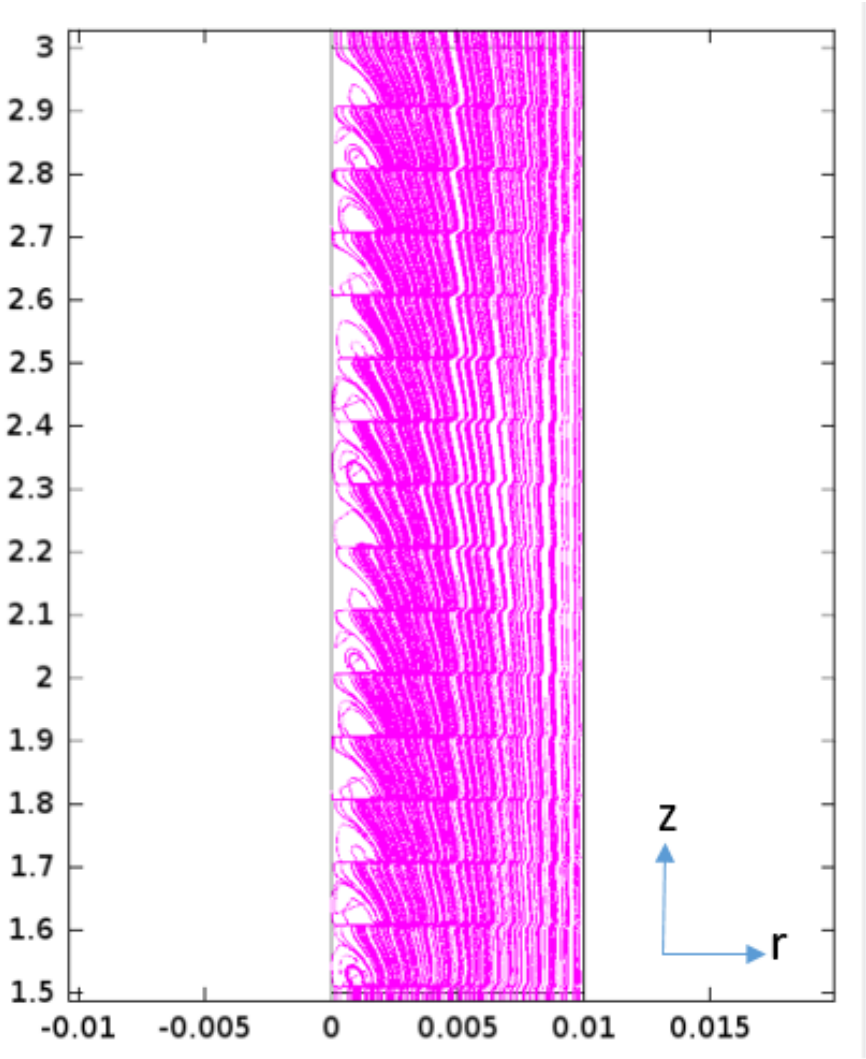

Figure 3.80. Distribution of the Stream Lines created by $I_0 = 300$ with frequency 10π at $Re = 50$ for $n = 0.75$

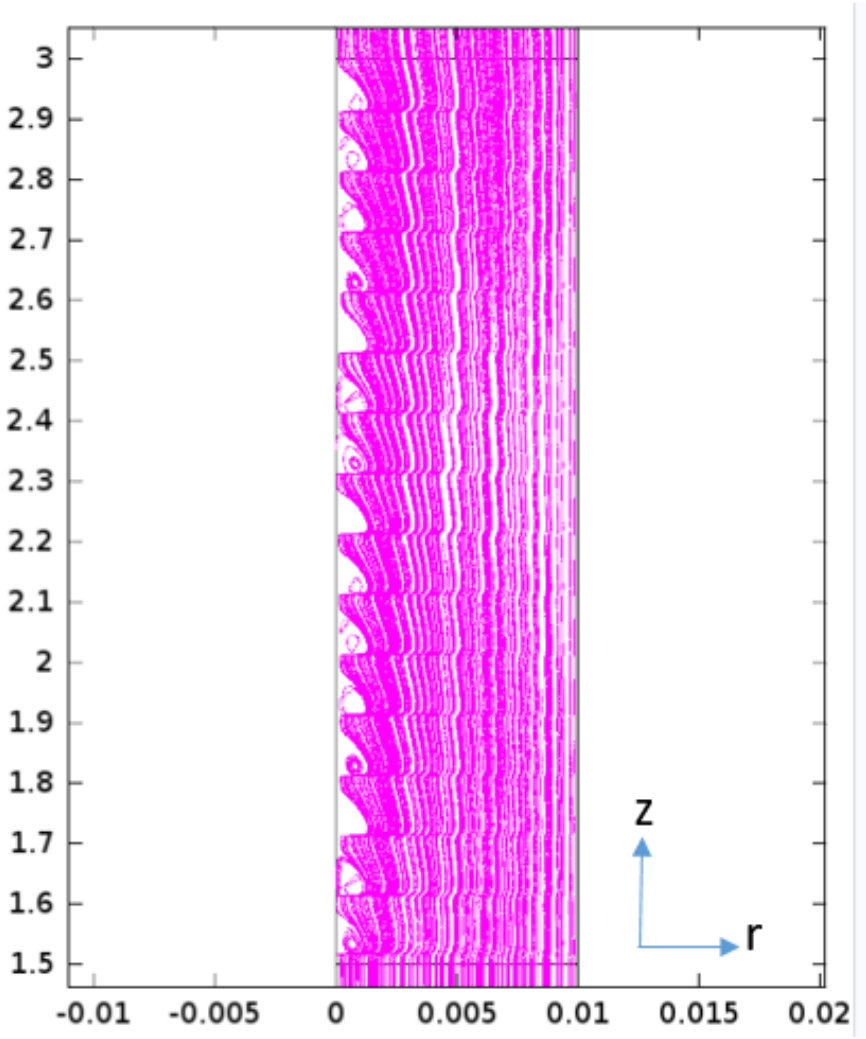

Figure 3.81. Distribution of the Stream Lines created by $I_0 = 300$ with frequency 10π at $Re = 50$ for $n = 0.75$

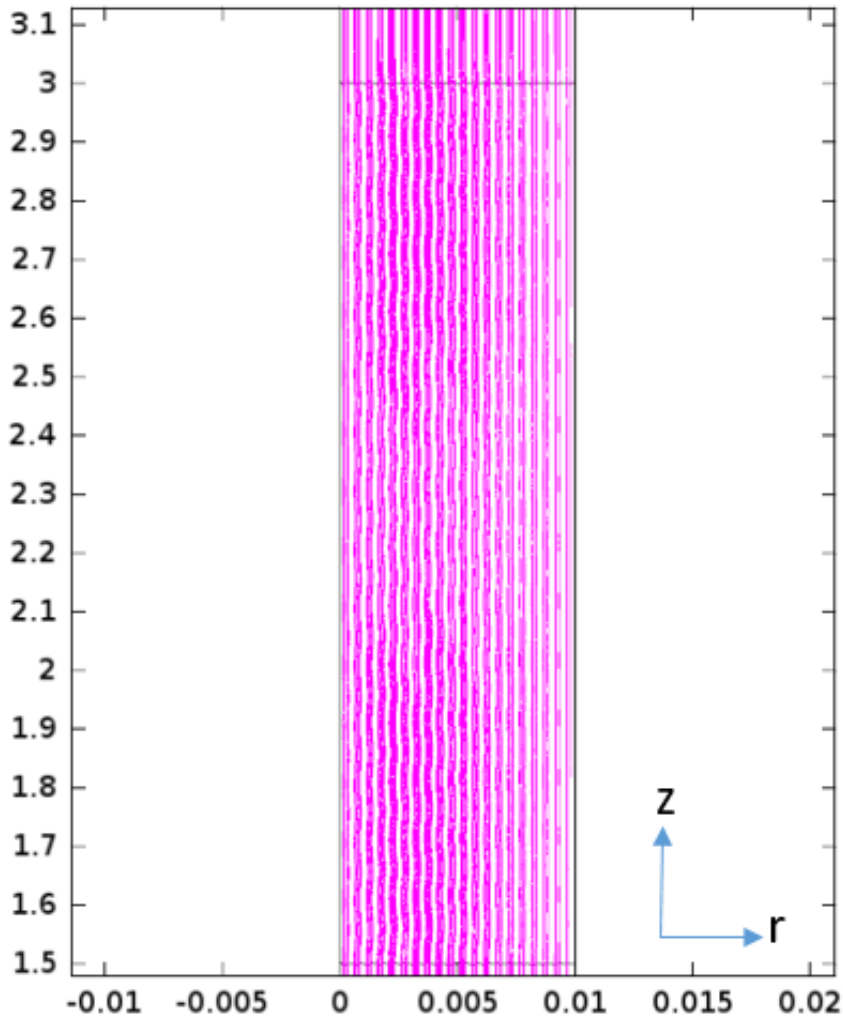

Figure 3.82. Distribution of the Stream Lines created by $I_0 = 75$ with frequency 10π at $Re = 50$ for $n = 0.85$

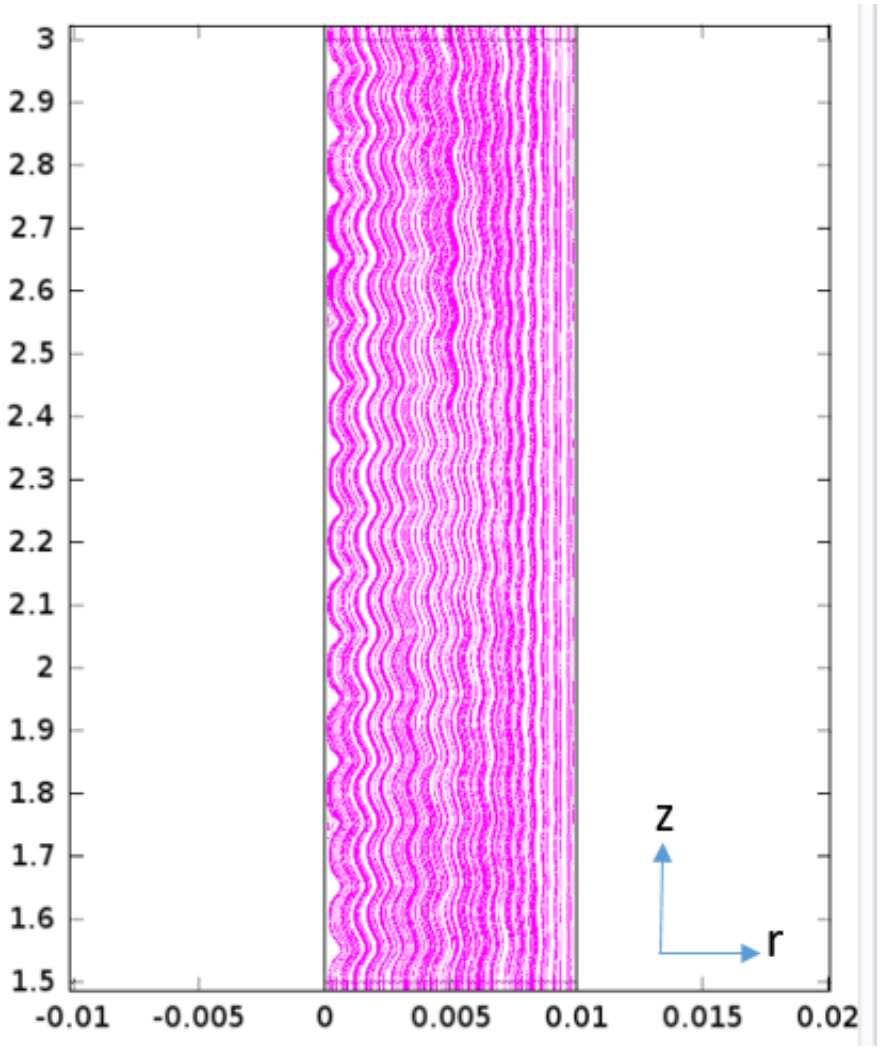

Figure 3.83. Distribution of the Stream Lines created by $I_0 = 150$ with frequency 10π at $Re = 50$ for $n = 0.85$

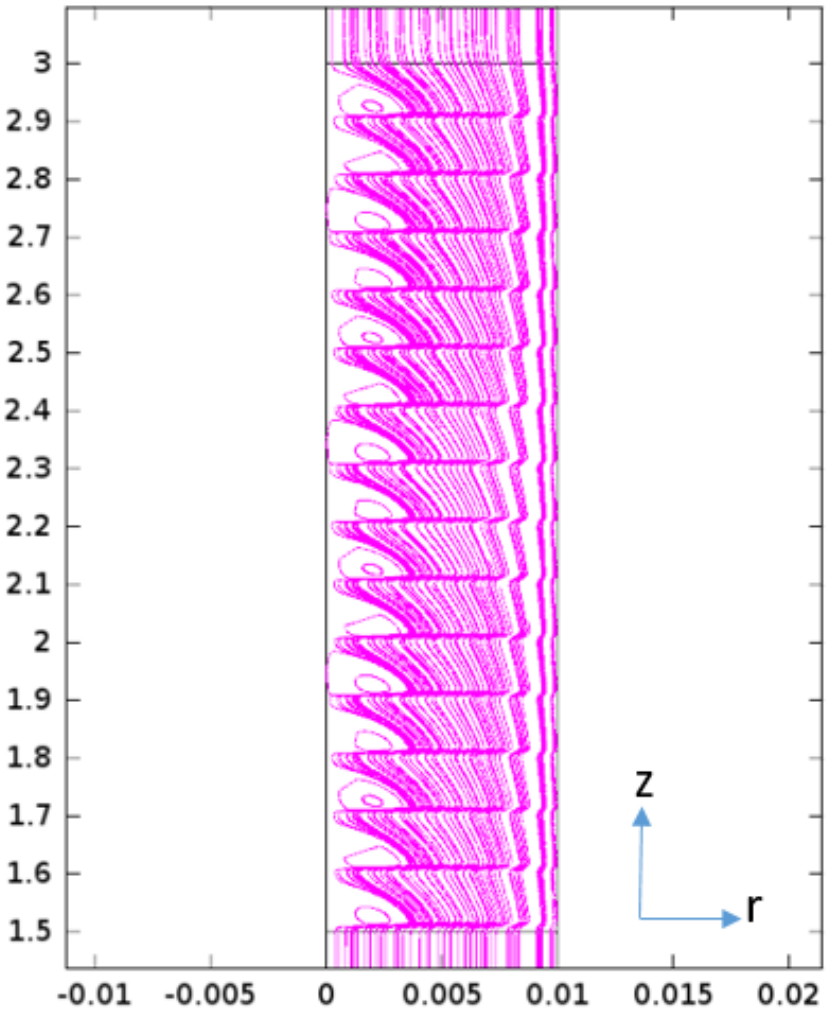

Figure 3.84. Distribution of the Stream Lines created by $I_0 = 300$ with frequency 10π at $Re = 50$ for $n = 0.85$

the oscillating magnetic field is higher. Comparing Figures 3.85 and 3.86 with 3.87, which is Newtonian ferro fluid, it can be seen that as the ferro fluid becomes more shear thinning the vortices start to occur and increase in the pipe. Under the same magnetic effect the vortices start to diminish and become less visible as fluid becomes Newtonian. Further increasing the power law index n to 1.1 vortices start to disappear and the wavy form of the stream lines become more straight.

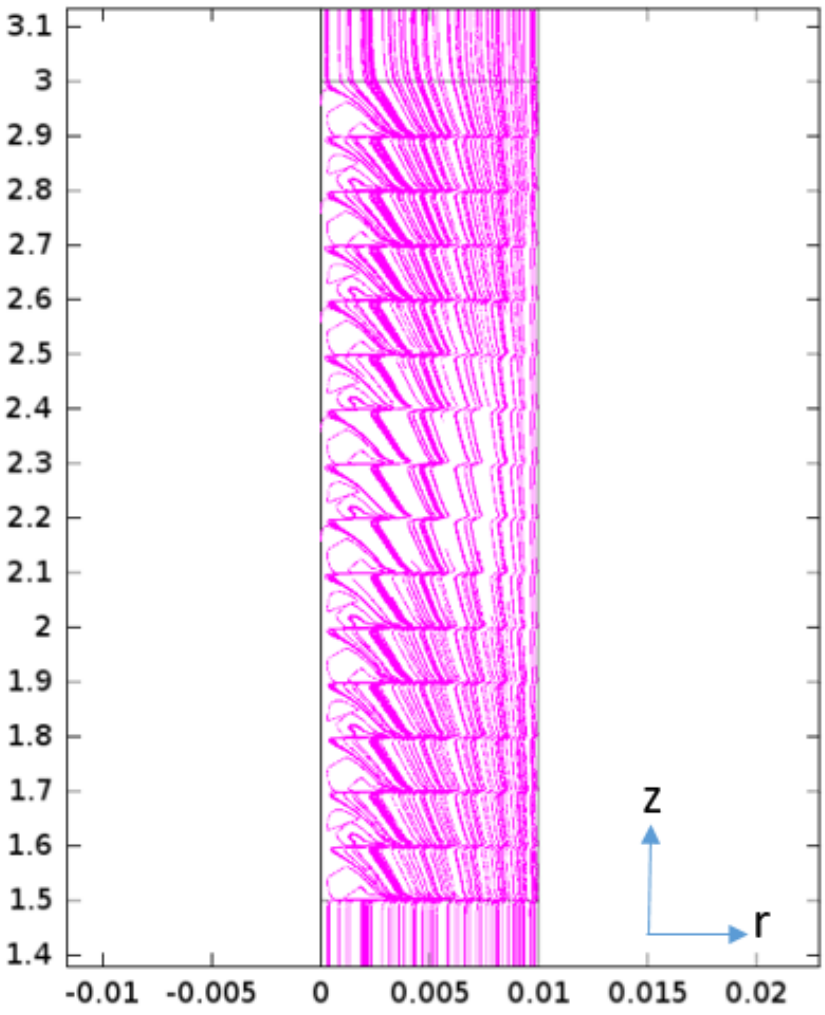

Figure 3.85. Distribution of the Stream Lines created by $I_0 = 300$ with frequency 10π at $Re = 50$ for $n = 0.75$

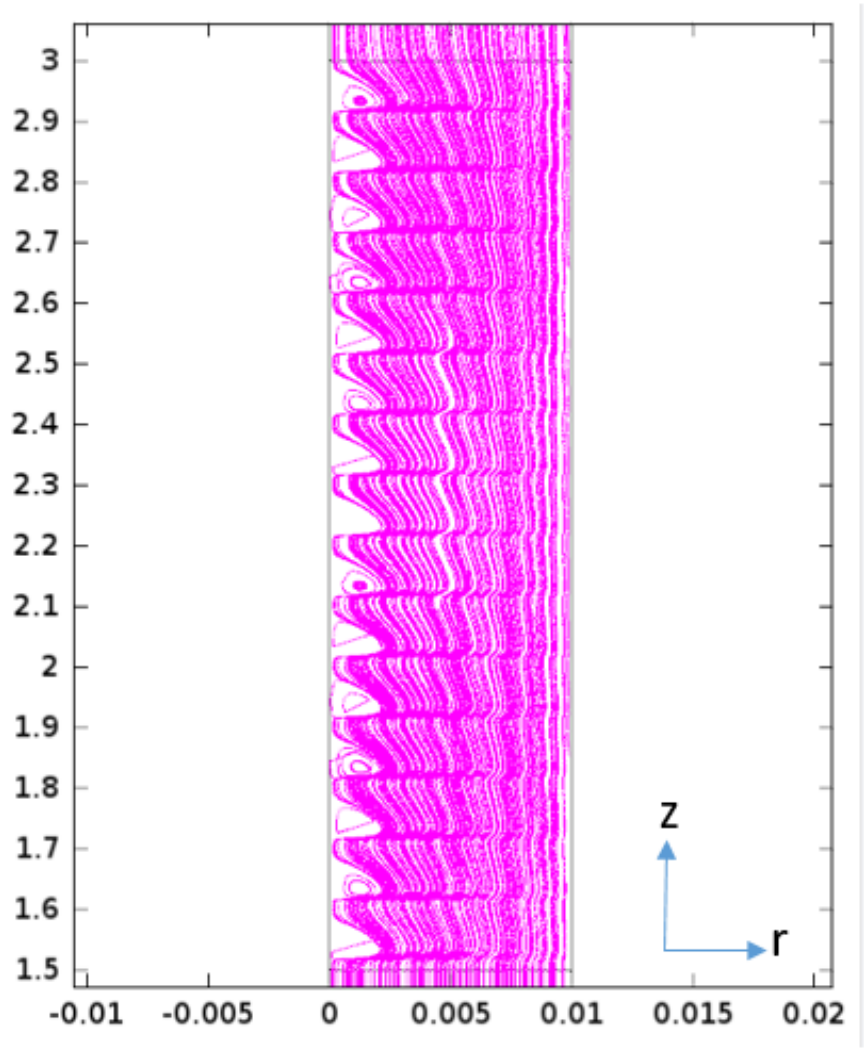

Figure 3.86. Distribution of the Stream Lines created by $I_0 = 300$ with frequency 10π at $Re = 50$ for $n = 0.85$

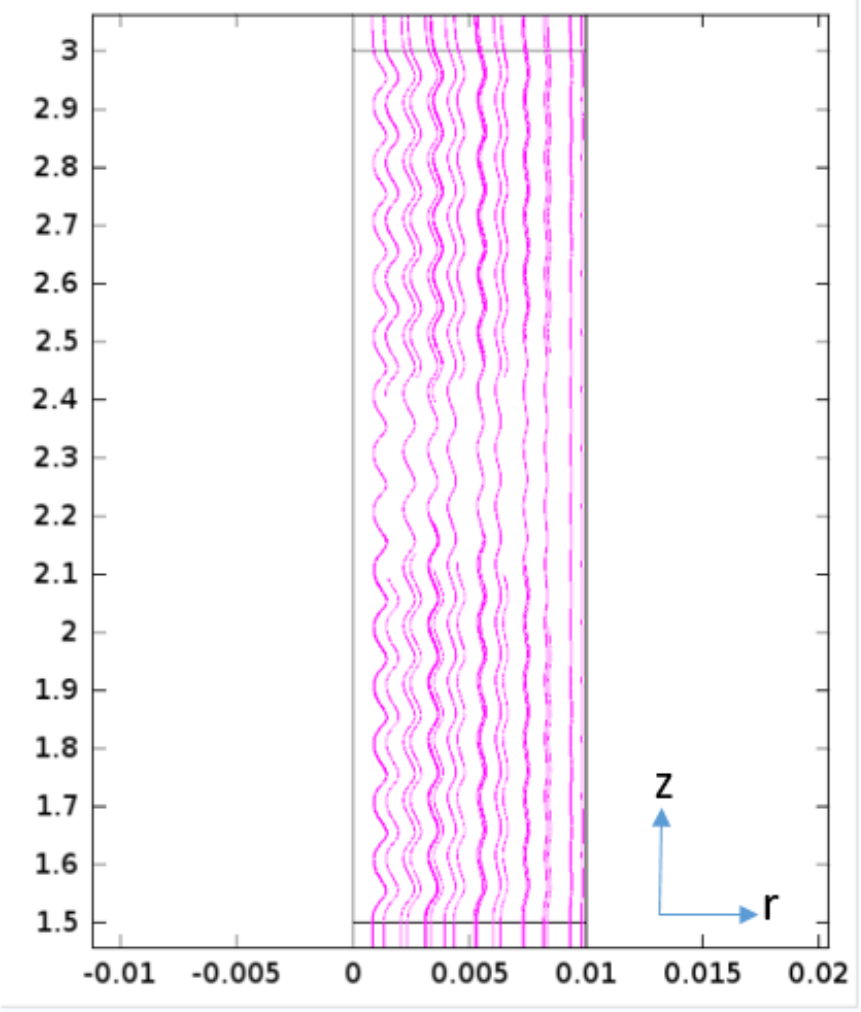

Figure 3.87. Distribution of the Stream Lines created by $I_0 = 300$ with frequency 10π at $Re = 50$ for $n = 1$

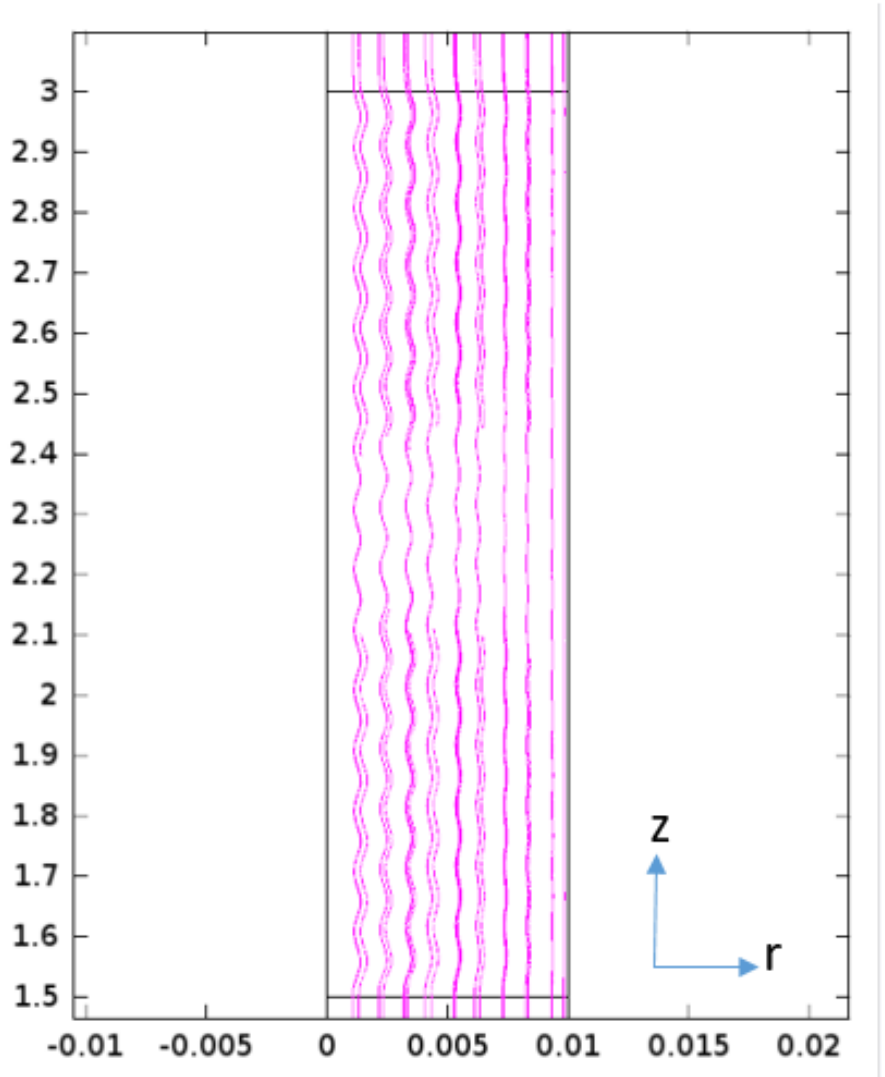

Figure 3.88. Distribution of the Stream Lines created by $I_0 = 300$ with frequency 10π at $Re = 50$ for $n = 1.1$

Akay *et al.* [8]. describes the non-dimensional vorticity as:

$$\overrightarrow{\bar{\Omega}} = \frac{curl\vec{V}D}{U_0} \tag{3.16}$$

where $\bar{\Omega}$ is the non-dimensional vorticity non-dimensionalized by velocity and the characteristic length which is diameter for the pipe. Figures 3.89 and 3.90 reveals the $\frac{I_0}{Re}$ vs. non-dimensional vorticity for oscillating magnetic fields created by $I_0 = 150$ and $I_0 = 300$ respectively for Reynolds 50,100, 200 and 300 for power law indices $n = 0.75$, $n = 0.85$, $n = 1$ and $n = 1.1$. The non-dimensional vorticities are strongly supported by the stream line results. Results reveal that as the ferro fluid becomes more shear thinning the magnitude of the non-dimensional vorticity increases for the same magnetic field value. Therefore streamlines at lower power law indices revealed larger vorticities and as the ferro fluid becomes more shear thickening the magnitude of the non-dimensional vorticity decreases. This is because at lower power law indices the magnetic effects are more dominant. Results also reveal that with increasing Reynolds number the value of the non-dimensional vorticity decreases. Streamline distribution also revealed the same as with increasing Reynolds number the vortices diminish and stream lines become flatter. With increasing Reynolds number the magnetic effects which are proportional to N/Re decrease and inertia effects start to dominate. It is also seen that the non-dimensional vorticity is directly proportional with the induced magnetic field. With increasing magnetic field stream lines start to take a wavy form and vortices start to develop and the increasing value of the non-dimensional vorticity with increasing magnetic field value reveals that. Figures 3.89 and 3.94 also reveal that similar to the previous cases a linear relationship between those non-dimensional parameters are observed and previous relationships are confirmed. The generalized equation revealing the peak non-dimensional vorticity value in terms of power law index, Reynolds number and non-dimensional electrical current is given as:

$$\bar{\Omega} = 16.94n^{-5.596}\frac{I_0}{Re} \tag{3.17}$$

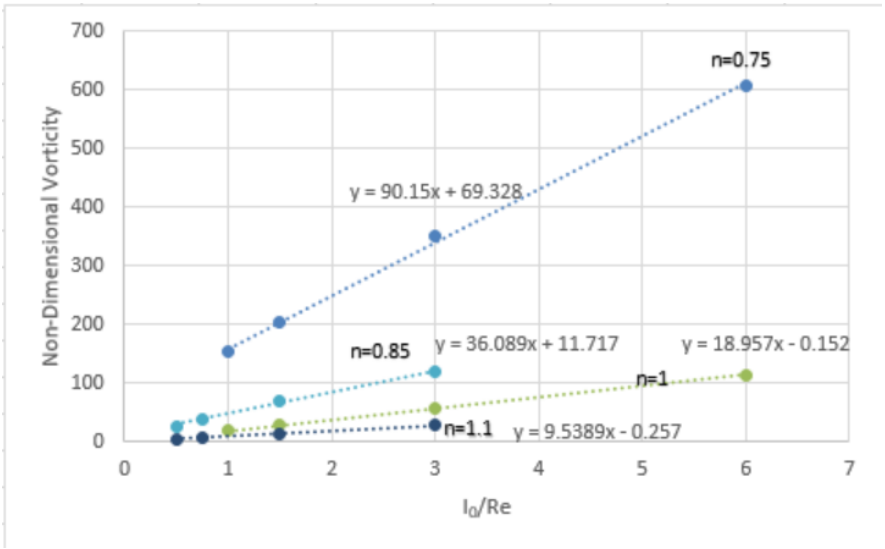

Figure 3.89. Non-dimensional vorticity at oscillating magnetic field created by $I_0 = 150$ with frequency 10π

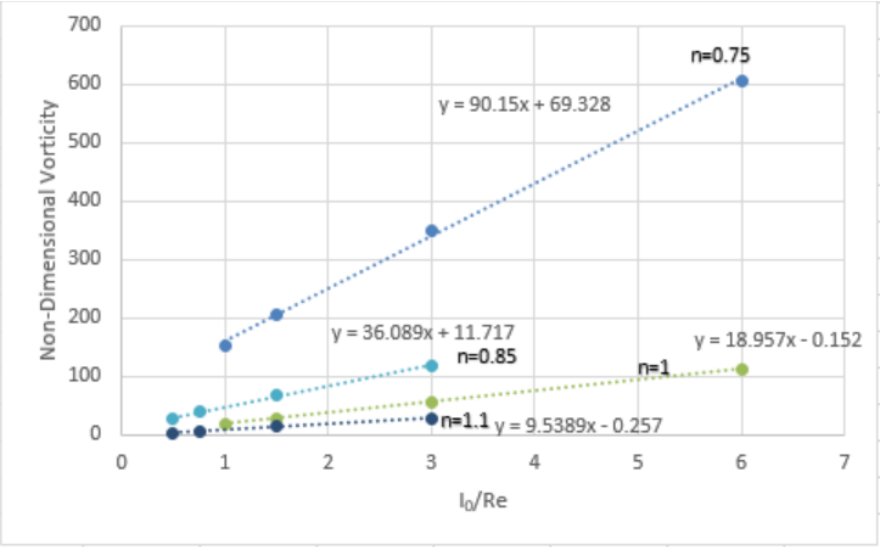

Figure 3.90. Non-dimensional vorticity at oscillating magnetic field created by $I_0 = 300$ with frequency 10π

4. CONCLUSION

The first half of this study is conducted for Newtonian and power law ferro fluid under the effect of constant magnetic field to see the effect on magnetic entrance length, friction factor and velocity profile. Analyses are performed for power law indices of $n = 0.6$, $n = 0.7$, $n = 0.8$, $n = 0.9$, $n = 1$, $n = 1.1$ and $n = 1.2$; which cover shear thinning, shear thickening and Newtonian ferro fluid cases; at Reynolds numbers from $Re = 100$ to $Re = 1200$, for non-dimensional electric current created by magnetic fields of $I_0 = 75$, $I_0 = 100$ and $I_0 = 150$. Magnetic entrance length L_m/D, friction factor C_f and non-dimensional velocity profile U/U_∞ are studied under the effect of the constant magnetic field. Results revealed that the magnetic entrance length is inversely proportional with the induced magnetic field and directly proportional with Reynolds number and power law index. The magnetic interaction parameter states the ratio of the magnetic effects to the inertia effects. With increasing magnetic field, which increases the magnetic interaction parameter, the magnetic effects become more dominant compared to inertia effects therefore when the ferro fluid enters to the magnetic region of the pipe it develops in a shorter entrance length. As the increase of the Reynolds number increases the inertia effects the influence of the magnetic field on the ferro fluid decreases and the inverse relationship between magnetic entrance length and the Reynolds number is observed. For power law ferro fluids, as the fluid becomes shear thinning viscous effects near the wall decrease so a more uniform profile is observed whereas as the fluid becomes more shear thickening as the viscosity near wall increases more sharp profile is observed and due to this the velocity profile develops sooner compared to the shear thinning fluids. Under the effect of the magnetic field this phenomena is still observed but due to the rheological effect of the magnetic field shorter entrance lengths are observed. The magnetic entrance length results are plotted in terms of Reynolds number, non-dimensional current and power law indices and linear relationships are observed for all cases. Different than the magnetic entrance length the friction factor is directly proportional with the induced magnetic field and inversely proportional with the Reynolds number and power law index. As the fluid becomes more shear thickening the viscous effects near the wall increase so does the friction factor. On

the other hand increase of the Reynolds number influence the inertia effects directly therefore decrease of the viscous effects decrease the friction factor. With increasing magnetic field the velocity profile starts to take a flatter shape. Due to this the fluid exhibits a higher skin friction factor. The important thing here is that as the fluid becomes more shear thinning the velocity profile takes a flatter shape too, however shear thinning fluids experience less viscous effects with increasing shear rate but in the case of a magnetic field this does not happen therefore the velocity profile becomes flatter without having changes in viscous behavior as a result the ferro fluid undergoes a flatter shape. Lastly the velocity profile becomes flatter with increasing power law index and magnetic field and decreasing Reynolds number. As the natural shape of the velocity of shear thinning fluid is flat due to the decreasing viscous effects near the wall it is easier for the magnetic field to make it flatter and with increasing power law index the velocity profile becomes sharper. As the inertia effects become more dominant with increasing Reynolds number the flatter velocity profile diminishes as it increases. The second half of the study is conducted for Newtonian and power law ferro fluid under the effect of oscillating magnetic field to see the effect on the stream lines and vortices developing within the fluid as well as the magnitude of the non-dimensional vorticity. Analyses are performed for power law indices of $n = 0.75$, $n = 0.85$, $n = 1$ and $n = 1.1$ at $Re = 50$, $Re = 100$, $Re = 200$ and $Re = 300$ for oscillating magnetic fields created by $I_0 = 0.75A$, $I_0 = 1.5A$, $I_0 = 3A$ and $I_0 = 6A$ with different frequencies. Results revealed that the when the magnetic field is applied oscillating it has different effects compared to constant magnetic field. With increasing magnetic field stream lines start to take a wavy shape and when the magnetic field further increases vortices start to occur in the pipe. Results revealed that the vorticity and velocity are influenced by the magnetic field shape, if it is constant it converges to a constant value and if it is oscillating it is in the form of a sinus wave. Also compared to constant magnetic field, as oscillating magnetic field has higher gradients than constant magnetic field, the magnetic force which is related to the gradient of the magnetic field is higher for oscillating magnetic field case as a result even the magnitude of the magnetic field is the same for both cases vortices with higher magnitudes are observed for oscillating magnetic cases. As a result vortices are obtained under the

oscillating magnetic field. As the flow becomes more shear thinning it becomes easier to develop vortices and higher values of non-dimensional vorticity. This is because the resistance of the fluid towards rate of deformation decreases with decreasing power law index. Lastly similar to the previous cases increasing inertia effects with increasing Reynolds number diminishes the vortices within the fluid.

REFERENCES

1. Oldenburg, "Numerical Simulation of Ferrofluid Flow for Subsurface Environmental Engineering Applications", *Kluwer Academic Publishers*, Vol. 38, 2000.

2. White, *Fluid Mechanics*, McGraw Hill, NY USA, 2011.

3. Moreau, R., *Magnetohydrodynamics*, Kluwer Academic Publishers, France, 1990.

4. P.A. Voltairas, L. M., D.I. Fotiadis, "Hydrodynamics of magnetic drug targetingl", *Journal of Biomechanics*, Vol. 35, 2002.

5. Malekzadeh, H. A., A. and Dabir, "Magnetic field effect on fluid flow characteristics in a pipe for laminar flow", *Journal of Mechanical Science and Technology*, Vol. 333, 2011.

6. Solis, K. and Martin, "Torque density measurements on vortex fluids produced by symmetry-breaking rational magnetic fields", *Soft Matter*, Vol. 10, 2014.

7. Sheikholeslami, G.-B. M. G. D., M. and Soleimani, "Heat flux boundary condition for nanofluid filled enclosure in presence of magnetic fields", *Journal of Molecular Liquids*, Vol. 193, 2014.

8. Akay, B., "Experimental investigation of the root fow in a horizontal axis wind turbine", *Wind Energy*, Vol. 17, 2014.

9. Omer Baris Adiguzel, K. A., "Magnetic field effects on Newtonian and non-Newtonian ferrofluid flow past a circular cylinder", *Applied Mathematical Modelling*, Vol. 42, 2017.

10. Weier, M., Gerbeth and Avilov, "Boundary layer control by means of electromagnetic forces", *ERCOFTAC Bulletin*, Vol. 44, 2000.

11. Calvo, A. M., "The Surface Charge In Electrospraying: It's Nature and Universal Scaling Laws", *Pergamon*, Vol. 30, 1998.

12. F. Gazeau, J.-C. B. R. P., C. Baravian and M. I. Shliomis, "Energy conversion in ferrofluids: Magnetic nanoparticles as motors or generators", *Phys*, Vol. 56, 1997.

13. P. K. Papadopoulos, P. M. H., P. Vafeas, "Ferrofluid pipe flow under the influence of the magnetic field of a cylindrical coil", *American Institute of Physics*, Vol. 24, 2012.